Nonlinear Optical Studies of Metallophtalocyanines and Hemiporphyrazines in Solution, Polymer Films and in the Presence of Nanomaterials

A thesis submitted in fulfilment of the requirements for the degree

of

Doctor of Philosophy

of

RHODES UNIVERSITY

By

Jonathan Britton

May 2013

Abstract

This thesis presents the study of the effects of CdTe-TGA quantum dots (QDs) on optical limiting ability of different phthalocyanine (Pc) complexes (**5**-**12**) containing Zn, Ga, In central metals and substituted with benzyloxyphenoxy, phenoxy, tert-butylphenoxy and amino groups in solution and in poly (methyl methacrylate) (PMMA) films. The optical limiting parameters of Pcs were higher for tert-butylphenoxy when compared to benzyloxyphenoxy and phenoxy substituents, in DMSO. Non-peripheral substitution decreased the optical limiting parameters. Third-order susceptibility ($Im[\chi^{(3)}]/\alpha$) values of Pcs in the absence and presence of CdTe QDs were in the 10^{-12} to 10^{-10} esu cm range. Hyperpolarizabilities (γ) ranged from 10^{-31} to 10^{-29} esu L for Pc alone or in mixture with QDs. The effect on the optical limiting abilities of twelve embedded phthalocyanines containing In, Ga, Zn and Al as central metals in polymer thin films was also examined. The effect of forming a covalent link zinc tetraamino phthalocyanine (**12**) with poly (methyl acrylic acid) (PMAA) and Zn (**13**) and OHAl (**14**) octacarboxy phthalocyanines to polyethylenimine (PEI) was also studied. The hyperpolarizability of the twelve phthalocyanines in polymer was found to be in the range of 10^{-26} to 10^{-24} esu.L. This is significantly higher than the hyperpolarizabilities of these phthalocyanines in solution. Non-linear optical (NLO) parameters were determined for phthalocyanine complexes containing In, Ga and Zn as central metals when embedded in PMMA polymer in the presence of quantum dots (QDs). The QDs mainly employed were CdTe-TGA (TGA = thioglylcolic acid). Triplet lifetimes increased as k (excited state (σ_{ex}) to ground state (σ_g) absorption cross section ratio) values decreased with the addition of the CdTe-TGA to the phthalocyanines. The saturation energy density (F_{sat}) values were smaller in the films

when compared to the solutions. Complex **7** tetrasubstituted with tert-butylphenoxy groups at non-peripheral positions was also studied in the presence of CdS-TGA, CdSe-TGA, fullerenes and single walled carbon nanotubes. There is a general improvement in optical limiting ability of Pc complexes in the presence of nano-materials (NMs). Degradation studies seem to indicate that placing a phthalocyanine within a polymer thin film may protect it slightly from photo- and thermal degradation.

3(4), 15(16)-Bis-(4 -*tert*-butyl-phenoxy)-10, 22-diaminohemiporphyrazinato chloroindium hemiporphyrazine was synthesized from 1, 3, 5-triaminobenzene and 4-tert-butyl-phenoxyisoindoline. The structure of the complex was confirmed using mass, nuclear magnetic resonance and infrared spectroscopies. The nonlinear parameters of the compound was also analyzed in dimethylformamide and found to be significantly greater than previously analyzed phthalocyanines.

Table of Contents

List of Symbols

f - f is Lorentz local field factor

F_{sat} – saturation fluence

I_{lim} – limiting intensity

Im[$\chi^{(3)}$] – imaginary component of the third order susceptibility

***k* value** - ratio of the absorption cross section of the singlet and triplet states

n - refractive index

N_A - Avogadro's constant

$^1O_2$ – singlet state oxygen

$^3O_2$ – triplet state oxygen

S_0 - ground singlet state

S_1 - excited singlet state

T_1 - first excited triplet state

T_n - nth excited triplet state

Z_0 – Rayleigh length

α – linear absorption coefficient

β - nonlinear absorption term

γ - hyperpolarizability

ε - molar extinction coefficient

ε_S - singlet state molar extinction

ε_T - triplet state molar extinction

σ_{ex} **-** absorption cross section of the excited state

σ_g **-** absorption cross section of the ground state

τ_T – triplet lifetime

Φ_{ISC} - inter system crossing quantum yield

Φ_T - triplet quantum yield

ω_0 – beam waist at the focus

ω* - frequency

List of Abbreviations

1-CNP - 1-chloronaphthalene

^{13}C-NMR – carbon nuclear magnetic resonance

^{1}H-NMR - proton nuclear magnetic resonance

A - absorption

Abs. – absorption

AFM - atomic force microscopy

BET - Brunauer Emmett Teller technique

DEPT - Distortionless Enhancement by Polarization Transfer

DMF - N,N'-dimethylformamide

DMSO – dimethylsulfoxide

EDC - N-(3-dimethylaminopropyl)-N'-ethylcarbodiimide hydrochloride

Fluor. – fluorescence

H_2Pc - metal-free phthalocyanine

HMBC - heteronuclear multiple-bond correlation

HOMO - highest occupied molecular orbital

HSQC - Heteronuclear Single Quantum Coherence

IC - internal conversion

IR – infrared

ISC – intersystem crossing

LUMO - lowest unoccupied molecular orbital

MPc – metallophthalocyanine

MOCPc - metallooctocarboxyphthalocyanine

NHS - N-hydroxysuccinimide

NLO - nonlinear optics

- nonlinear optical

NM - Nanomaterial

NOESY - nuclear Overhauser effect spectroscopy

Pc – phthalocyanine

PDT - photodyanamic therapy

PEI - polyethylenimine

PMAA - poly (methyl acrylic acid)

PMMA – Poly (methyl methacrylate)

QD – quantum dot

RSA - reverse saturable absorption/absorber

SA – saturable absorption/absorber

SEM - scanning electron microscopy

Std. – standard

STM - scanning tunnelling microscopy

SWCNT – single-walled carbon nanotube

TEM - transmission electron microscopy

TGA - thioglycolic acid

- thermogravimetric analysis

THF - tetrahydrofuran

UV/Vis - ultraviolet/visible

XRD - X-ray powder diffraction

List of Figures

List of Tables

List of Schemes

Chapter 1

Introduction and Objectives

1. Introduction

1.1 Phthalocyanines and Hemiporphyrazines

1.1.1 Introduction and General Applications

Phthalocyanines (Pcs) were discovered by chance in 1907 by Braun and Tcherniac. The brightly coloured compound, blueish in colour, was a by-product of synthesis of o-cyanobenzamide from phthalamide [1, 2]. Twenty years later, other phthalocyanine (Pc) derivatives were again obtained from the synthesis of phthalonitriles from o-dibromobenzene and cuprous cyanide by de Diesbach and von der Weid [3]. The structure of the metal free, unsusbstituted Pc was determined only about a quarter of a century later by the comprehensive research of Linstead and co-workers [4 – 7]. Linstead was the first to use the term phthalocyanine [4] which was derived from the Greek words *naphtha* (rock oil) and *cyanine* (blue), while the X-ray diffraction analysis of Pcs were carried out by Robertson and co-workers [8 – 10].

A Pc molecule is a planar macrocycle with an 18 π- electron system (see Fig. 1.1a). The structure of Pcs grants them their renowned stability, both chemical and thermal. The pyrrole nitrogen atoms form a cavity into which metal ions can be incorporated [11]. More than seventy metals/metalloids can be (and have been) incorporated into the phthalocyanine core.

A hemiporphyrazine (Hp) (Fig. 1b) is a phthalocyanine analogue where two opposite facing isoindoles are replaced by either benzenes or pyridine rings, thus giving tautomers A and B a D_{2h} symmetry and C a C_s symmetry. There have also been reports of Hps being able to accommodate a large variety of central metals into their

cavities, similar to a Pcs. Interestingly, despite their similarity in structure to Pcs, Hps have an absorbance spectra without any absorption in the visible and near-infrared [12]. In fact their absorbances can be found around the near UV. Hps can also exist in polymers, in what is termed a ladder configuration [13].

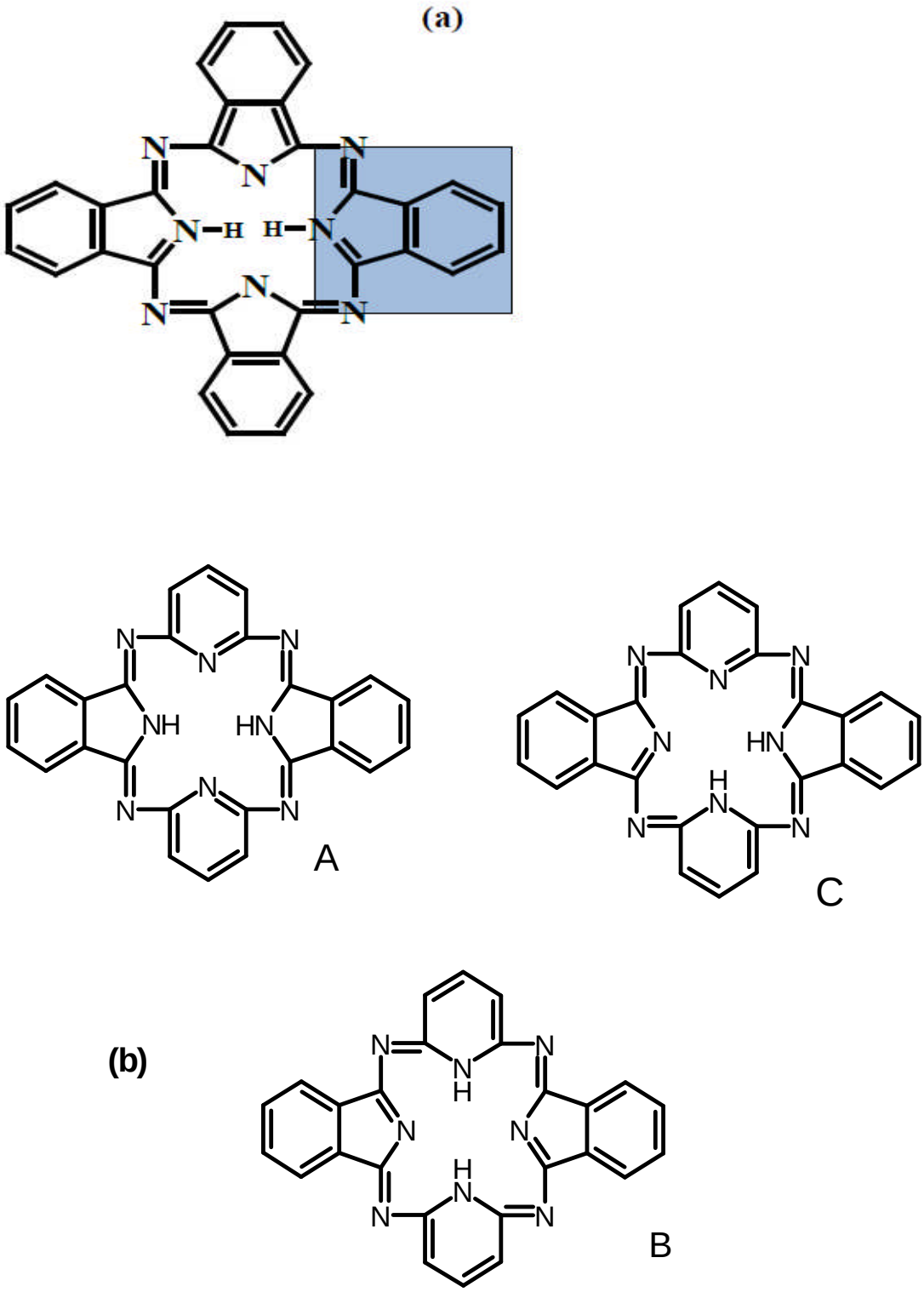

Fig. 1.1: (a) Indication of the four units which constitute an unmetallated phthalocyanine's structure. (b) Structures of an unmetallated hemiporphyrazine (shown are tautomers A-C).

Phthalocyanines have already been used for a diverse array of applications. Copper phthalocyanines are used as dyes in the textile and paper industry [11]. Phthalocyanines are also used in high-speed CD-R media and often act as the donor molecule in organic solar cells [14 – 25]. Probably the most significant application of phthalocyanines is in photodynamic therapy [1].

Photodynamic therapy (PDT) is a form of cancer treatment which involves a photosensitizer, a light source and oxygen present around the cancerous tissue. The photosensitizers most used are porphyrins and phthalocyanines, due to the fact that they are able to remain in cancerous tissue for a long time and that they can be engineered to possess the necessary energy requirements to produce singlet oxygen. Applications of Hps are mainly in optical limiting which will be discussed below.

1.1.2 General Synthesis of Phthalocyanines and Hemiporphyrazines

Phthalocyanines are synthesized through the cyclization of benzene derivatives (Scheme 1.1) to form the planar macrocyle.

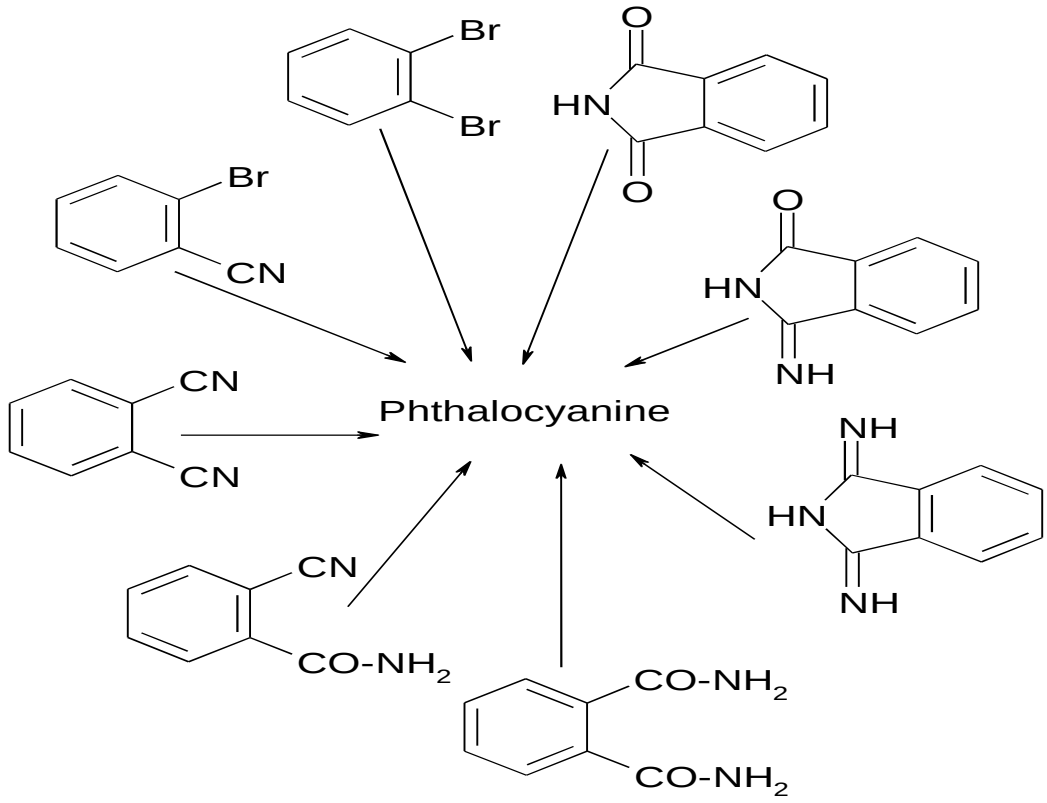

Scheme 1.1: Possible benzene derivatives used for Pc synthesis.

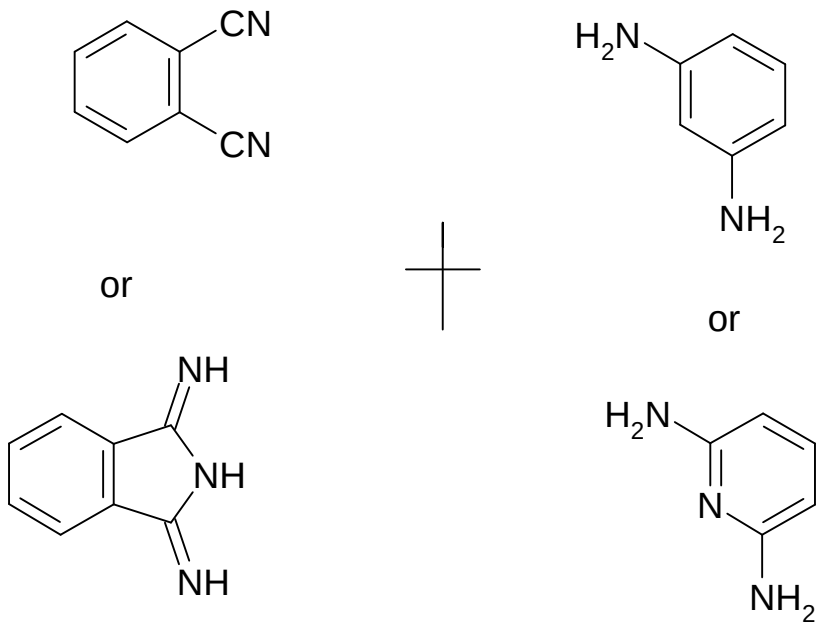

Fig. 1.2: Possible derivatives used for Hp synthesis.

Hps are synthesized through the reaction of substituted phthalonitriles or isoindolines with substituted 2, 5-diaminopyridine or 1, 3-diaminobenzene (see Figure 1.2) to form the unmetallated Hp.

1.1.3 Phthalocyanine and Hemiporphyrazine Absorption Spectra

A metal free phthalocyanine, H_2Pc, has a square planar, D_{2h} symmetry. When a metal is incorporated into the phthalocyanine cavity, the symmetry increases from D_{2h} to D_{4h}. The increase in symmetry results in the reduction of allowed transitions.

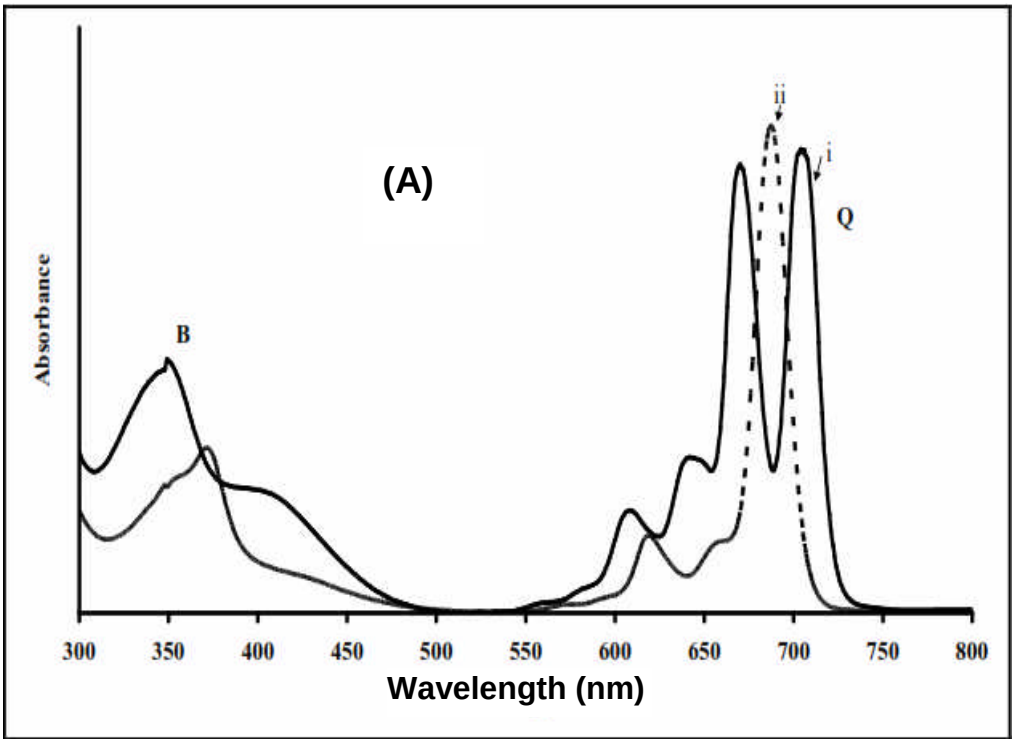

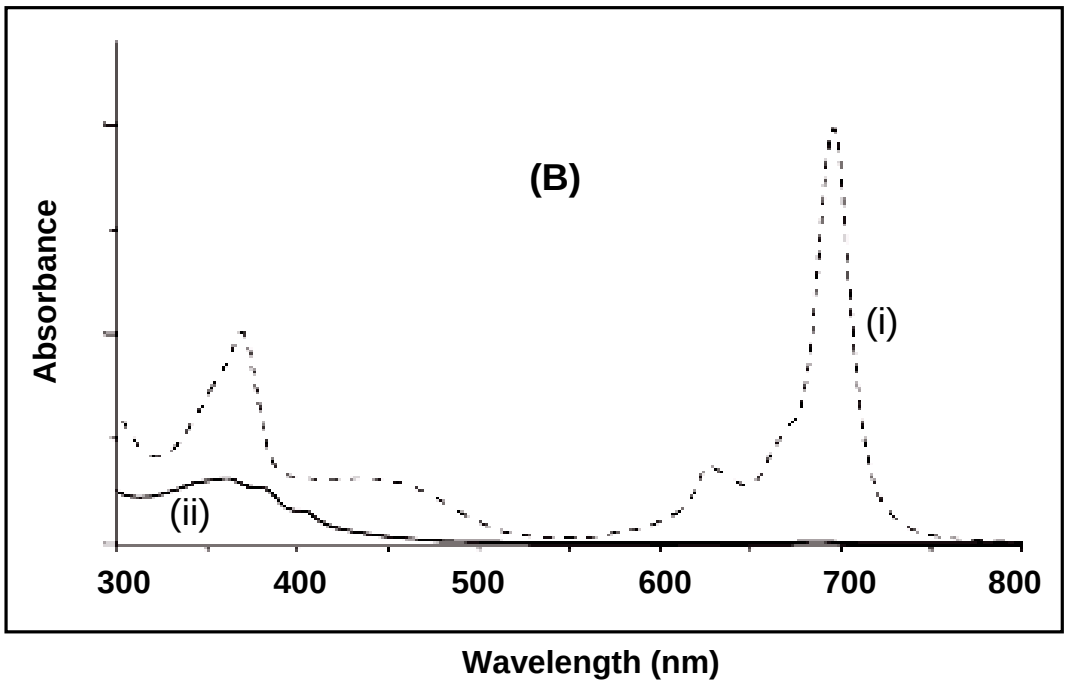

Fig. 1.3: Ground state electronic absorption of (A) an unmetallated phthalocyanine (i) and metallated phthalocyanine (ii) [unpublished work] and (B) absorbance spectra of (i) metallophthalocyanine (ii) hemiporphyrazine [26].

Metallophthalocyanines (MPcs) are known for their distinctive, strong absorption in the visible region of the spectrum (~ 670nm), called the Q band and weaker, broader, absorptions at around 350nm called the B bands [27], Fig. 1.3A, which is made up of two bands, B_1 and B_2. The assignment of the Q and B bands are based on the four-orbital model (Fig. 1.4), proposed by Gouterman's group [27 - 29]. The Q and B bands come from π - π * transitions and can be best explained in terms of a linear combination of transitions from a_{1u}, a_{2u} and b_{2u}, the highest occupied molecular orbitals (HOMO) of the MPc ring to the lowest unoccupied molecular orbitals

(LUMO), e_g*. The low symmetry of an unmetallated Pc results in the splitting of the Q band (Fig. 1.3A).

There are other bands which are characteristic of MPcs, namely the N, L and C bands which will not be discussed in great detail here. These are found at higher energies (below 300 nm) in the ground state electronic absorption spectra and are primarily due to π - π* transitions [30]. The N band is also strongly related to variations in the electron density of the pyrrole nitrogen atoms. The N band originates from a transition of the b_{2u} to the e_g and the L band is the a_{2u}/b_{2u} to e_g transition. As can be seen, there is some ambiguity regarding the L and N bands.

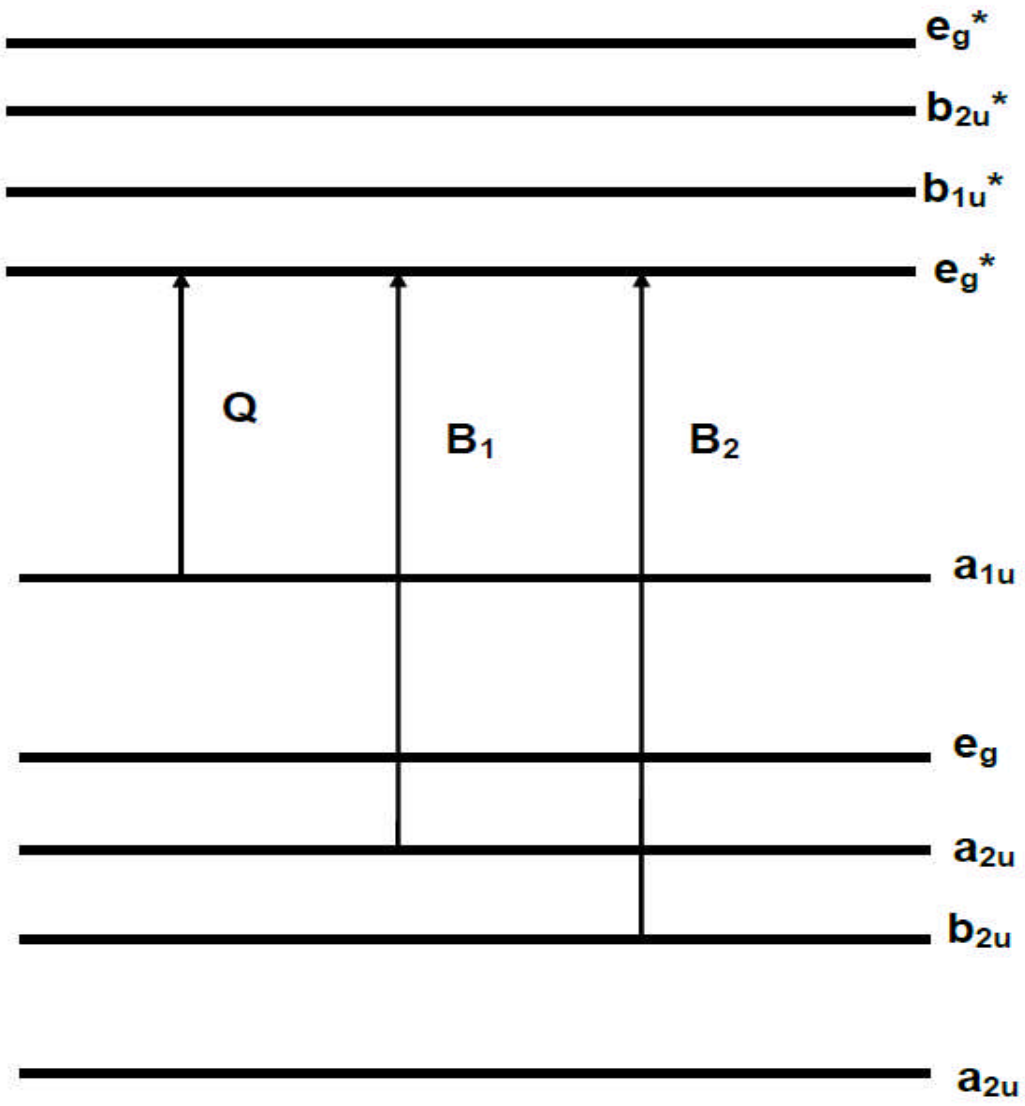

Fig. 1.4: Electronic transitions in phthalocyanines

Hps have a C_{2v} symmetry and absorbance bands around the 350 - 400 nm region, with a similarity to a Pc's Soret bands (Fig. 1.3B).

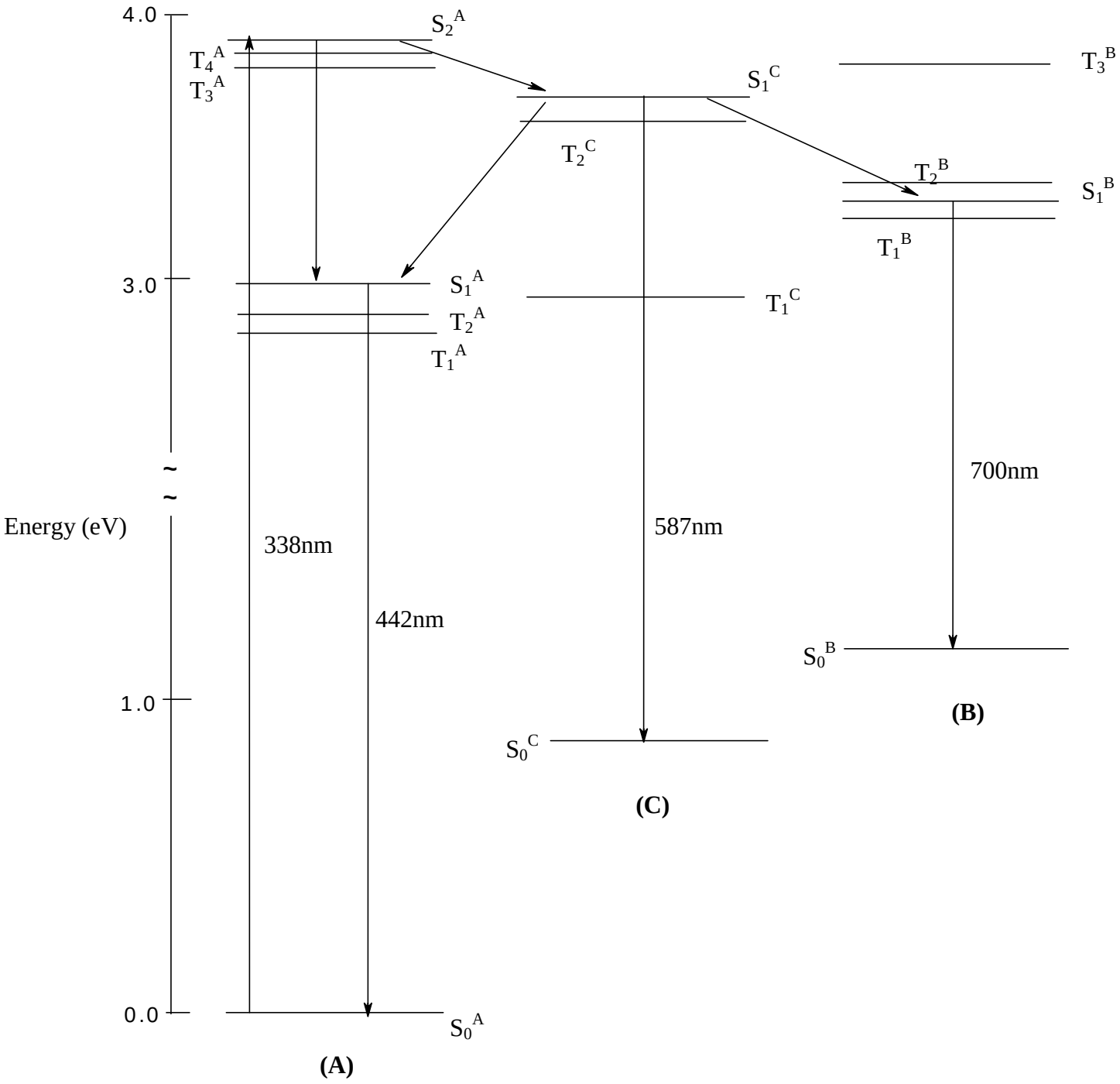

Fig. 1.5: Electronic transitions of the 3 tautomers of H_2Hp [31].

Figure 1.5 is a Jablonski diagram [31] showing the singlet and triplet transition of the three H_2Hp tautamers (A, B and C) shown in Figure 1.1b.

1.2 Quantum Dots and other nano-materials

In this work the nonlinear properties of quantum dots (QDs), single walled carbon nanotubes (SWCNTs) and fullerenes will be studied together with Pcs. Since three types of QDs were used in the study, they are discussed in more detail.

1.2.1 Introduction

Nanostructured materials have attracted exceptional interest over the past decades because of their unique architectures, tailored physicochemical properties, central roles in fabricating nanoelectronics and potential applications in bionanotechnology [32 – 37].

Quantum dots (QDs) are semiconductor nanocrystals that have diameters in the nanometer range. Their size is smaller than the exciton Bohr radius of the bulk semiconductor material from which the quantum dot is constructed, thus enabling confinement of an exciton in all three dimensions. QDs are therefore considered dimensionless. The energy levels of the semiconductor nanocrystals now become discrete (Fig. 1.6), as compared to the valence and conductance bands which exist when the semiconductor is in its bulk form. What this ultimately means is that the quantum dots have numerous discrete energy levels that they can occupy when excited, usually by a photon of light, giving the quantum dot a rather broad absorption spectrum. However, the quantum dot can only emit energy as fluorescence from the lowest energy level in the former conductance band to the highest energy level in the former valence band. This means that the emissions of quantum dots is very specific and size dependent (Fig. 1.7) [38, 39].

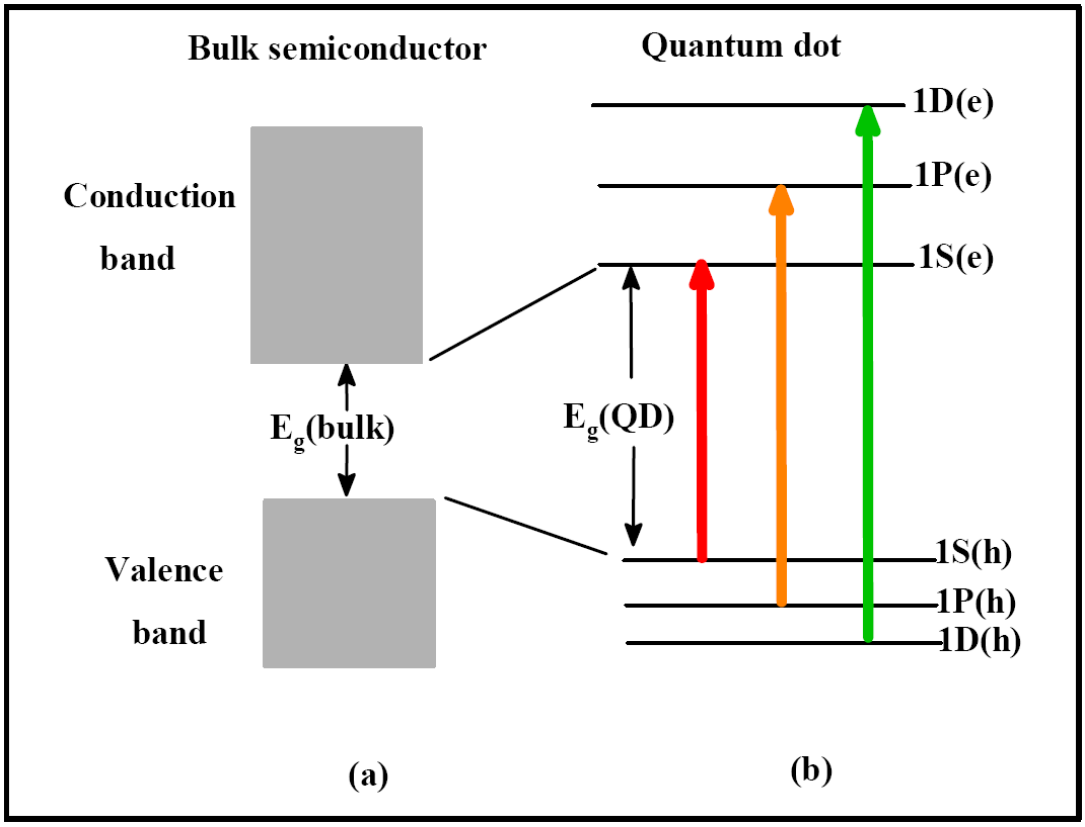

Fig. 1.6: Band gap in bulk crystals and QDs showing (a) continuous conduction and valence energy bands separated by a "fixed" energy gap, E_g(bulk) (b) QD characterized by discrete atomic-like states with energies that are determined by the QD radius [39].

Another effect of the exciton quantum confinement is that the energy gap is larger than that between the conduction and valence bands of the bulk. The emission is thus blue-shifted compared with that of the bulk semiconductor. As the quantum dots grow in size and begin to assume a structure that more closely resembles the bulk's structure, the energy gap progressively decreases, thus red-shifting the emission. This is useful because it means that the quantum dots' emission region can be tuned to where it can be most useful (see Fig. 1.7a) [38 – 44].

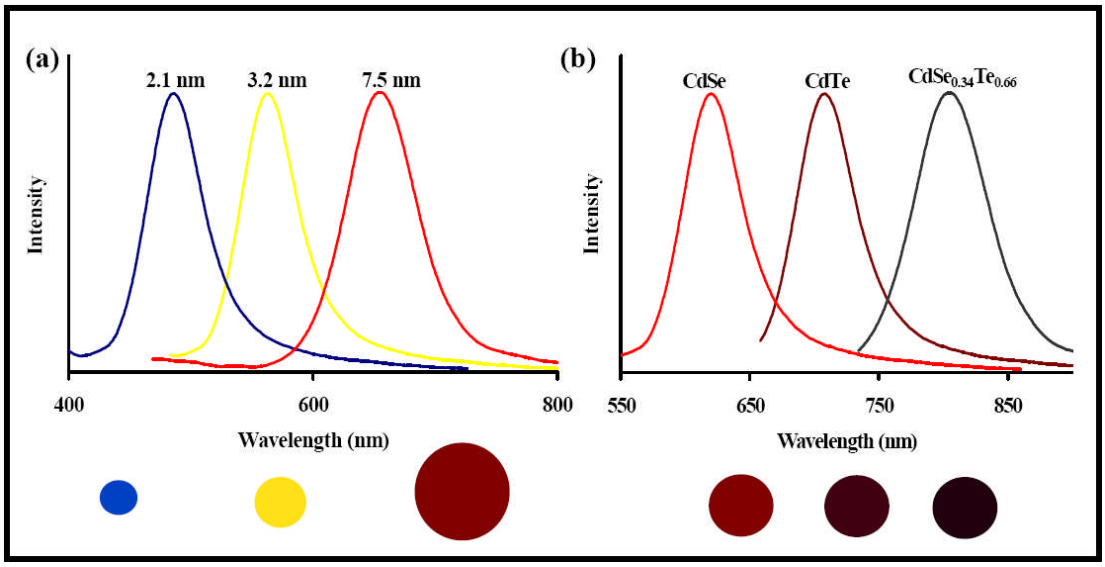

Fig. 1.7: QD emission wavelength tuned by changing the nanoparticle (a) size or (b) composition [39].

QDs have evolved a great deal since their initial creation in the early 1980s [45]. Mainly CdTe and CdSe QDs were being made in the early days. Currently QDs can be created with nearly every semiconductor in existence, as well as with many metals and insulators. Along with the expansion of the types of atoms which may be involved in the formation of the QDs, with different emission spectra (see Fig. 1.7b), there are also many different techniques to creating QDs from one, two or three types of atoms in many differing ratios, as well as the possibility to create a “quantum dot shell” around an existing quantum dot [45].

While all these possibilities for QD formation do exist, there does appear to be a favouring of the combination of group III and group V elements and the group II and IV elements. In addition, since many QDs are formed from semiconductors, the possibility of doping the QD exists, which may add unique properties to the QD or merely enhance pre-existing ones [46].

QDs are capped during synthesis to stabilize them and help regulate the growth. Capping can also help “trap” the QD’s atoms within its structure. To elaborate, the capping agent is bound around the surface of a QD, effectively encapsulating it (bar a few defects which may arise). This makes it rather unlikely that an atom or ion from the QD lattice will escape into the surrounding environment. An added benefit of the capping agent is that, depending on its structure, different properties may be incorporated into the QD. These can range from water solubility to giving the QD terminal groups which may be used to create bonds with other molecules.

Quantum dots themselves have some ability to create singlet oxygen and radicals, meaning that they may be used for photodynamic therapy (PDT) to a certain degree as well, and, with their much broader absorption spectrum, excitation should be significantly easier and more flexible compared to the narrow absorption regions present in phthalocyanines for example [44, 47, 48]. However, unless the QD can be cleared quickly from the body, it is likely that the capping agent will end up degrading, leaving a “naked” QD within the body which may do more harm than good [44].

All these properties allow for the exploitation of QDs in a variety of fields. Some fields of application of QDs include biological labeling, use in optoelectronic devices and, as stated above, they also have a potential for use in photodynamic therapy (PDT) and other biomedical applications [49 - 60]. QDs are also known to show optical limiting (OL) behaviour [61]. Thus both phthalocyanines and QDs are good candidates for optical limiters and combining the two could result in improved OL behavior.

The other nano-materials (NMs) used were fullerenes (Buckminsterfullerene, C_{60}) and single-walled carbon nanotubes (SWCNTs). Buckminsterfullerene is the smallest fullerene molecule containing pentagonal and hexagonal rings in which no two pentagons share an edge (which can be destabilizing). Fullerenes and related compounds show considerable promise as catalysts. Fullerene-based materials could also have important photonic device applications. The reason for this is fullerenes have a very large non-linear optical response, which makes them suitable for a range of telecommunication applications and as optical limiters [62 - 76]. Single-walled carbon nanotubes are usually only a few nanometres wide, but they can range from less than a micrometer to several millimetres in length. They often have closed ends, but can be open-ended as well. Their unique molecular structure results in extraordinary macroscopic properties, including high tensile strength, high electrical conductivity, high ductility, high heat conductivity, and relative chemical inactivity [77 - 85]. They also show ultrafast second- and third-order nonlinearities responses, meaning they are able to sustain high repetition rates, and saturable absorption (SA) in the near infrared (NIR) region [86 – 90]

1.2.2 Synthesis of Water Soluble Quantum Dots

There are generally two different pathways towards producing quantum dots referred to as the top-down and bottom-up approaches. Basically, one can either build up quantum dots from atoms or break down lattices to form them. Within the top-down pathway there exists one general method, which will be mentioned in a rather generalized sense. This method involves progressively confining the exciton of a lattice by slowly removing parts of the lattice in a process called etching until it cannot move in any dimension (which is the definition of a QD). The process may be

achieved using photolithography, electron beam lithography or using ball-milling. In this way quantum wells (which have the exciton confined in one dimension) and quantum wires (which confine the exciton in two dimensions) are also formed [45].

The bottom-up method is the most well established of the methods, having originated in the 1980s [61], and this is the method used to synthesize the QDs used in this thesis. The process involves the initial combination of the compounds of interest and capping agent, called nucleation. This is followed by the heating of the solution to grow the QDs to the desired size, a process called Ostwald ripening [91, 92].

The water soluble nature of a quantum dot is determined by the type of capping agent used. In this work, for example, thyoglycolic acid (TGA) was used because it ends in a carboxyl group, thus meaning that the resultant QDs would be water soluble.

1.2.3 Quantum Dot Size Characterization

The size of the QDs may be characterized using UV-Vis spectroscopy, X-ray powder diffraction (XRD), atomic force microscopy (AFM), transmission electron microscopy (TEM) and the Brunauer Emmett Teller (BET) technique, to name a few. With UV-Vis spectroscopy, only the size of CdTe quantum dots can be estimated using the polynomial fitting function derived in the literature [93], equation 1.1:

$$D = (9.8127 \times 10^{-7})\lambda^3 - (1.7147 \times 10^{-3})\lambda^2 + (1.0064)\lambda - (194.84) \qquad (1.1)$$

where λ is the absorption maxima of the QDs. When using XRD, size may be confirmed using the Scherrer equation 1.2 [94]:

$$d\left(\mathring{A}\right)=\frac{k\lambda}{\beta\cos\left(\theta\right)} \qquad (1.2)$$

where k is an empirical constant equal to 0.9, λ is the wavelength of the X-ray source, (1.5405 Å for Cu), β is the full width at half maximum of the diffraction peak (in radians), and θ is the angular position of the peak (in degrees).

Whilst all of the microscopic techniques (AFM, TEM and SEM) operate on different principles, the method each uses for size determination is the same and it is based on the comparison of the diameter of an image of a quantum dot to a determined scale for the image. The only real difference between them is resolution and operation speed. For example, SEM operates faster than TEM, but has about 40 times lower resolution than TEM, and cannot be used with samples smaller than 30 Å [95]. Another issue which can arise, especially in AFM, is the aggregation of the quantum dots, thus making them appear larger than they actually are [96]. The reason why it can often arise in AFM, as well as TEM and SEM, is the preparation of the sample tends to cause the compounds to aggregate together. Lastly, all of these techniques generally only look at a small region of the total sample and the quantum dot sizes present there, whereas XRD which will give an average size for the entire sample [97].

BET is also useful for QD size determination. The amount of gas adsorbed onto the QD to form a monolayer is determined. Used with the cross-sectional area that the gas particles occupy, the QD diameter can be calculated as an average, though it tends to give larger values than other techniques [98 – 100] and the result can also be disrupted due to aggregation of the QDs.

Photoluminescence and photoluminescence excitation are also possible size determination techniques, though it is unclear exactly how this technique operates. There seems to be some involvement of the luminescence intensity as an indicator of particle size, with the argument being that nanoparticles contain fewer defects to quench their luminescence than the bulk material does [101, 102]. Also, the luminescence would give an indication of the energy band gap of the particle, so perhaps these factors are used together to determine size [101, 102].

Lastly, there are two techniques that could be used appear to operate in the same manner as XRD, in that scattering patterns obtained are used to determine the particle's size. These two techniques are Raman scattering spectroscopy and dynamic light scattering [97]. In this work XRD is employed to determine the size of the QDs synthesized. Something which should be noted is that regardless of the technique used, the measurement obtained for the compound in question will either be an average of a range of sizes or given as a range of sizes.

1.3 Photophysics

1.3.1 The Jablonski diagram

A Jablonski diagram is a representative diagram of the energy transitions and spin alterations that electrons of a molecule can undergo. The triplet-triplet absorption is indicated by the T_1 to T_n transition, while the S_0 is the ground state (Fig. 1.8) of the molecule. S_0 to S_1 indicates absorption (abs.), whilst S_1 to S_0 is fluorescence (fluor.). The S_1 to T_1 transition represents intersystem crossing (ISC). Transition between the S and T levels involves an alteration in electron spin, which is ordinarily forbidden to

happen but due to the closeness of the S_1 and T_1 energy levels and spin orbit coupling it can occur.

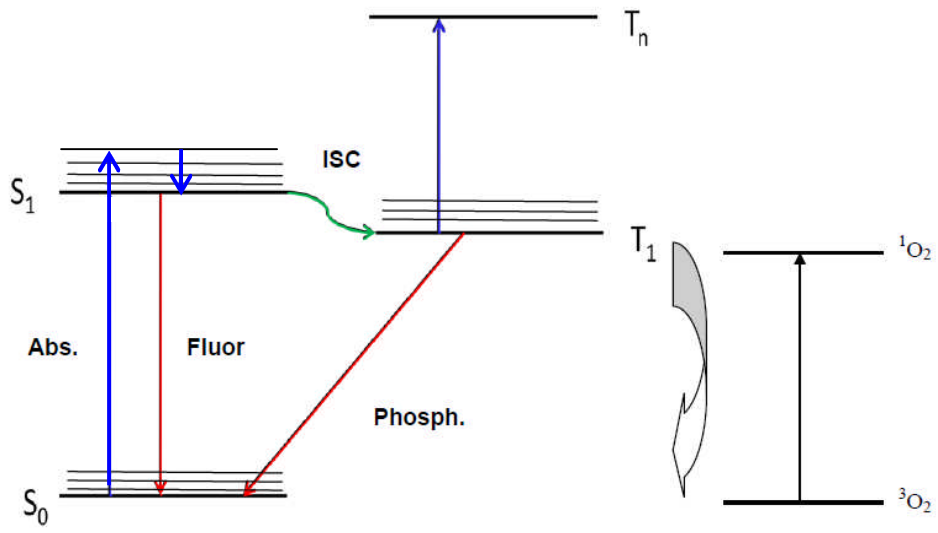

Fig. 1.8: Jablonski diagram.

Phthalocyanines can cause cancer cell death in PDT due to their ability to produce singlet oxygen, which can kill cells through apoptosis or necrosis. The singlet oxygen is produced when energy from phthalocyanines in the triplet state is transferred to triplet oxygen (Fig. 1.8), forming singlet oxygen, whilst the phthalocyanines return to their singlet ground state. Due to the fact that the phthalocyanines and PDT light are localized mainly around the cancerous tissue, the damage the singlet oxygen does is only localized there. Another more recent application of Pcs and Hps is as optical limiters due to the presence of strong nonlinear absorptions which originate from strong triplet-triplet absorption and strong intersystem crossing.

1.3.2 Triplet Quantum Yields and Lifetimes

The triplet quantum yield is an indication of how many molecules have entered the triplet state per photon of light absorbed. The triplet decay is measured using laser flash photolysis and the data is analysed using OriginPro 7.5 software. The triplet quantum yield is obtained using equation 1.3 [103]:

$$\Phi_T = \Phi_T^{Std} \frac{\Delta A_T \varepsilon_T^{Std}}{\Delta A_T^{Std} \varepsilon_T} \qquad (1.3)$$

where ΔA_T and ΔA_T^{Std} are the changes in the triplet state absorbances of the MPc derivatives and the standard, respectively. ε_T and ε_T^{Std} are the triplet state molar extinction coefficients for the MPc derivatives and the standard, respectively. Φ_T^{Std} is the triplet quantum yield for the standard, e.g. ZnPc.

Equation 1.4 is used to obtain the triplet state molar extinction coefficients:

$$\varepsilon_T = \varepsilon_S \frac{\Delta A_T}{\Delta A_S} \qquad (1.4)$$

where ε_S is the singlet state molar extinction coefficient, and the ΔA_T and ΔA_S are the triplet and singlet state absorbances respectively.

1.4 Nonlinear Optics (NLO)

All matter possesses an electromagnetic field of various intensities, and it is because of this field that matter and light are able to interact. Nonlinear optics is a branch of study of this interaction, more specifically how matter interacts with intense laser

light. Higher intensity light can result in behaviour which does not occur when the light of a lower intensity is used with certain materials.

Optical limiting (OL) is a specific branch of nonlinear optics, and it deals with how certain materials are able to regulate light intensity. This means that certain materials do not transmit light linearly at high intensities, but, instead, have a fixed intensity transmission, (Fig. 1.9). Fig. 1.9 merely represents the idea that the light transmitted by material A is the same intensity when both low and high intensity light is applied to it, indicating that the optical limiting response is arising from the triplet-triplet absorption (see Fig. 1.9) of A.

The development of optical limiting materials has attracted considerable attention as a means of providing protection for light sensitive objects such as the eye from laser radiation [104 - 113]. Materials with strong reverse saturable absorption (RSA) can effectively limit the output energy of incident light; hence such materials are of prime importance in optical limiting applications [113].

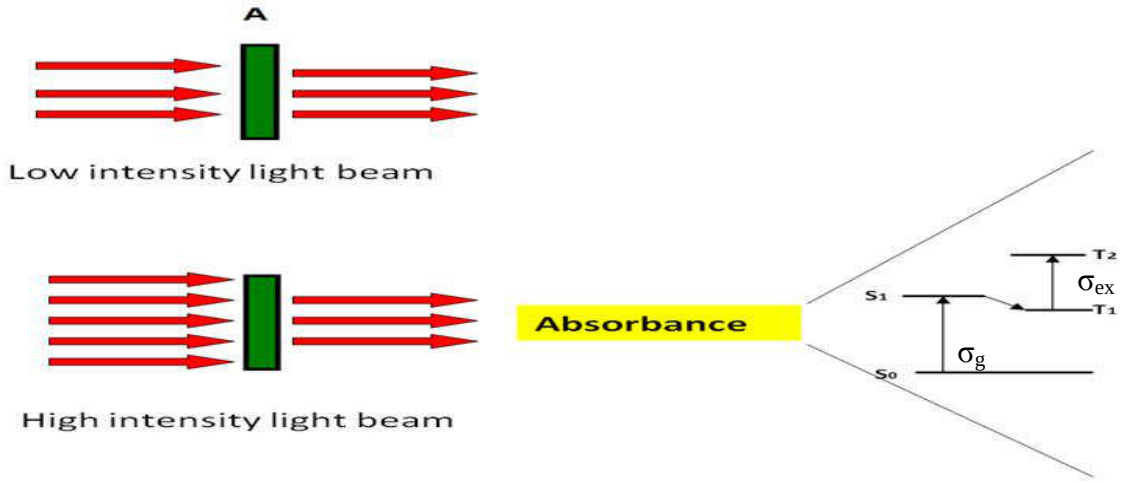

Fig. 1.9: Schematic representation of the ideal functioning of a phthalocyanine optical limiter under low and high intensity light.

This optical limiting phenomenon has also been observed in nano-materials, and in the case of phthalocyanines it is the triplet-triplet ($T_1 – T_2$) absorption (Fig. 1.9) which is responsible for the decrease in the transmitted light after the intense laser light causes two-photon absorption and intersystem crossing to the triplet state.

1.4.1 Optical Limiting of Phthalocyanines, Hemiporphyrazines and Nano-materials

Metallophthalocyanines (MPcs) have been shown to be excellent OL materials with high absorption cross section ratio of excited triplet state to ground state in the absorption range 400–600 nm [114 - 125]. The nonlinear optical properties of MPcs can be modified by substituting different metal atoms into the ring or altering peripheral and axial functionalities [125]. Combining MPc complexes with NMs such as SWCNTs, fullerenes or QDs is expected to result in enhanced NLO behavior due to the synergistic effect.

The phthalocyanines that are mostly used as optical limiters are those containing heavy central metals such as indium, gallium, lead and antimony, as well as those with peripheral groups that help with the solubility and disaggregation of the phthalocyanine. It is possible also to utilize the peripheral groups to increase the ratio of excited state to ground state absorption cross section [126 - 129].

Hps with heavy metal centers have also shown great promise as optical limiters due to the presence of a large nonlinear absorption [12]. As an added benefit over Pcs, Hps have little to no visible absorption present, meaning that little visible light obstruction will occur whereas Pcs absorb red light and cause the transmitted light to appear green [26, 31, 130 - 134]. Other than the loss of the Q-band, Hps behave

remarkably similarly to Pcs and have their triplet absorption around the same wavelength region as Pcs.

The use of NMs in OL and as NLO materials has also attracted considerable attention [135 - 137]. SWCNTs, fullerenes and QDs all show some OL or NLO behaviour [138 – 147].

Phthalocyanines have been studied extensively as optical limiters due to the ease with which a Pc enters a triplet state, where the optical limiting behaviour originates from. Aside from the enhanced intersystem crossing, heavy metals tend to disrupt the Pcs original symmetry. This is because the heavy metals rarely fit into the Pc cavity and, instead, are held slightly above the ring, and this altered symmetry also appears to be beneficial to good optical limiting ability [148, 149]. Pc aggregation also tends to disrupt the symmetry, resulting in improved optical limiting.

The QDs do show some minor OL ability, but their main contribution is the fact that they are synthesized from heavy elements. Bringing a Pc into close proximity to these QDs will end up enhancing the intersystem crossing to the triplet state of these molecules in a manner similar to introducing a heavy atom to the central cavity, thus resulting in larger NLO responses from them.

With regards to the fullerenes it is more of a cumulative NLO response from both the fullerene and Pc. This is because almost all the light absorbed by the fullerene is transitioned to the triplet state, thus resulting in a moderate OL response. It is also formed from carbon atoms, so there is little chance that they will enhance intersystem crossing in Pcs. This is also true of single walled carbon nanotubes (SWCNTs). Non-chiral SWCNTs, which were used in this study, do not have much OL ability and are more likely to cause scattering of the laser light, which would

decrease the intensity but may end up distorting the transmitted image. Chiral SWCNTs have been known to exhibit second-order optical limiting.

1.4.2 Nonlinear Optical Parameters – Equations used in this work

One of the more common methods for determining optical limiting parameters is the use of a Z-scan, which essentially provides the nonlinear refraction (closed-aperture setup) and nonlinear absorption (open-aperture setup) directly from the device's measurements. These are the two major factors which help explain the processes involved in optical limiting.

Once the open aperture data was collected with the Z scan, it could be analyzed by using the procedure described by Sheikh-Bahae *et. al* [150], using equation 1.5:

$$T(z) = \frac{1}{\sqrt{\pi}\, q_0(z)} \int_{-\infty}^{\infty} ln\left[1 + q_0(z) e^{-\tau^2}\right] d\tau \qquad (1.5)$$

where $\Delta T(z)$ is the normalized transmittance of the sample and $q_0(z)$ is given by equation 1.6:

$$q_0(z) = \beta I_0 L_{eff} / (1 + z^2/z_0^2) \qquad (1.6)$$

and L_{eff} by equation 1.7:

$$L_{eff} = \frac{1 - e^{-\alpha L}}{\alpha} \qquad (1.7)$$

where I_0 is peak irradiance at focus, L_{eff} is the effective sample length (calculated using equation 1.7), L is actual sample length, α is the linear absorption coefficient and β is the nonlinear absorption coefficient. z is the position of the sample with respect to the focal position. z_0 is the Rayleigh length, and is defined as the distance along the propagation direction of a beam from the focal waist to where the beam cross section doubles.

Equation 1.5 is however, not well suited to fit directly to the data and a numerical representation of this equation was therefore employed as a fit function to obtain $q_0(z)$, equation 1.8:

$$T(z) = 0.363e^{\left(\frac{-q_0(z)}{5.60}\right)} + 0.286e^{\left(\frac{-q_0(z)}{1.21}\right)} + 0.213e^{\left(\frac{-q_0(z)}{24.62}\right)} + 0.096e^{\left(\frac{-q_0(z)}{115.95}\right)} + 0.038e^{\left(\frac{-q_0(z)}{965.08}\right)} \quad (1.8)$$

The $q_0(z)$ can then be used in Equation 1.6, along with Equation 1.7, to obtain β and β is then used in the equations below. Equation 1.8 can only be used when certain assumptions are made to simplify the analysis:

- The analysis assumes only a $\chi^{(3)}$ nonlinearity.
- The analysis assumes a Gaussian spatial and temporal pulse.
- The sample length is smaller than the Rayleigh length.
- The full transmittance equation is used in analysis of open aperture Z-scan.
- Fit parameters. The only free parameters used in the analysis of an open aperture Z-scan is the Rayleigh length, z_0 , and the product of the nonlinear absorption coefficient and the intensity, β x I_0, which is treated as a single parameter.

This is not the only method which can be used though. Another involves the use of triplet quantum yield and triplet lifetime measurements in the calculation of these parameters. The first parameter is the limiting intensity (I_{lim}), which essentially indicates the intensity at which the optical limiting response will begin to occur, and can be calculated using equation 1.9 [151, 152]:

$$I_{\lim} = \frac{h\omega}{2\pi\sigma_{13}\tau_{21}} \qquad (1.9)$$

where ω^*, σ_{13} and τ_{21} are the frequency at which the system absorbs, singlet state absorption cross section and triplet lifetimes, respectively, and 1 = S_0, 2 = T_1 and 3 = S_1. There is no specified optimal range for I_{lim} values, however the lower they can be the better the optical limiter because the optical limiting behaviour will occur sooner. The I_{lim} values for this work were obtained graphically from plotting incident intensities against emergent intensities of a sample.

The imaginary component of the third order susceptibility is also representative of the nonlinear absorption, equation 1.10:

$$\mathrm{Im}[\chi^{(3)}] = n^2\varepsilon_0 c_0 \lambda\beta / 2\pi \qquad (1.10)$$

where n and c_0 are, respectively, the linear refractive index of the medium the compounds reside in and the speed of light in a vacuum; ε_0 is the permittivity of free space, λ is the wavelength of the incident light and β is the nonlinear absorption coefficient, given by equation 1.11.

$$\beta = 5.3\,\varepsilon_s \varepsilon_T c_{mol} \Phi_{ISC} \qquad (1.11)$$

where ε_S and ε_T are extinction coefficients for the ground and triplet state, respectively, c_{mol} is the concentration of active species in the triplet state and Φ_{ISC} is the intersystem crossing quantum yield [151, 153], equation 1.11. The optimal range for $\mathrm{Im}[\chi^{(3)}]$ is 10^{-9}-10^{-11} [151]. Equation 1.11 can be used to obtain the triplet quantum yield of a sample if the other factors are known. This can be done because the

intersystem crossing quantum yield and triplet quantum yield could be considered equivalent. This was used as reinforcing evidence of the calculated triplet quantum yields of the compounds in thin films.

Another term to consider is called hyperpolarizability. Whilst the imaginary component of the third-order susceptibility of the compound gives the nonlinear absorption, it is for the whole solution. Hyperpolarizability gives the nonlinear absorption per mole of compound, which is useful when it comes to comparison of the effectiveness of multiple compounds. Hyperpolarizability is calculated using equation 1.12 [151, 154]:

$$\gamma = \frac{\mathrm{Im}[\chi^{(3)}]}{f^4 c_{mol} N_A} \qquad (1.12)$$

where N_a is Avogadro's constant, c_{mol} the concentration of the active species in the triplet state and f is Lorentz local field factor, $f = (\eta^2 + 2)/3$. Optimal values of γ are between 10^{-29}-10^{-34} [151].

The last parameter is the k term (Equation 1.13), and it is an indication of the ratio of triplet absorption cross section to singlet absorption cross section at a particular wavelength. In this case the particular wavelength is 532 nm. This is important because in the case of phthalocyanines it is the triplet absorption which is most involved in optical limiting:

$$k = \sigma_{ex} / \sigma_g \qquad (1.13)$$

Also, the modified Jablonski diagram (Fig. 1.9) helps to describe where the two terms (σ_{ex} and σ_g) originate from. For any significant optical limiter this ratio needs to be larger than one – ideally considerably larger.

Tables 1.1 to 1.3 (and Figs. 1.10 to 1.14) list a selection of Pc derivatives that have been studied for their nonlinear optical behaviour [124, 126, 151, 155 - 161].

Table 1.1: Nonlinear optical limiting parameters for InPc and GaPc Derivatives.

Compound	**Solvent/ Polymer**	**Method**	**k**	**I_{lim} ($J.cm^{-2}$)**	**Im[$\chi^{(3)}$] (esu)**	**$\gamma/10^{-32}$ (esu)**	**[Ref.]**
ClInPc					0.15×10^{-11}		[151]
(tri-(n-hexyl)siloxy)InPc	Toluene	Frequency Doubling	16	0.24			[126]
1a	$CHCl_3$	Z-scan	16.1	10.1	1.2×10^{-11}	7.3	[156]

Compound	**Solvent/ Polymer**	**Method**	**k**	**I_{lim} ($J.cm^{-2}$)**	**Im[$\chi^{(3)}$] (esu)**	**γ/10^{-32} (esu)**	**[Ref.]**
1b	$CHCl_3$	Z-scan	16.2	9.5	1.3×10^{-11}	8.1	[156]
1c	$CHCl_3$	Z-scan	15.9		3.99×10^{-6}		[157]
1c	PMMA[a]	Z-scan	8.3		1.41×10^{-4}		[157]
1d	$CHCl_3$	Z-scan	14.8		3.66×10^{-6}		[157]
1d	PMMA[a]	Z-scan	9.1		1.45×10^{-4}		[157]
2a	Toluene	Pump and Probe		0.25			[124]
2a	Toluene	Z-scan	27.5		1.6×10^{-11}	1.30	[159]

Compound	Solvent/ Polymer	Method	k	I_{lim} ($J.cm^{-2}$)	$Im[\chi^{(3)}]$ (esu)	$\gamma/10^{-32}$ (esu)	[Ref.]
2b	Toluene	Pump and Probe		0.09			[124]
2c	Toluene	Pump and Probe		0.09			[124]
2d	Toluene	Pump and Probe		0.66			[124]
2e	DMSO[b]	Calculation	41.4	1.16	4.59×10^{-11}	0.002	[155]
2f	DMSO[b]	Calculation	53.4	1.92	2.87×10^{-11}	0.00307	[155]
2g	DMSO[b]	Calculation	9.44	1.47	6.81×10^{-11}	0.00297	[155]
2g	PMMA[a]	Z-scan	7.5		2.48×10^{-2}		[157]

Compound	**Solvent/ Polymer**	**Method**	**k**	**I_{lim} ($J.cm^{-2}$)**	**Im[$\chi^{(3)}$] (esu)**	**γ/10^{-32} (esu)**	**[Ref.]**
2h	$CHCl_3$	Z-scan	18.5		5.65×10^{-6}		[157]
2h	PMMA[a]	Z-scan	7.4		2.72×10^{-2}		[157]
2i	$CHCl_3$	Z-scan	16.8		4.99×10^{-6}		[157]
2i	PMMA[a]	Z-scan	7.6		3.50×10^{-3}		[157]
2j	$CHCl_3$	Z-scan	15.7		4.32×10^{-6}		[157]
2j	PMMA[a]	Z-scan	8.6		3.54×10^{-3}		[157]
2k	DMF[c]	Z-scan			9.79×10^{-12}		[158]

Compound	Solvent/ Polymer	Method	k	I_{lim} ($J.cm^{-2}$)	$Im[\chi^{(3)}]$ (esu)	$\gamma/10^{-32}$ (esu)	[Ref.]
2k	Toluene	Z-scan	13.5		1.2×10^{-11}	0.84	[159]
2A(i)	Toluene	Z-scan	12.4		1.5×10^{-11}	2.40	[159]
2A(ii)	Toluene	Z-scan	11.3		1.3×10^{-11}	1.76	[159]
2A(iii)	Toluene	Z-scan	10.0		1.1×10^{-11}	1.50	[159]

[a] = PMMA = Poly (methyl methacrylate)

[b] = DMSO = Dimethylsulphoxide

[c] = DMF = Dimethylformamide

Table 1.2: Nonlinear Absorption Coefficients for InPc and GaPc Derivatives (see Table 1.1 for abbreviations).

Compound	**Solvent/Polymer**	**Method**	**Linear Absorption Coefficient (cm^{-1})**	**Nonlinear Absorption Coefficient ($cm\ W^{-1}$)**	**Ref.**
1e	$CHCl_3$	Z-scan	1.4	2.37×10^{-7}	[160]
1e	PMMA	Z-scan	265		[160]
1f	$CHCl_3$	Z-scan	1.4	1.93×10^{-7}	[160]
1f	PMMA	Z-scan	286		[160]
2l	$CHCl_3$	Z-scan	1.4	3.89×10^{-7}	[160]
2l	PMMA	Z-scan	115		[160]

Compound	Solvent/Polymer	Method	Linear Absorption Coefficient (cm^{-1})	Nonlinear Absorption Coefficient ($cm\ W^{-1}$)	Ref.
2m	$CHCl_3$	Z-scan	1.4	2.93×10^{-7}	[160]
2m	PMMA	Z-scan	387		[160]

Table 1.3: Linear Transmittance at Focus for InPc and GaPc Derivatives.

Compound	Solvent/Polymer	Method	Concentration (M)	Linear Transmittance at Focus	Ref.
2a	Toluene	Z-scan	8×10^{-5}	0.88	[161]

Compound	Solvent/Polymer	Method	Concentration (M)	Linear Transmittance at Focus	Ref.
2n	Toluene	Z-scan	4.8×10^{-4}	0.86	[161]
2o	Toluene	Z-scan	1.2×10^{-4}	0.86	[161]
2p	Toluene	Z-scan	2.6×10^{-4}	0.72	[161]
3	1-CNP*	Z-scan		0.78	[161]
4	Pyridine	Z-scan	6×10^{-5}	0.88	[161]

* 1-chloronaphthalene.

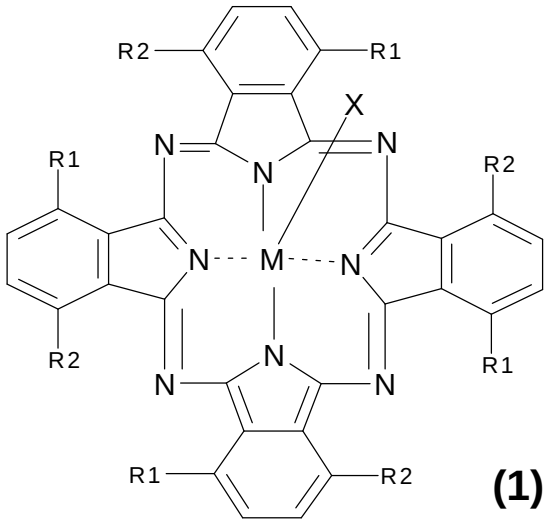

(1)

R1 = R2 = C_6H_5, X =Cl, M = In **(a)**

R1 = R2 = C_6H_5, X =ArF, M = In **(b)**

R1 = H, R2 = 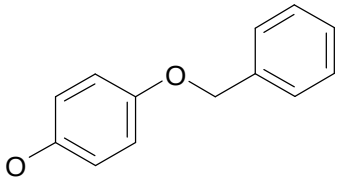 X = Cl, M = Ga **(c)**

R1 = H, R2 = 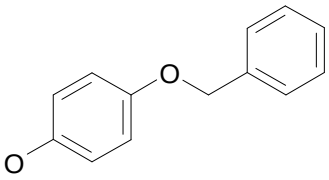 X = Cl, M = In **(d)**

R1 = 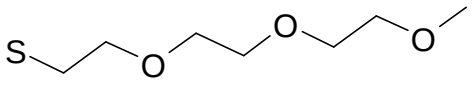 , R2 = H, X = Cl, M = In **(e)**

R1 = 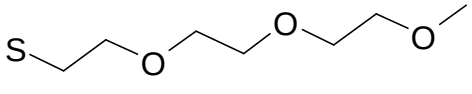 , R2 = H, X = Cl, M = Ga **(f)**

Fig. 1.10: Tetra Substituted InPc Derivatives **1a** – **f**.

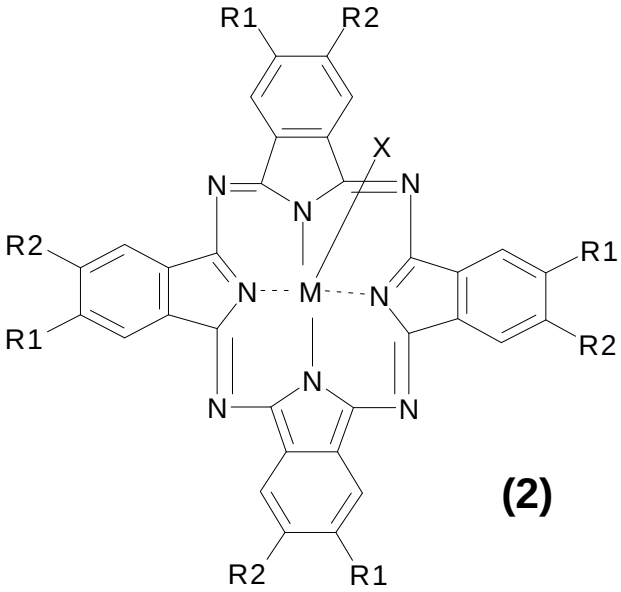

(2)

M = In, X = Cl, R1 = H, R2 = $-C(CH_3)_3$ **(a)**

M = In, X = Br, R1 = H, R2 = 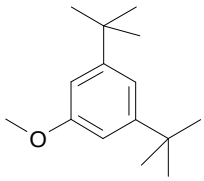 **(b)**

M = In, X = I, R1 = H, R2 = 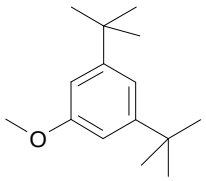 **(c)**

M = In, X = $OCOCF_3$, R1 = R2 = 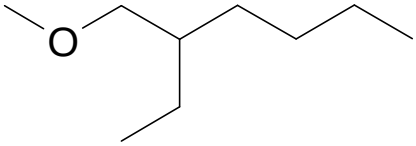 **(d)**

M = In, X = Cl, R1 = R2 = 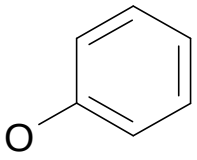 **(e)**

M = In, X = Cl, R1 = R2 = 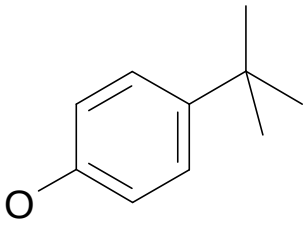 **(f)**

M = In, X = Cl, R1 = R2 = 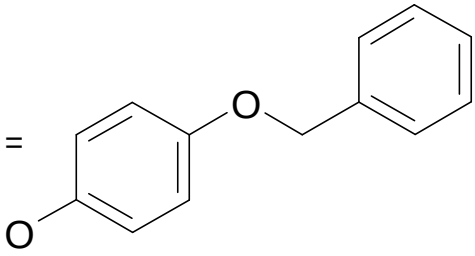 **(g)**

M = Ga, X = Cl, R1 = R2 = 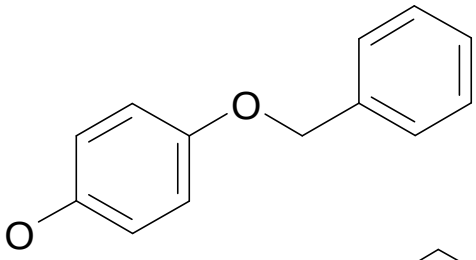 **(h)**

M = Ga, X = Cl, R1 = H, R2 = 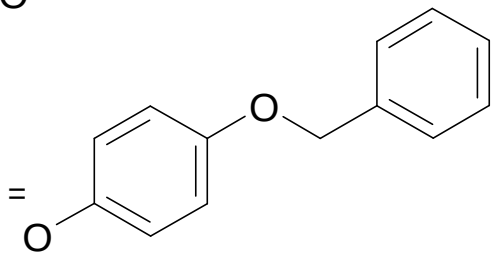 **(i)**

M = In, X = Cl , R1 = H, R2 = 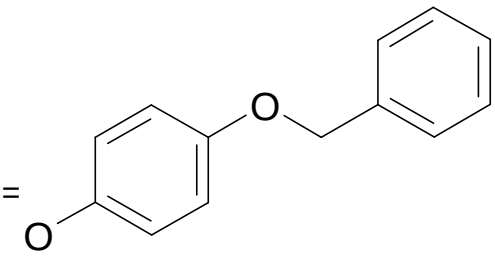 **(j)**

(k)

M = Ga, X = Cl, R1 = H, R2 = -$C(CH_3)_3$

R1 = 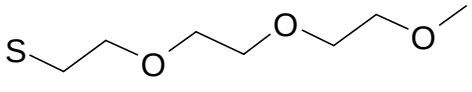

, R2 = H, X = Cl, M = In **(l)**

R1 = 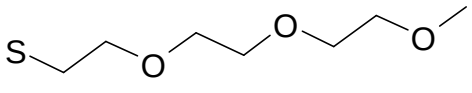

, R2 = H, X = Cl, M = Ga **(m)**

R1 = R2 = 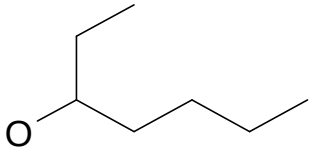

, X = Cl, M = Ga **(n)**

R1 = R2 = 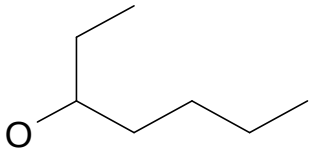

, X = Cl, M = In **(o)**

R1 = R2 = 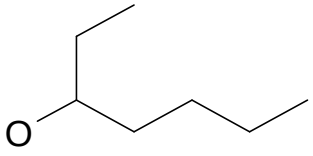

, X = 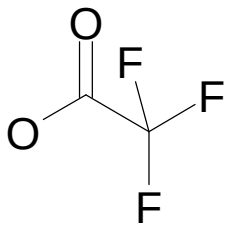

, M = In **(p)**

Fig. 1.11: Octa Substituted InPc Derivatives **2a**-**p**.

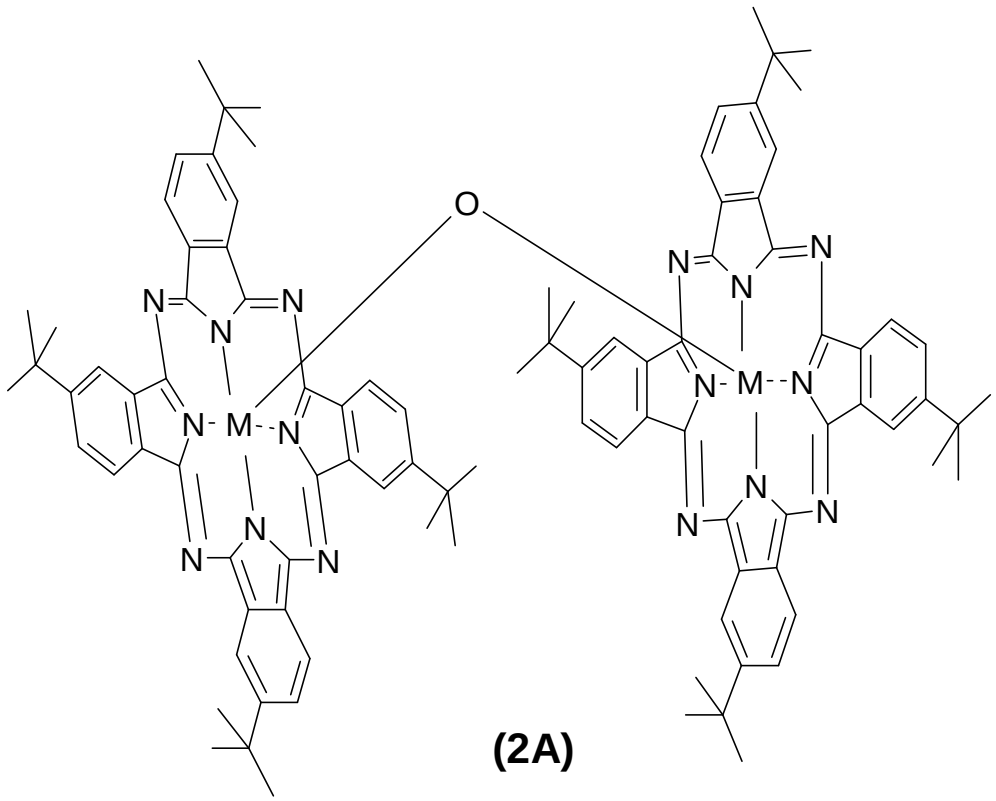

(2A)

M = In, M = In **(i)**

M = Ga, M = Ga **(ii)**

M = In, M = Ga **(iii)**

Fig. 1.12: Oxo-bridged InPc and GaPc derivatives **2A(i)** – **(iii)**.

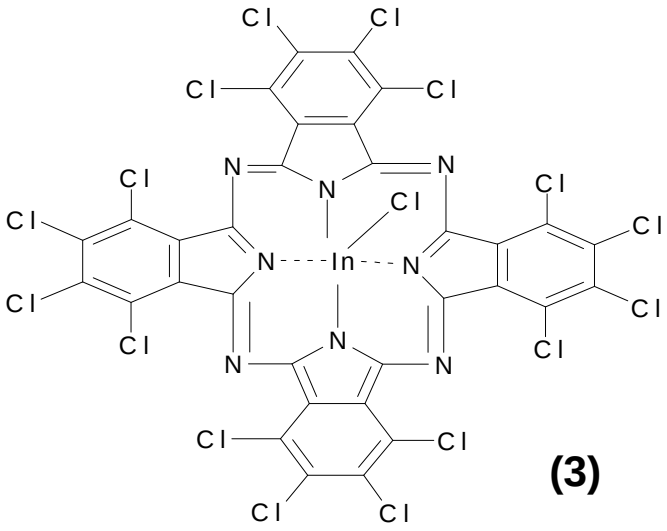

Fig. 1.13: Hexadeca Substituted InPc **3**.

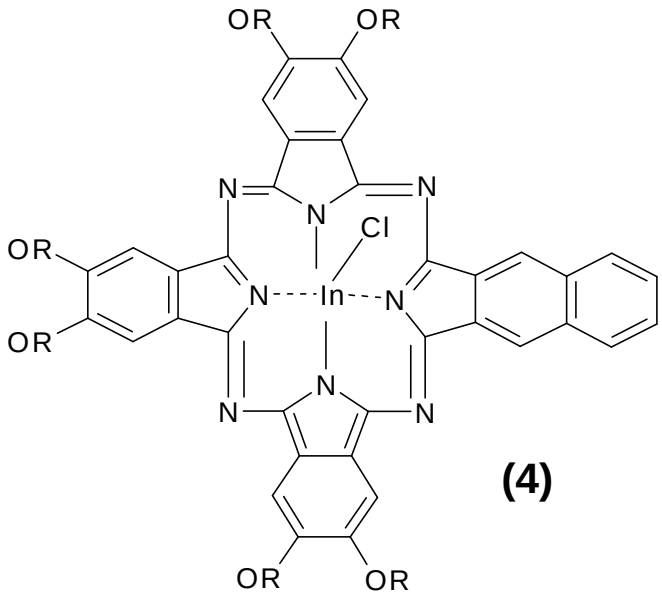

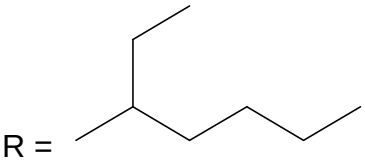

Fig. 1.14: Unsymmetrical InPc derivative **4**.

As can be seen from Tables 1.1 to 1.3, InPc and GaPc derivatives (Figs. 1.10 to 1.14), the parameters which were studied in Table 1.1 include k values, $Im[\chi^{(3)}]$ and γ. Table 1.2 is more focused on nonlinear absorption coefficients or β, and comparisons with a compound's linear absorption coefficient or α. Lastly, Table 1.3 shows the linear transmittance at the laser focal point for certain compounds. This gives a qualitative indication to what extent the transmission of the laser light is limited by the compound. From these tables it can be seen that there is a fair number of $Im[\chi^{(3)}]$ and k values determined, but not so many γ, F_{sat} and I_{lim} values. F_{sat} (saturation fluence) and I_{lim} are fairly closely related to one another, but the I_{lim} should ideally be lower than the F_{sat}. The I_{lim} is the intensity threshold where nonlinear optical behaviour starts to occur in a compound and F_{sat} is the energy at which singlet absorption saturation of the compound is reached. As can be seen, these two parameters are virtually identical to one another and it is important for these values to be low enough to limit the transmitted radiation to a safe level, but not too low as to cause the optical limiter to behave more like a filter. This thesis looks to remedy the lack of certain of the above mentioned values by examining all of them for 13 compounds with indium, gallium or zinc as central metals.

1.5 Aims of the Thesis

Tables 1.1 to 1.3 show that there have been few systematic studies of the effects on nonlinear ability of compounds with different substituents at different attachment positions (α vs β), only benzyloxyphenoxy and substituents **(e)** or **(f)** from Fig. 1.10 has been studied at α and β positions with the same central metal, and different numbers of substituents (tetra- vs octa-). Only the benzyloxyphenoxy is listed in the tables as studied as tetra- and octa-substituted compounds using indium and gallium

central metals. Along with this is the lack of nonlinear studies involving the combination of Pcs with NMs. PMMA is mostly used as the polymer of choice when performing polymer film studies.

Hence this study presents the analysis of nonlinear characteristics of Pcs substituted at the α- and β-positions for a series of substituents (Fig. 1.15) in order to see whether the substituents' positions has any effect on nonlinear properties. In addition to this is the nonlinear differences between octa- and tetra-substituted Pcs, using a wide variety of substituents, were also studied.

Nonlinear absorption studies involving NMs mixed with Pcs in solution and in polymer films are virtually non-existent. It therefore presents an interesting area of study due to the unknown properties that such combinations would possess. As has already been alluded to, any compound in close enough proximity to the conjugated ring system of the phthalocyanine tends to create an enhanced triplet-triplet absorption and QDs are generally made from heavy elements, so it stands to reason that QDs in close proximity to a Pc should enhance the Pc's triplet quantum yield and consequently its photophysical and nonlinear behaviour. And this is the part of the aim of the current work.

Most studies of the NLO of InPcs and GaPcs have been in solution, as Tables 1.1 to 1.3 show, with a few exceptions. Embedding the phthalocyanines within a transparent polymer thin film for OL applications adds some protection to the phthalocyanines against degradation. Also, practical optical limiting devices require the casting of the optically active compounds in the solid state. Poly (methyl methacrylate) (PMMA) has been the preferred polymer for embedding Pcs for OL [157], but poly (methyl acrylic acid) (PMAA) and polyethylamine (PEI) were also

employed in this work. The PMAA and PEI also allow the testing of linking a Pc to a polymer via an amide bond, and what sort of altered nonlinear ability occurs compared to when the Pc and polymer are simply mixed.

Some of this work compares the NLO behaviour of phthalocyanine complexes embedded in PMMA in the presence and absence of nanomaterials. The Pc complexes were chosen for their good solubility due to limited aggregation behaviour in solution as a result of peripheral non-peripheral substitution. The central metals (In, Ga and Zn) were chosen for their size which will enhance intersystem crossing due to the heavy atom effect. Pcs employed in this work are shown in Fig. 1.15 as complexes **5** – **16**. The complexes are isomeric mixtures and hence the determined NLO parameters are going to be an average of all the isomers present. Compounds **9** and **10** are the same as compounds 2h and 2g respectively. CdTe-TGA QDs was used with the Pc complexes, whereas CdSe-TGA QDs, CdS-TGA QDs, single walled carbon nanotubes (SWCNTs) and fullerenes were used with one Pc complex only as an example.

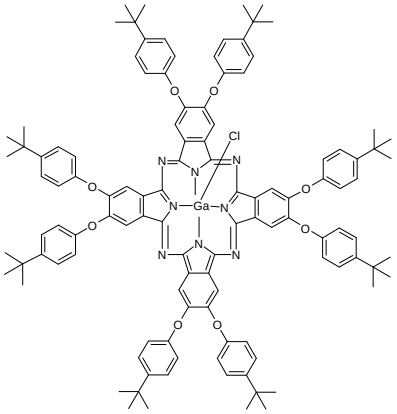

Complex **5**,

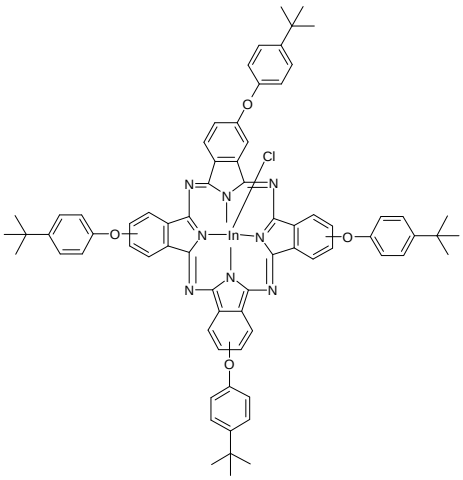

Complex **6**,

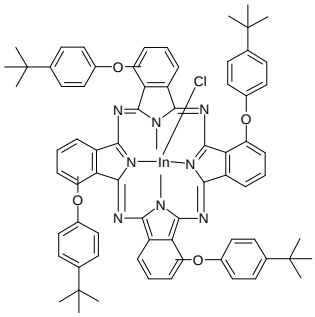

Complex **7**,

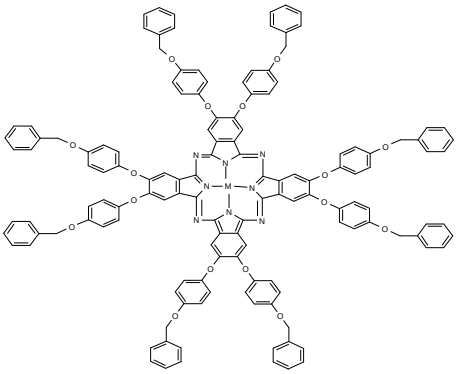

M = Zn (Complex **8**,), GaCl (Complex **9** ,) and InCl (Complex **10**,)

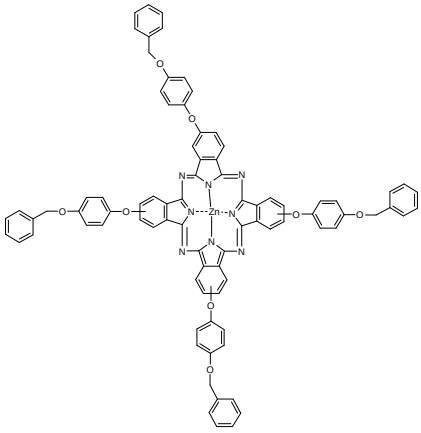

Complex **11**,

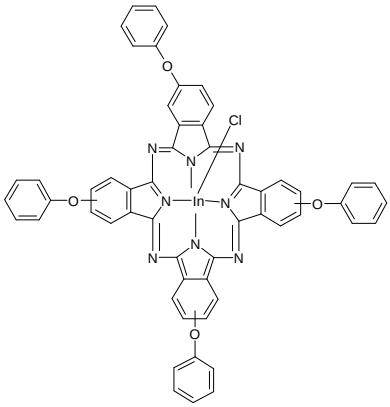

Complex **12**,

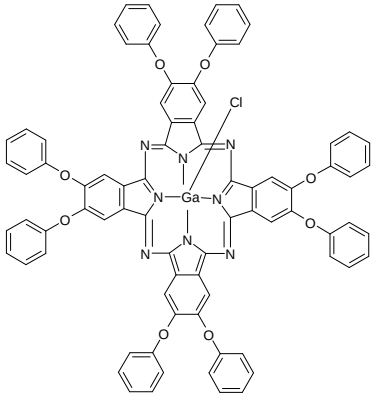

Complex **13**,

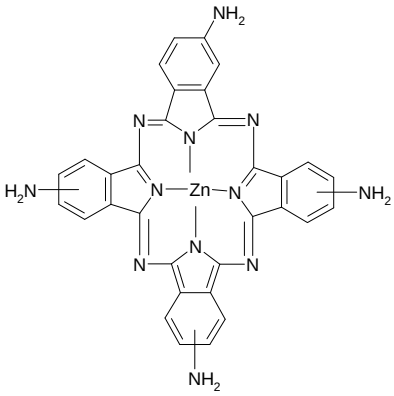

Complex **14**,

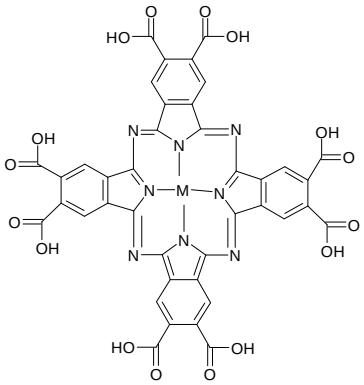

M = Zn (Complex **15**),

AlOH (complex **16**)

Fig. 1.15: Chemical structures of the phthalocyanines studied here.

This work also reports on an In hemiporphyrazine (ClInHp) containing two *tert*-butyl phenoxy substituents (see Fig. 1.16). The two amino groups were designed for future linking to polymers for NLO studies. It was discovered that the formation of an amide link between compound **14** and poly (methyl acrylic acid) caused compound **14** to start behaving like a saturable absorber (SA) instead of undergoing the usual reverse saturable absorption (RSA) observed for Pcs, hence Hps will be studied with this in mind. Hps containing *tert*-butyl phenoxy have been reported [12, 162], and those containing secondary amine groups are also known [13, 163]. This work reports for the first time an Hp containing both a *tert*-butyl phenoxy and primary amine groups.

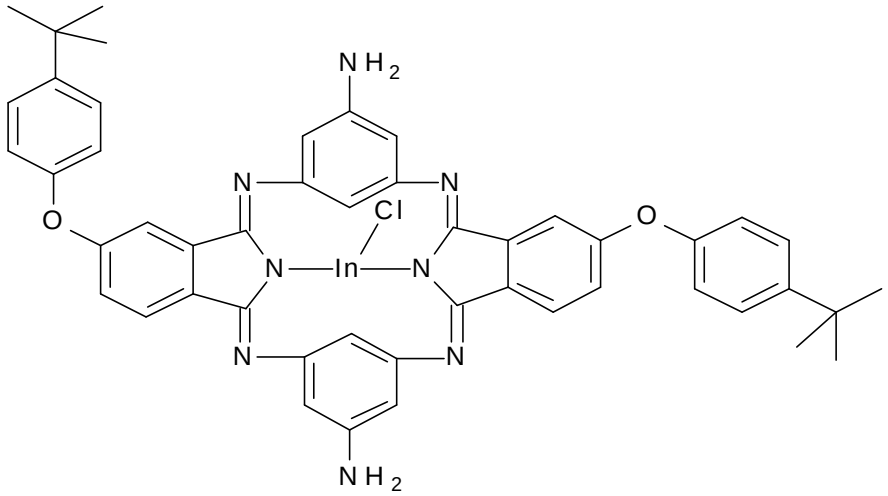

Fig. 1.16: Chemical Structure of ClInHp.

Indium was chosen as a central metal due to its mass, which should enhance intersystem crossing and consequently the triplet quantum yields necessary for improved NLO.

RSA is the process whereby one gets a decrease in the transmitted laser light passing through a compound as the compound approaches the focal point an intense light beam (see Fig. 1.17). The reasoning for this is that the higher intensity allows the compound to undergo two-photon absorption to the B bands, and from here the compound undergoes internal conversion and intersystem crossing to reach the triplet state where the amount of absorption increases since there is usually better triplet absorption than singlet absorption for the compound at the laser wavelength.

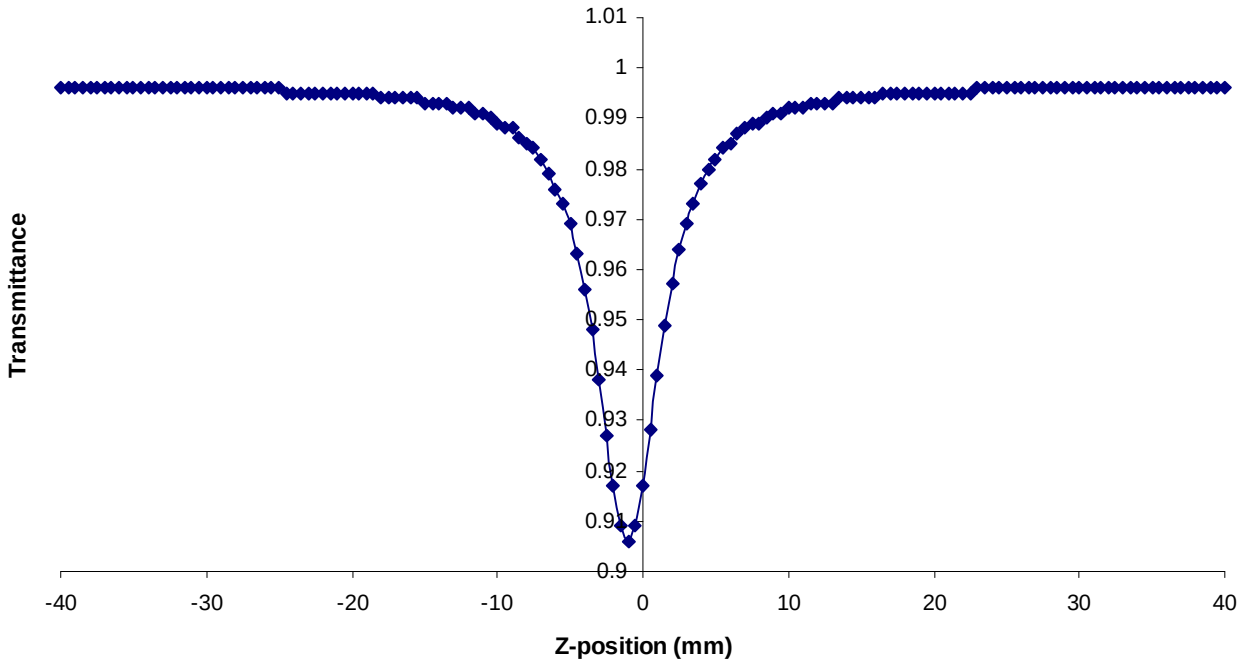

Fig. 1.17: Example Z-scan of compound undergoing RSA [unpublished data].

SA usually occurs when the compound finds itself unable to undergo two-photon absorption to the triplet state. As the compound approaches the focal point of the laser light an increase in transmittance is experienced (see Fig. 1.18). The reasoning behind this is said to be that since so many of the compound's electrons end up in the excited singlet state around the triplet point that there aren't any left in the ground state to absorb the now rather intense laser light. This causes the compound to "become more transparent" and allowing more light through than it usually would.

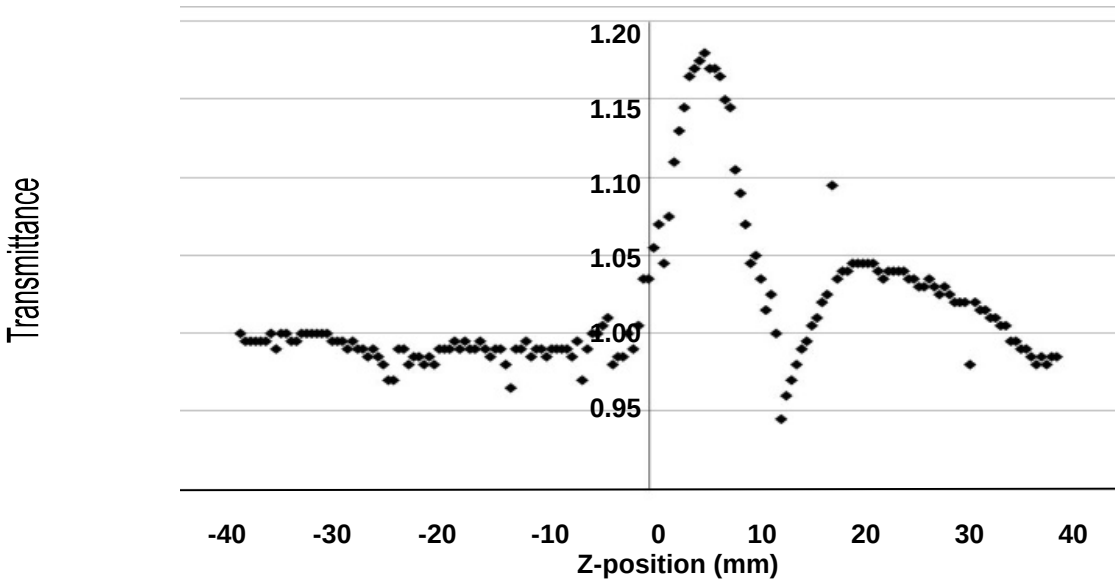

Fig. 1.18: Example Z-scan of compound (ZnPc) undergoing SA [unpublished data].

To summarize objectives:

- To study the nonlinear behaviour of the MPcs (**5** – **16**) in the presence and absence of NMs.
- To synthesize, characterize and test the nonlinear behaviour of InHp.
- To study the effect on the nonlinear behaviour of embedding MPcs and NMs in polymer film.
- To test the effect on nonlinear properties of Pcs linked to polymers.

Chapter 2

Synthesis and Methodologies

2. Experimental

2.1. Materials

The syntheses of phthalocyanine complexes (**5** to **16**) used in this work (see Figure 1.15) have been reported before [155, 157, 164 -169]. The general synthesis involved the reaction of a phthalonitrile with the desired substituent with the desired metal salt in solution. The solution was heated to reflux to achieve cyclisation.

2.1.1 Solvents

Dimethylsulfoxide (DMSO), dichloromethane (DCM) and N,N'-dimethylformamide (DMF) were obtained from Saarchem and dried over molecular sieves before use. Methanol (MeOH), ethanol (EtOH) and tetrahydrofuran (THF) were obtained from Sigma-Aldrich. Triply deionised water was employed for aqueous solutions.

2.1.2 Synthesis Reagents

N-hydroxysuccinimide (NHS) was obtained from Fluka. HCl and cadmium chloride were purchased from Merck. Thioglycolic acid (TGA), tellurium powder, selenium powder and N-(3-dimethylaminopropyl)-N'-ethylcarbodiimide hydrochloride (EDC) 3, 5-dinitroaniline, 4-nitrophthalonitrile, 4-tert-butyl-penol, palladium on activated carbon, celite, potassium carbonate, sodium methoxide, ammonia gas and indium chloride were obtained from Sigma-Aldrich. Sodium borohydride, sulphuric acid and sodium hydroxide (NaOH) pellets were obtained from Saarchem. 1, 3, 5-triaminobenzene was synthesized according to literature reports [170].

2.1.3 Polymers and Nanomaterials

Poly (methyl methacrylate) (PMMA, average molecular weight: ~120000 g/mol), poly (methyl acrylic acid) (PMAA oligomer, average molecular weights: ~670 g/mol, ~900 g/mol and ~1100g/mol), polyethylenimine (branched PEI, average molecular weight: ~10000 (determined by gel permeation chromatography) – 25000(determined by light scattering)), single walled carbon nanotubes (SWCNT) (diameter = ~1.5 nm; Length = 1 – 5 μm) and fullerenes were obtained from Sigma-Aldrich.

2.2. Equipment

- ^{1}H Nuclear Magnetic Resonance (^{1}H NMR) spectra were obtained on a Bruker AMX 400MHz spectrometer.
- X-ray powder diffraction patterns were recorded on a Bruker D8, Discover equipped with a proportional counter, using Cu-Kα radiation (λ = 1.5405 Å, nickel filter). Data were collected in the range from 2θ = 5º to 60º, scanning at 1º min^{-1} with a filter time-constant of 2.5 s per step and a slit width of 6.0 mm. Samples were placed on a silicon wafer slide. The X-ray diffraction data were treated using the Eva (evaluation curve fitting) software. Baseline correction was performed on each diffraction pattern by subtracting a spline function fitted to the curved background and the full-width at half-maximum values used in this study were obtained from the fitted curves.
- Infrared spectra were recorded using the Bruker Vertex 70, using potassium bromide discs formed with the samples imbedded within them, whilst the

Raman spectra were obtained using a Bruker RAM III, using compacted sample mixed with KBr to form a small disc.

- A convenient and fast experimental method to assess materials for NLO (including optical limiting) is the open aperture Z-scan experiment (see Fig. 2.1). This measures the total transmittance through the sample as a function of incident laser intensity while the sample is gradually moved through the focus of a lens (along the z-axis). The Z-scan equipment employed in this work was fabricated at the University of Stellenbosch in South Africa. All experiments described in this study were performed using a tunable laser system consisting of a Q-switch pump laser (355 nm, 135 mJ/4-6 ns, repetition rate = 20 Hz) pumping an optical parametric oscillator (OPO,30 mJ/3-5 ns) with a wavelength range of 420 - 2300 nm (NT-342B, Ekspla).

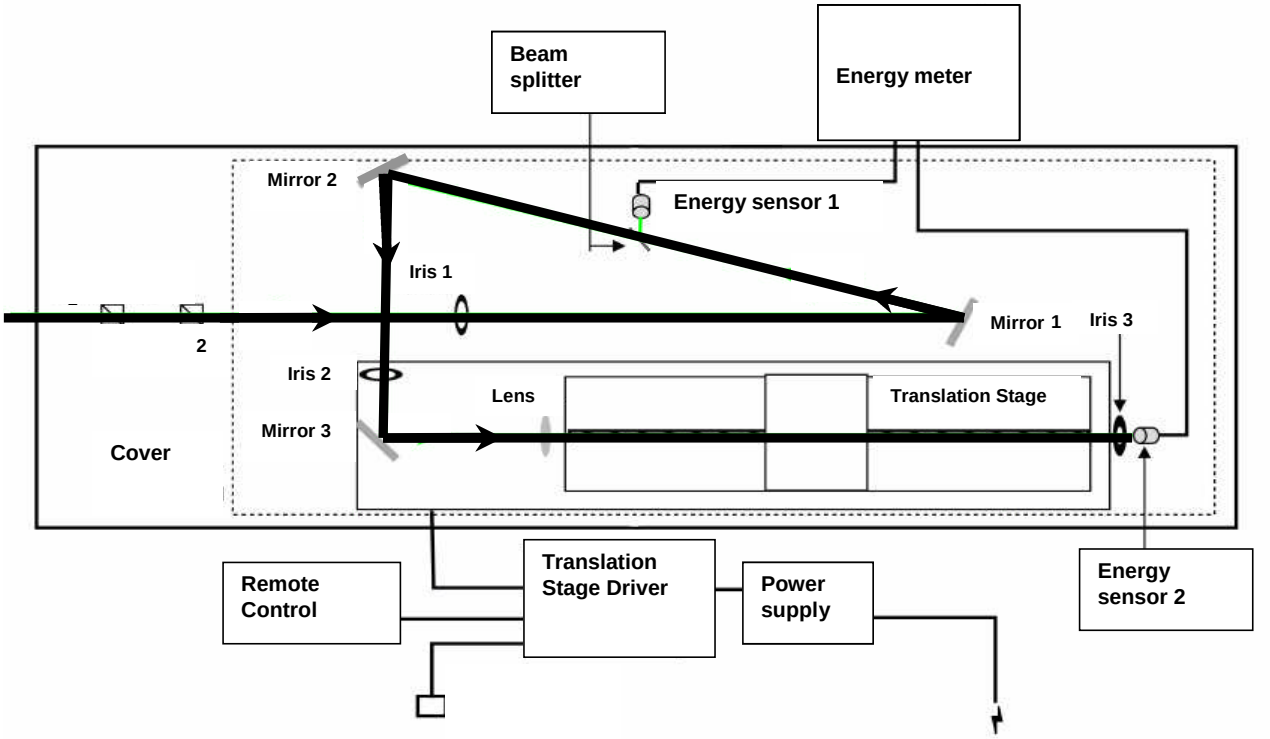

Fig. 2.1: Schematic diagram of Z-scan setup.

- Triplet quantum yields for solutions were determined by recording the triplet absorption and decay kinetics using the same laser system as the z-scan with a Thermo Oriel xenon arc lamp, a photomultiplier tube as a detector and a 3032C Tektronix 300MHz two-channel digital real-time oscilloscope (Fig. 2.2). Triplet lifetimes were determined using OriginPro 7.5 software. The Pcs and NMs embedded in the polymer films were placed in the sample cell holder at an angle so as to have the laser light and xenon lamp light both striking it. This setup was used to determine the triplet lifetimes of the embedded polymer films, with their triplet quantum yields being determined using their nonlinear absorption coefficient (β).

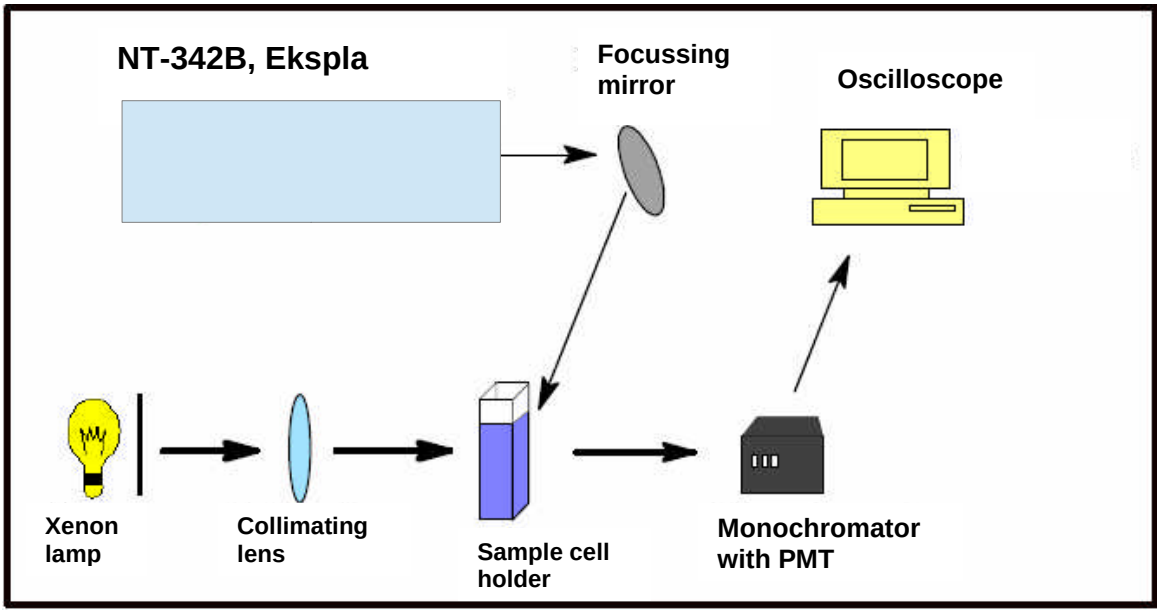

Fig. 2.2: Schematic Diagram of Laser Flash Photolysis Setup.

- UV-visible spectra were recorded on a Shimadzu UV-2550 spectrophotometer.

- Mass spectrometer used was a Bruker MALDI-TOF/TOF Mass Spectrometer (Autoflex III), with the compound placed in a α-cyano-4-hydroxycinnamic acid matrix with sodium trifluoroacetate included in the mixture.
- Fluorescence measurements were taken on a Varian Eclipse spectrofluorimeter.
- Thermal gravimetric analysis (TGA) was carried out using a Shimadzu Simultaneous Thermogravimetry/Differential Thermal Analyser, Model DTG-60H at a heating rate of 10 °C min^{-1} in a high-purity nitrogen atmosphere.
- For photodegradation studies, the polymers were irradiated at room temperature and in air using a General Electric Quartz lamp (300W, 120 V). The white light from the lamp was used with only water filtering the infrared radiation from it (see Fig. 2.3). Light intensities were measured with a POWER MAX5100 (Molelectron detector incorporated) power meter and were found to be 3.657 x 10^{15} photons s^{-1} cm^{-2}**.**

The thin films of phthalocyanine alone or Pc mixed with polymer were mounted at about 3 cm in front of the light for photodegradation studies. This allowed the thin film of Pc/polymer or phthalocyanine alone to be exposed to the full electromagnetic spectrum generated by the lamp, as well as causing an increase in heat to the analysed substances. This setup should therefore cause thermal and light stresses upon the thin film of Pc/polymer or phthalocyanine alone as thin films, allowing us to examine the protection the polymer offers to the phthalocyanine within it compared to the same phthalocyanine alone on a glass side.

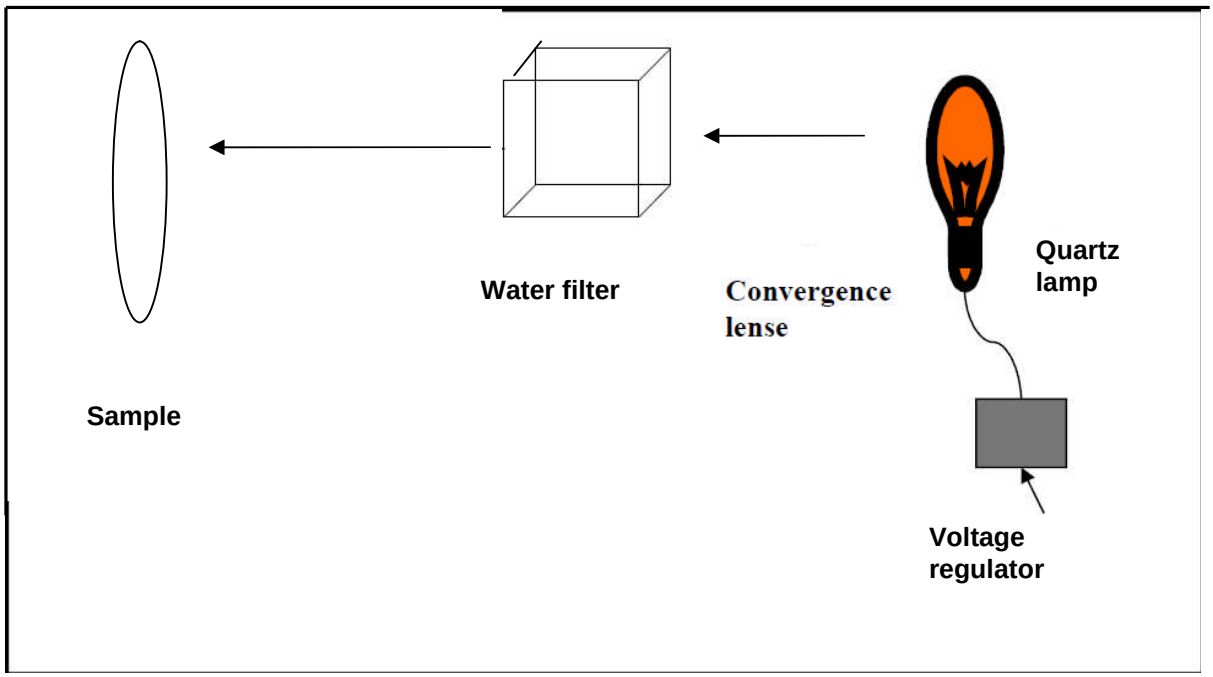

Fig. 2.3: Photodegradation setup.

2.3 Synthesis

2.3.1 Hemiporphyrazines

*2.3.1.1 Synthesis of 4-tert-butyl-phenoxyisoindoline (**19**), Scheme 3.1*

4-Nitrophthalonitrile, (**17**), (0.50 g, 2.89 mmol) and 4-tert-butyl-phenol, (**18**), (0.43 g, 2.89 mmol) were stirred overnight in DMSO in the presence of excess potassium carbonate. The resulting compound was purified over silica column using DMSO as an eluent; the solvent removed and then the compound was rinsed with water to remove any remaining potassium carbonate and allowed to dry. The compound (0.56 g, 2.02 mmol) was then placed in methanol, along with sodium methoxide (0.11 g, 2.02 mmol) and ammonia gas was bubbled through the solution under stirring at room temperature for six hours until the solution took on a pale green colour. After removing the solvent, the residue was dissolved in toluene and washed several times with water.

Yield 0.47 g (80%) ^{1}H NMR (THF-d_8): δ = 8.62 (3H, s, NH), 7.99 (2H, d, Ar-H), 7.33 (2H, d, Ar-H), 7.14 (1H, s, Ar-H), 7.06 (1H, d, Ar-H), 6.80 (1H, d, Ar-H). IR spectrum: 2949 cm^{-1} (=C-H stretch), 1598 cm^{-1} (C=C aromatic), 1533 cm^{-1} (C=C aromatic), 1506 cm^{-1} (C=C aromatic), 1435 cm^{-1} (CH_3 bending), 1269 cm^{-1} (C-O-C stretch), 1229 cm^{-1} (C-O-C stretch), 1144 cm^{-1} (C-O-C stretch), 1053 cm^{-1} (C-O-C stretch).

2.3.1.2 Synthesis of indium hemiporphyrazine (ClInHp), Scheme 3.1

ClInHp was synthesized by combining 4-tert-butyl-phenoxyisoindoline, (**19**), (0.18 g, 0.63 mmol), $InCl_3$ (0.14 g, 0.63 mmol) and 1, 3, 5-triaminobenzene, (**20**), (0.077 g, 0.63 mmol) in methanol and stirring under reflux overnight. The product was then

purified using silica column and THF, followed by THF:water 40:60 mixture and finally EtOH as eluents, so as to separate all the components. The final product in EtOH fraction was the compound of interest.

ClInHp: Yield: 0.16 g, 28 %. Uv-Vis (DMF): λ_{max} nm (log ε) 392.5 (3.29), 424.5 (3.18), 454 (2.99). IR spectrum: 3321 cm^{-1} (N-H stretch), 1711 cm^{-1} (C=N groups), 1645 cm^{-1} (N-H bending), 1357 cm^{-1} (C-N aryl stretch), 1313 cm^{-1} (C-N aryl stretch), 1222 cm^{-1} (aromatic ether), 1020 cm^{-1} (aliphatic amine). Mass Spectrum Calculated: 912.2 amu. Found: 913.1 amu $[M+1]^+$.

2.3.2 Synthesis of CdTe, CdSe and CdS QDs capped with thioglycolic acid (TGA)

The preparation of CdTe-TGA capped QD was performed via a modified method adopted from literature [171, 172] (Fig. 2.4). The formation of the CdSe-TGA and CdS-TGA QDs was done using other modified methods adopted from literature [173, 174]. Briefly, 2.35 mmol of $CdCl_2.H_2O$ was dissolved in 125 ml of water and 5.7 mmol of the TGA stabilizer was added under stirring. The solution was adjusted to pH 11 by the dropwise addition of NaOH. Nitrogen gas was bubbled through the solution for about 1 hour, and this aqueous solution subsequently reacted with H_2Te, H_2Se or H_2S gas. The H_2Te and H_2Se gases were generated by the reaction of $NaBH_4$ with Te or Se powder in the presence of 0.5 M H_2SO_4 under a flow of nitrogen gas, whilst H_2S gas was purchased already. The solution was then refluxed under air at 100^oC for different times to control the size of the QDs. On cooling, the QDs were precipitated out of the solution using excess ethanol, and the solutions were then centrifuged to harvest the QDs.

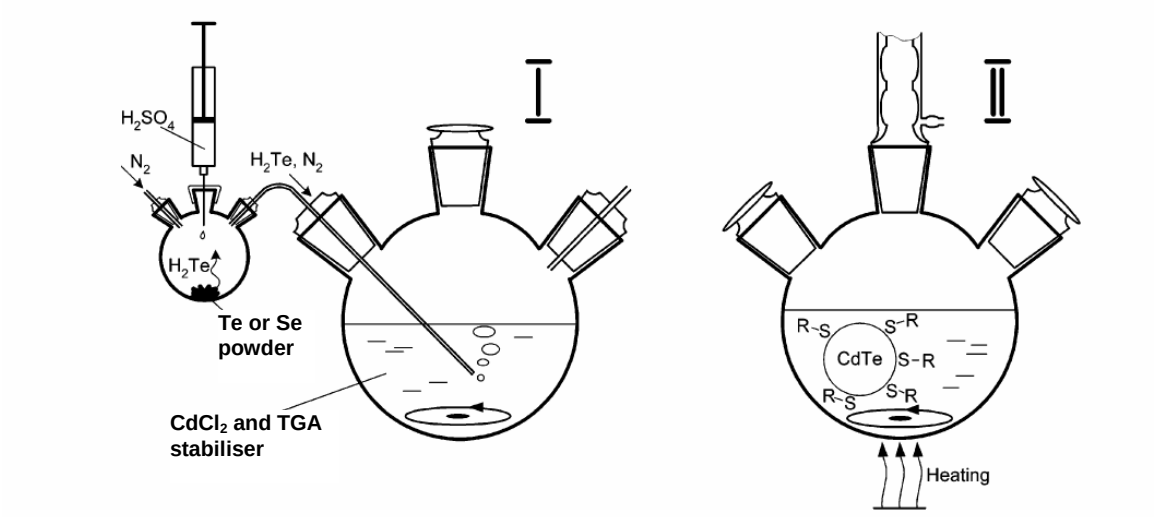

Fig. 2.4: Setup for synthesis of water-soluble CdTe-TGA, CdSe-TGA and CdS-TGA Quantum Dots [47].

2.3.3 Preparation of the Phthalocyanine/Nano-Material Films

Fabrication of the solid state films of investigated phthalocyanines and nano-material (NM) was done using a Pc/NM/polymer solution in DMF:water 9:1 or DMF:toluene (solubility was obtained for SWCNT-COOH after some sonication). The DMF:toluene mixture was used for the phthalocyanine/fullerene film because fullerenes are soluble in toluene. The 9:1 mixture was used to establish a 9:1 molar ratio between the phthalocyanine and NM because the phthalocyanines and nanomaterials were initially in separate solutions of near identical concentration before mixing. The thin films of Pc alone, NM alone or Pc/NM in polymer were formed by a drop-dry method of placing the solution on a glass slide, followed by the evaporation of the solvent. The polymer solution in which the phthalocyanines were dissolved in was 15% by weight. The structures of the polymers employed are shown in Fig. 2.5.

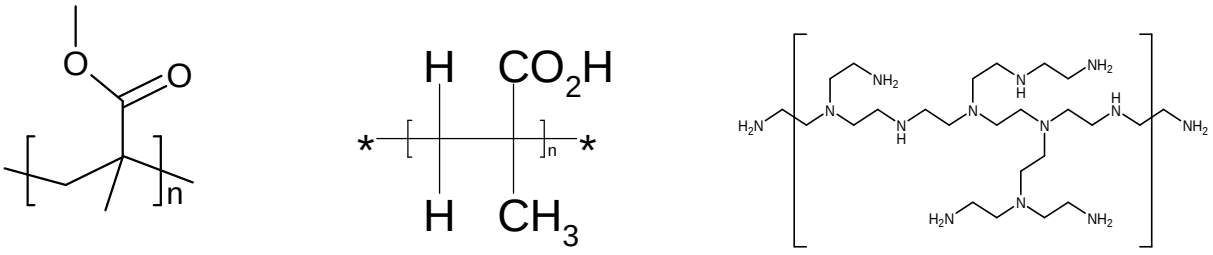

PMMA **PMAA** **PEI**

Fig. 2.5: Chemical structures of the studied polymers.

2.3.4 Linking of Pcs to polymers.

Amide linkages were formed between complex **14** (zinc tetraamino phthalocyanine, $ZnPc(NH_2)_4$) and PMAA, as well as complexes **15** and **16** (metallo octacarboxyphthalocyanines, $Pc(COOH)_8$, M = Zn, Al) and PEI. The MOCPcs complexes **15** and **16** Pcs (~1.05×10^{-4} mol) were first dissolved in a DMF:water mixture (2:1) (4 mL), then EDC (5 mM) and NHS (2 mM) were added to convert the carboxylic group (–COOH) of the MPcs into an active carbodiimide ester group. The mixture was left to stir at room temperature under a nitrogen atmosphere for 1 h. After this time, 1 g (0.04 – 0.1 mmol) of PEI was added to the activated Pc and the mixture stirred for 1 h to allow the conjugation of the Pc to the PEI to take place. For the conjugation of PMAA to complex **14** ($ZnPc(NH_2)_4$), the carboxylic group (–COOH) of the PMAA was first activated by stirring a mixture of the PMAA with EDC (5 mM) and NHS (2 mM) in DMF:water for 1 h, followed by addition of $ZnPc(NH_2)_4$ and further stirring for 1 h. The linked Pc-polymers were separated from the unlinked polymer and phthalocyanines by size exclusion chromatography using Biobeads and DMF as the eluant.

The linked complex was then formed into a thin film for analysis, along with the thin film of a mixture of these two compounds without a chemical bond. The molar ratio of PEI or PMAA to Pc was kept the same for the linked and mixed complexes. However the ratio of polymer to Pc in the linked and mixed complexes will differ in the final product due the activation and purification steps in the former.

Chapter 3

Characterisation Results

The results presented in this thesis have been published in journals listed below:

1. J. Britton, C. Litwinski, T. Nyokong, Optical limiting behaviour of ring substituted zinc, indium and gallium phthalocyanines in the presence of quantum dots, *J. Porphyr. Phthalocya.*, 15 (2011) 1239.

2. J. Britton, C. Litwinski, E. Antums, M. Durmuş, V. Chauke, T. Nyokong, Optical limiting analysis of phthalocyanines in polymer thin films, *J. Macromol. Sci. A.*, 50(1) (2013) 110.

3. J. Britton, M Durmuş, S. Khene, V. Chauke, T. Nyokong, Third order nonlinear optical properties of phthalocyanines in the presence of nanomaterials and in polymer thin films, *J. Porphyr. Phthalocya. (Special issue Lukyanets)*, in Press

4. J. Britton, M. Durmuş, V. Chauke, T. Nyokong, Polymethyl acrylate films containing metallo phthalocyanines in the presence of CdTe quantum dots: nonlinear optical behaviour and triplet state lifetimes, *Polyhedron*, Submitted 14-05-2013

5. J. Britton, E. Antunes, T. Nyokong, Synthesis and nonlinear optical examination of 3(4),15(16)-Bis-(4-*tert*-butyl-phenoxy)-10,20-diaminohemiporphyrazinato chloroindium, *J. Mol. Struct.*, in Press

3. Synthesis and Characterization

3.1 Phthalocyanines in the absence of QDs

The synthesis of Pc complexes **5** – **16** have been reported before [155, 157, 164 – 169]. Their spectra are discussed here for comparative purposes.

Figure 3.1 shows the UV-Vis spectra of the diverse selection of phthalocyanines being employed in this work, with Q-band absorptions ranging from about 671 nm to 715 nm in DMSO or DMSO:water (9:1), Table 3.1. The DMSO:water (9:1) solvent mixture was employed because examination of Pcs mixed with CdTe QDs are done in this solvent mixture in order to incorporate these two compounds in solution, hence the spectra of the Pc complexes also needed to be recorded in this solvent mixture as shown in Table 3.1. In general, there is not much change in the spectra on going from DMSO alone to DMSO:water in Table 3.1. In DMSO only complexes **8**, **10** and **14** show broadening between 600 and 650 nm region due to the presence of aggregates, Fig. 3.1. Complex **8** in particular shows a large peak due to the aggregates, monomerization of **8** could be achieved by addition of a surfactant (Tritox X 100). Aggregation in phthalocyanines is characterized by splitting or broadening of the Q band, with a blue shifted absorption band being due to the H aggregates. Aggregation in Pcs is dependent on the concentration, nature of the solvent, peripheral substituents, complexed metal ions and temperature [11]. The rest of the complexes were monomeric with a typical sharp Q band in DMSO. Phthalocyanine aggregates do have optical limiting ability, however aggregation reduces triplet state quantum yields.

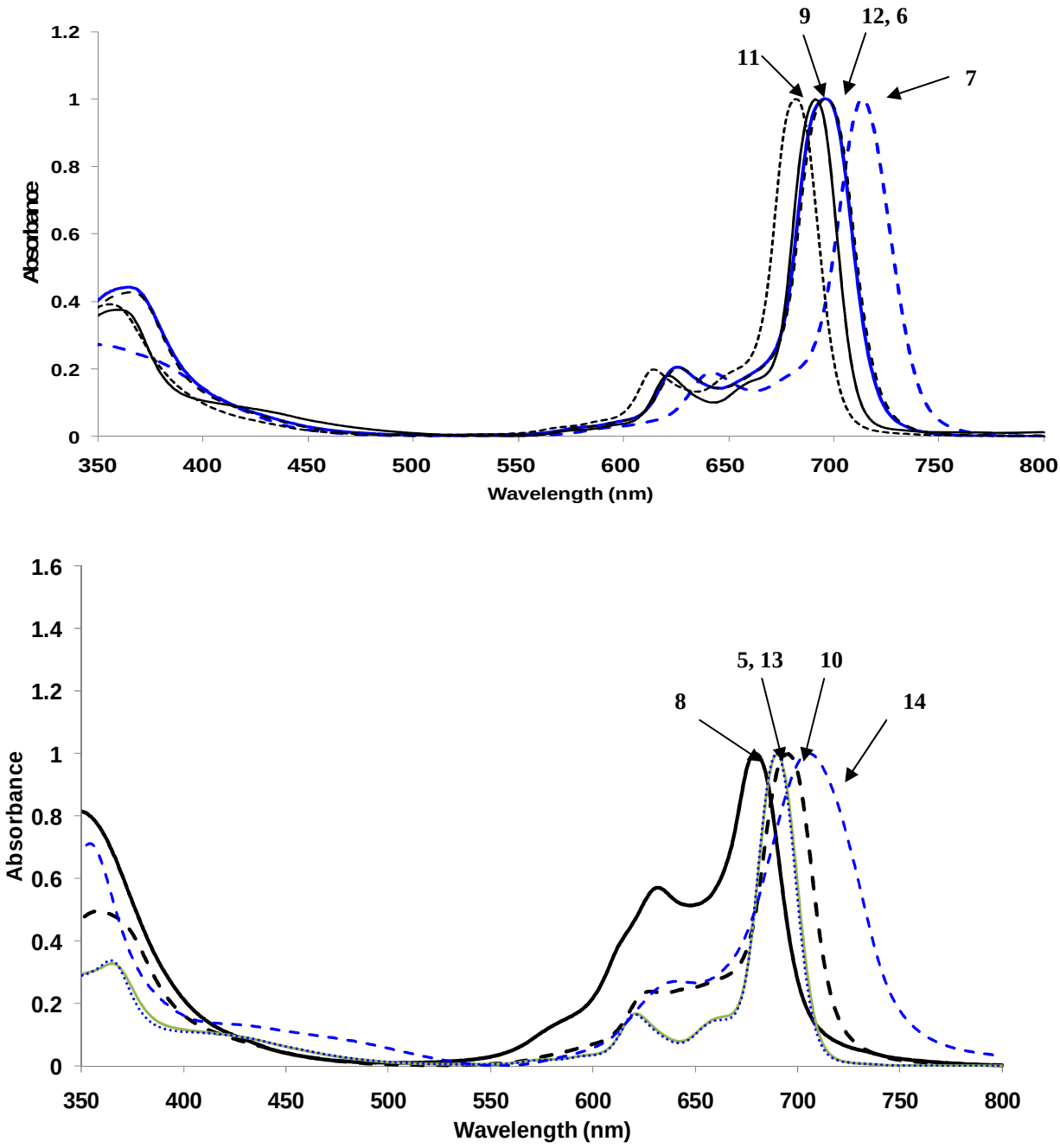

Fig. 3.1: Absorption spectra of examined phthalocyanines in DMSO. Concentration range: 2.68 x 10^{-6} to 1.75 x 10^{-5} M.

Table 3.1: Absorption spectral data for the studied phthalocyanine complexes in various solvents as indicated. The ratio of Pc:QDs of 97:1 was employed.

Complex	**Solvent**	**Q_{band}/nm (log ε)**	**FWHM (nm)**
5	DMSO DMSO:water (9:1)	688 (5.31) 688	22
5 + CdTe-TGA	DMSO:water (9:1)	685	-
6	DMSO DMSO:water	692 (5.14) 691	28
6 + CdTe-TGA	DMSO:water (9:1)	690	-
7	DMSO DMSO:water (9:1)	710 (5.20) 710	28
7+CdTe-TGA	DMSO:water (9:1)	709	-
8	DMSO DMSO:water (9:1)	676[a] (5.18) 672	69
8 + CdTe-TGA	DMSO:water (9:1)	671	-
9	DMSO DMSO:water (9:1)	688 (5.43) 688	23
9 + CdTe-TGA	DMSO:water (9:1)	684	-
10	DMSO DMSO:water (9:1)	692 (5.43) 688	29
10 + CdTe-TGA	DMSO:water (9:1)	688	-
11	DMSO	680 (5.23)	22

	DMSO:water (9:1)	680	
11 + CdTe-TGA	DMSO:water (9:1)	678	-
12	DMSO DMSO:water (9:1)	691 (5.29) 689	28
12 + CdTe-TGA	DMSO:water (9:1)	689	-
13	DMSO DMSO:water (9:1)	692 (5.10) 687	22
13 + CdTe-TGA	DMSO:water (9:1)	687	-
14	DMSO DMSO:water (9:1)	715 (4.83) 715	53
14 + CdTe-TGA	DMSO:water (9:1)	715	-

[a]the Q band of the monomer peak only has been provided

In DMSO:water, complexes **5**-**14** have a reasonably low amount of absorbance at the 532 nm region, Fig. 3.1, which is a region of interest in the OL studies in this work. Comparing the spectra in DMSO:water with that in DMSO alone (Fig. 3.2) shows that the is no change in the monomeric nature for complexes **5**, **6**, **7**,**11**, **12** and **14**, these complexes remain monomeric. For complexes **8**, **9** and **10**, aggregation is evident in the presence of water, while for **13** only a small increase in intensity observed between 600 and 650 nm in DMSO:water solvent mixture (Fig. 3.2). Aggregation in complex **8** intensified as judged by the enhancement of the blue shifted band at 630 nm.

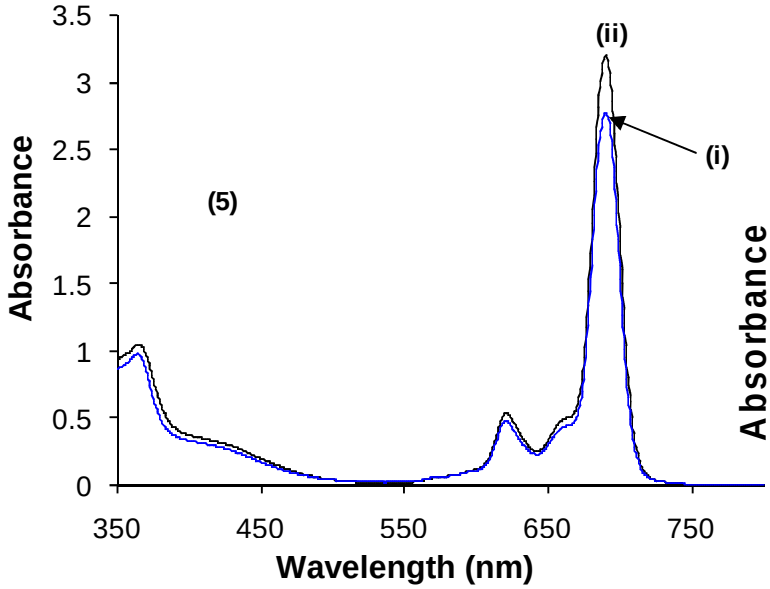
Absorbance
Wavelength (nm)
(5)
(i)
(ii)

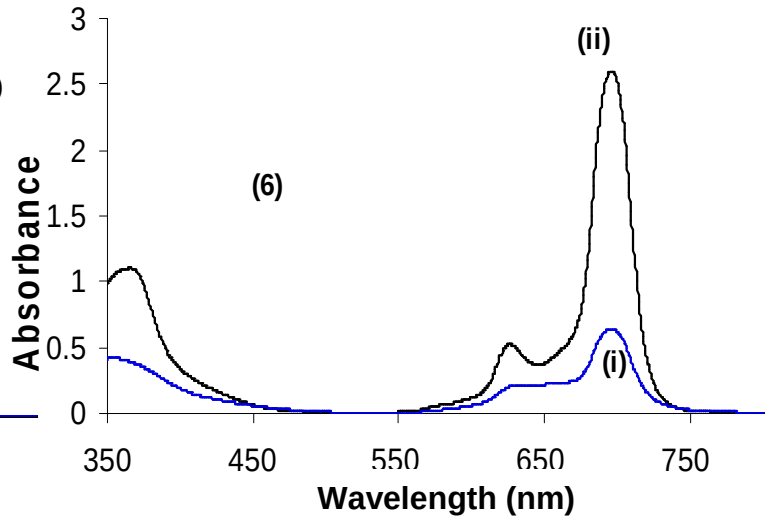
Absorbance
Wavelength (nm)
(6)
(i)
(ii)

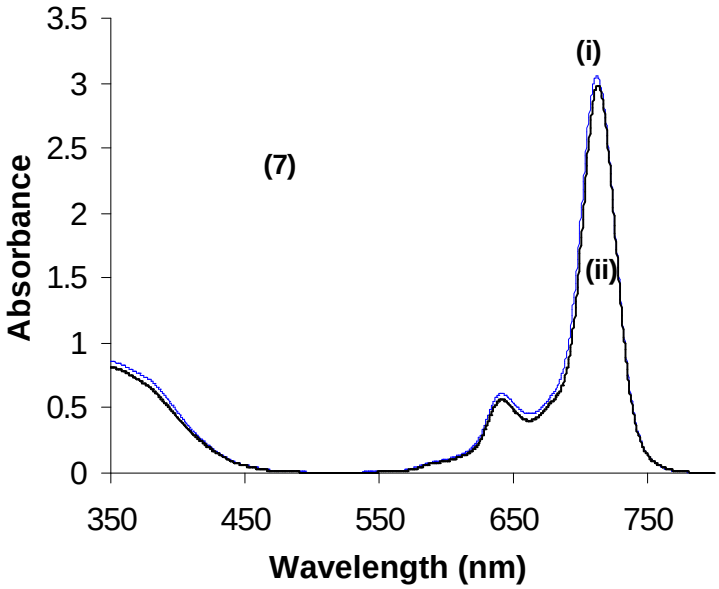
Absorbance
Wavelength (nm)
(7)
(i)
(ii)

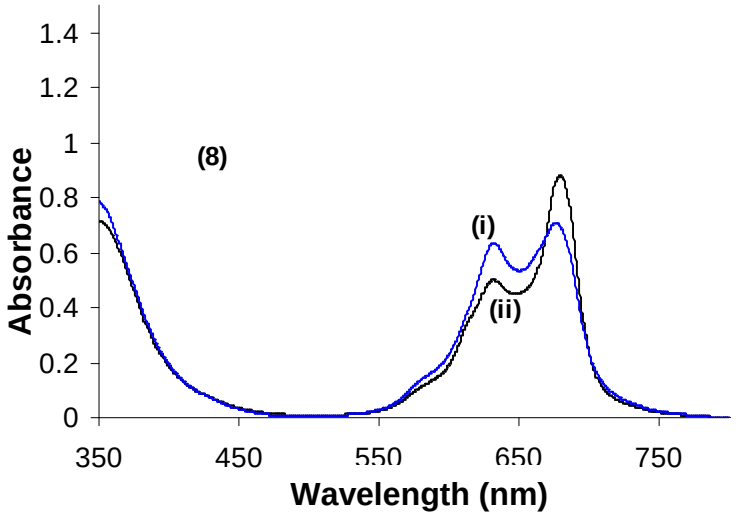
Absorbance
Wavelength (nm)
(8)
(i)
(ii)

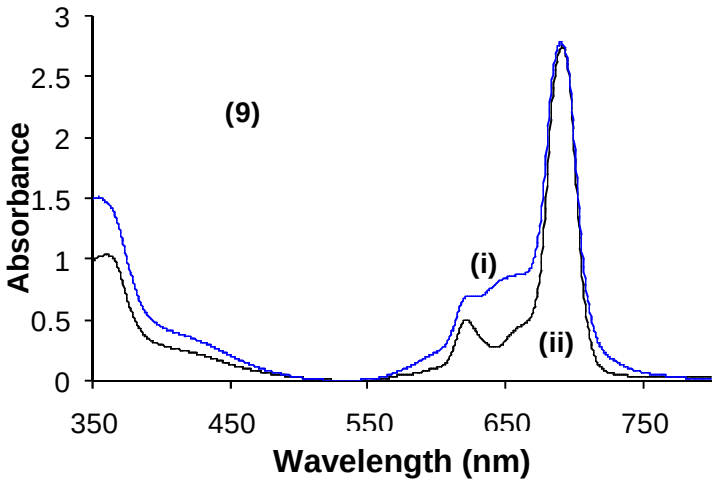
Absorbance
Wavelength (nm)
(9)
(i)
(ii)

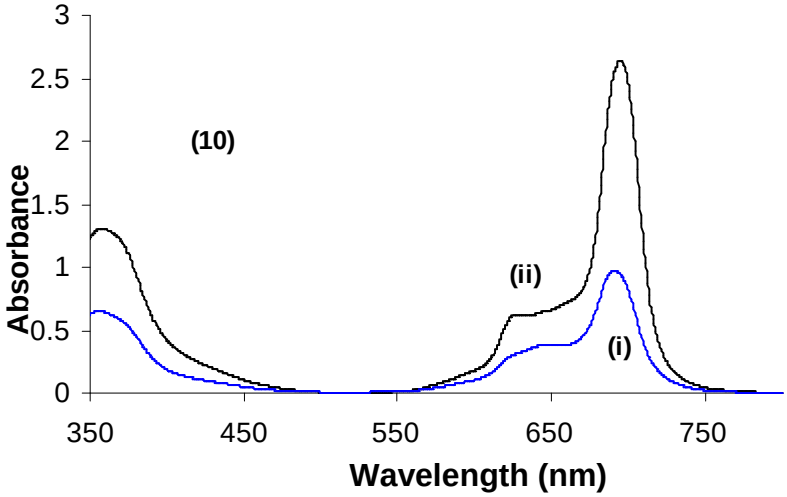
Absorbance
Wavelength (nm)
(10)
(i)
(ii)

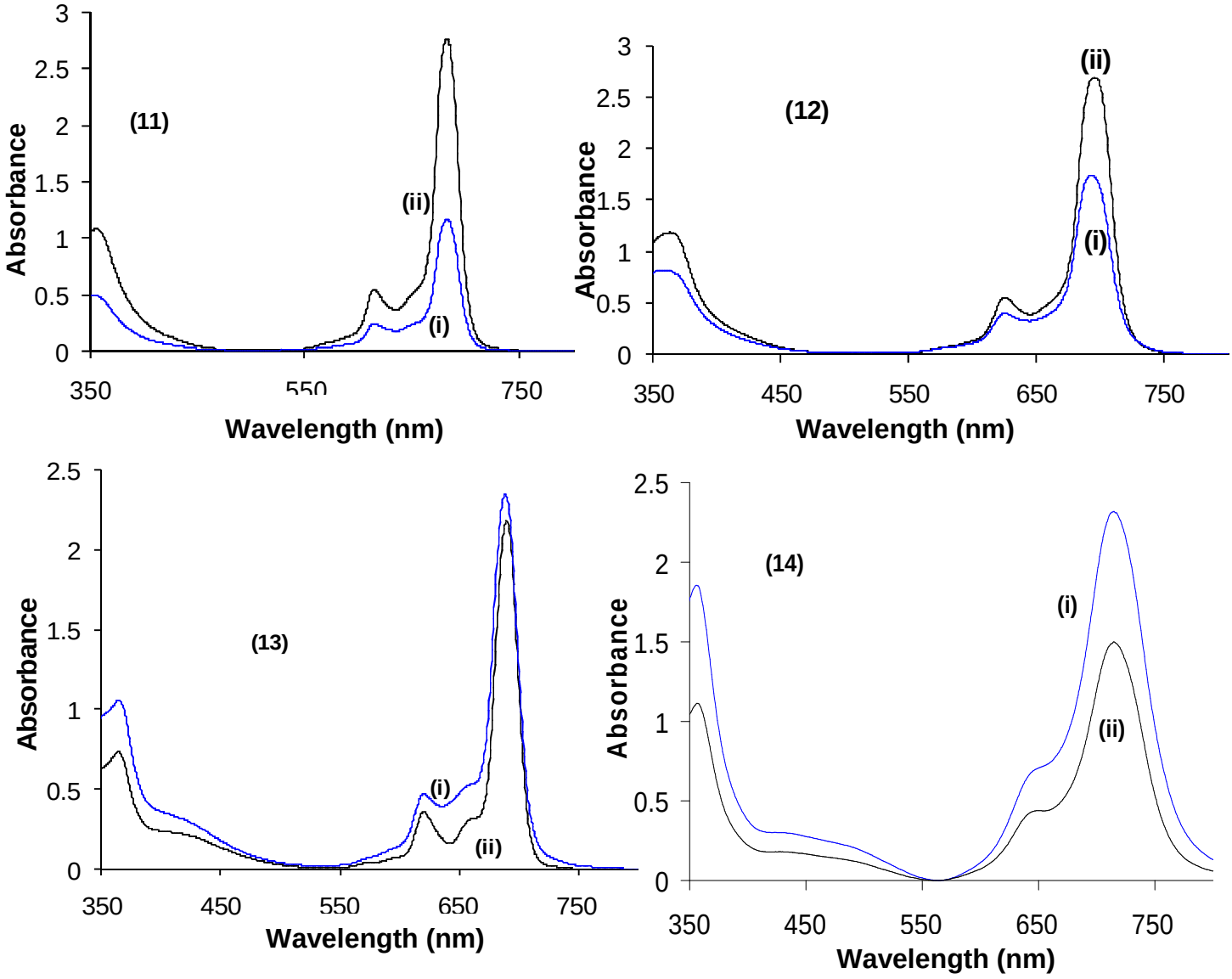

Fig. 3.2: Absorbance spectra of phthalocyanines **5**-**14** (i) in DMSO:water and (ii) DMSO alone.

3.2 Chloroindium hemiporphyrazine

The ClInHp was synthesized from 4-tert-butyl-phenoxyisoindoline and 1,3,5-triaminobenzene, Scheme 3.1. A molecular ion for the ClInHp was observed at 913.1 amu in the mass spectra data acquired, which corresponds to [M+1]. A yield of 28% was obtained for the ClInHp.

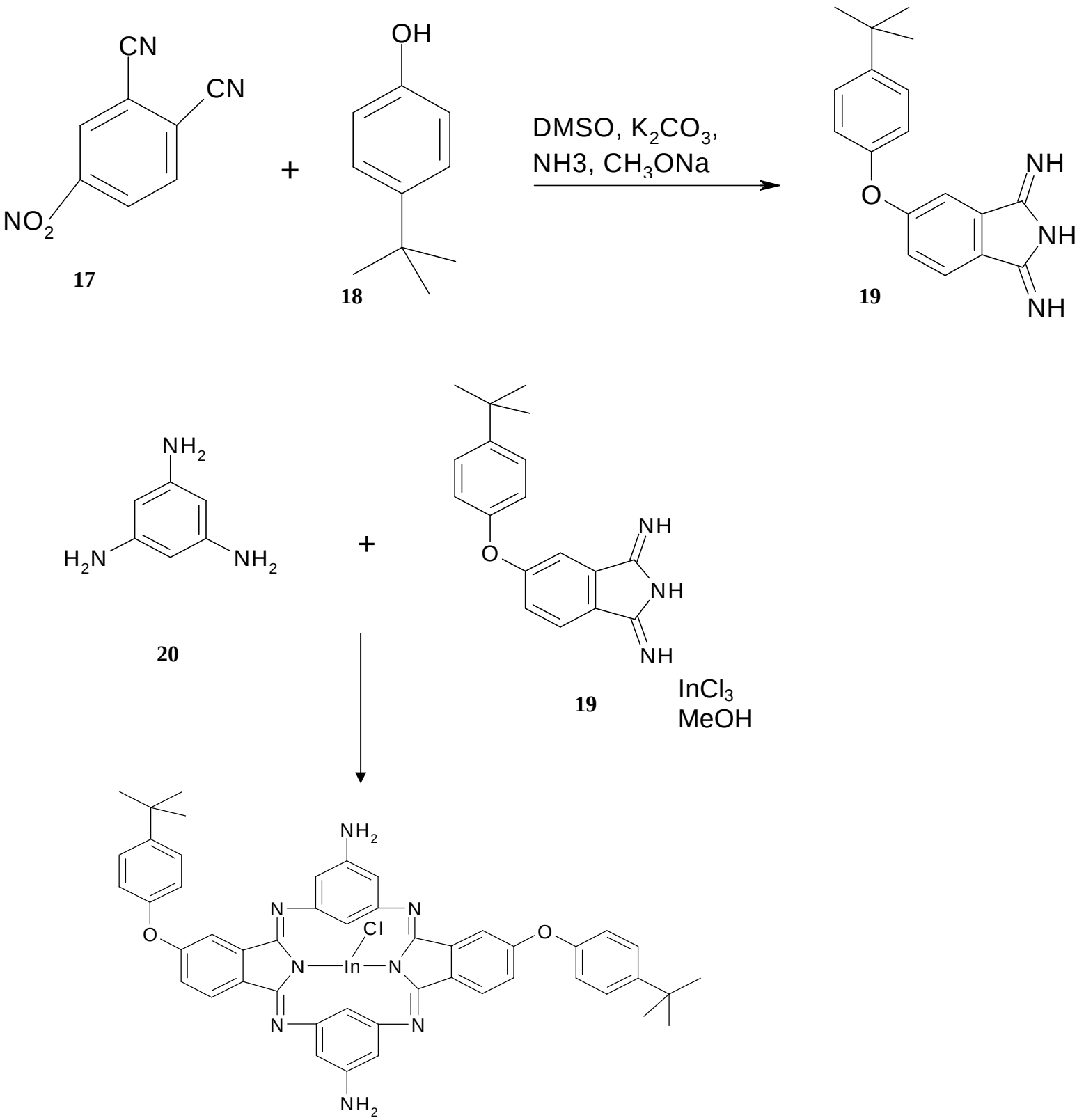

Scheme 3.1: Synthetic route for the creation of ClInHp

3.2.1. IR spectra.

Fig. 3.3 shows the infrared spectra of the ClInHp and its starting materials. The infrared spectrum of the ClInHp shows a broad peak around 3300 cm^{-1} that can either be attributed to an O-H stretch (from water) or an N-H stretch from the amine groups. The 1645 cm^{-1} band corresponds to the N-H bending. The 1711 cm^{-1} band is from C=N groups within the Hp molecule. In conjunction with this, is the 1020 cm^{-1} band for aliphatic amines, along with the 1357 cm^{-1} and 1313 cm^{-1} bands for the C-N aryl stretch. Lastly, there is the 1222 cm^{-1} band for aromatic ethers, which should correspond to the phenoxy substituents. The remaining bands are relatively weak and seem to mostly correspond to various C-H vibrations.

From Fig. 3.3 it can be seen that ClInHp and triaminobenzene have more defined peaks around the 3200 to 3300 cm^{-1} region than isoindoline, though the ClInHp peak is large and broad and probably corresponds more to an O-H bend. The two weak bands that triaminobenzene has around 3200 cm^{-1} do correspond to the N-H stretches for a primary amine, whilst the isoindoline appears to only have one band in this region. This would correspond to the N-H stretch observed for a secondary amine.

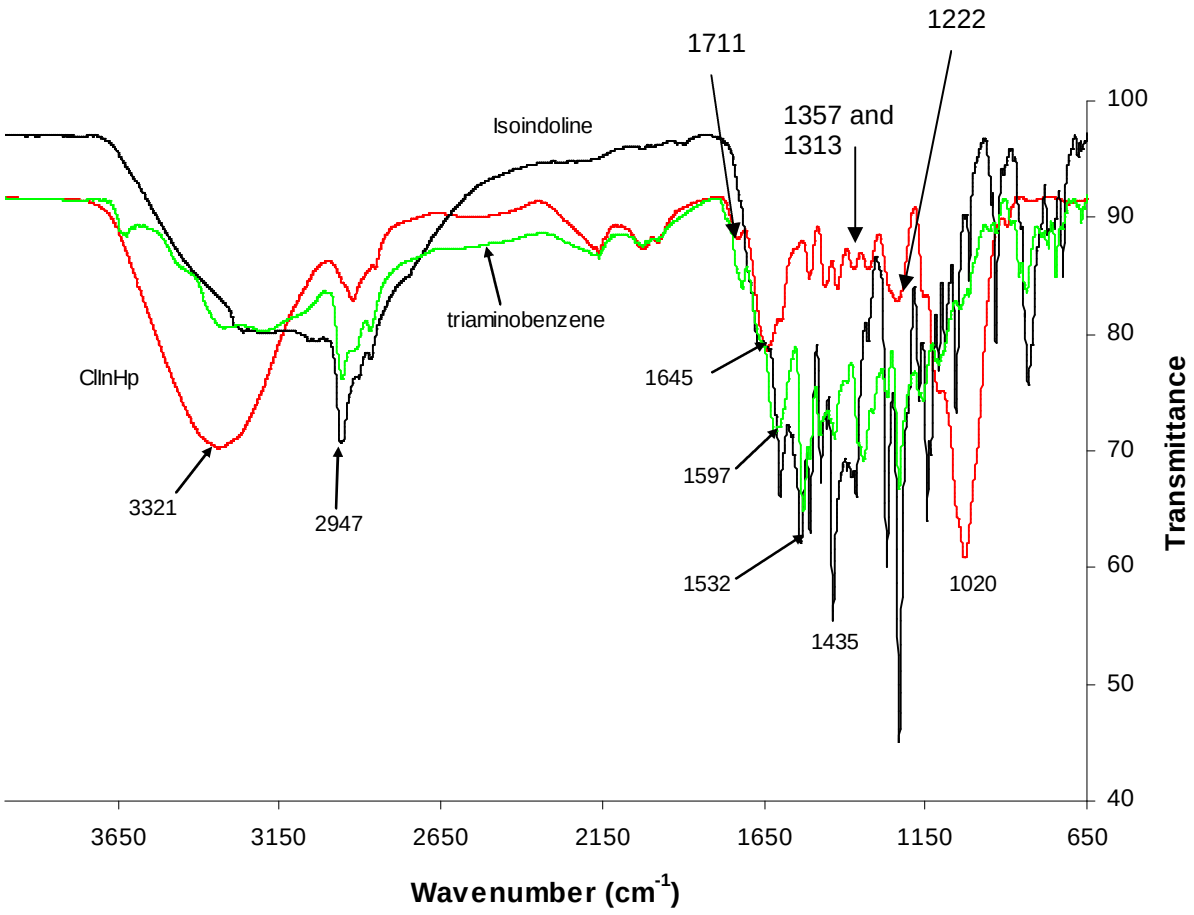

Fig. 3.3: Infrared spectrum of ClInHp and compounds used to form it.

3.2.2. NMR spectra.

The NMR data for the ClInHp are tabulated in Table 3.2 and numbers of protons are shown in Fig. 3.4. The proton NMR spectrum (Fig. 3.5) for ClInHp shows a number of aromatic signals at 7.75 (H-8), 7.48 (H-7), 7.29 (H-9), 7.27 (H-11) and 7.05 (H-10) ppm (see Fig. 3.4 for numbering), including a broad singlet at 10.1 ppm which indicates the presence of a heteroatom such as NH_2. As indicated by the coupling constants (i.e. J = 8.5 Hz), the doublet H-10 is coupled to the proton at 7.48 ppm (H-7). Both integrate to 4 protons and are assigned to the *t*-butyl phenoxy subunit.

Table 3.2: 1D and 2D NMR data for ClInHp acquired in THF-d_8 (^{1}H at 600 MHz; ^{13}C at 150 MHz).

	^{13}C (ppm)	**^{1}H (ppm)[a]**	**HMBC (ppm)**	**NOESY (ppm)**
1/2'	168.8 (s)[b,c]	-	-	
2/2'	168.6 (s)[b,c]	-	-	
3	164.3 (s)	-	-	
4	154.0 (s)	-	-	
5	148.8 (s)	-	-	
6	136.8 (s)	-	-	
7a 7b	128.0 (s)[c] 128.0 (d)[c]	- 7.48 (d, *J* = 8.5 Hz, 4H)	- C-4, C-7b, C-13	- 7.05
8	125.6 (d)	7.75 (d, *J* = 8.2 Hz, 2H)	C-1/C-2, C-3, C-6, C-9, C-11	7.29
9	123.0 (d)	7.29 (dd, *J* = 8.2 Hz, 2Hz, 2H)	C-3, C-7a, C-11	7.75
10	120.5 (d)	7.05 (d), *J* = 8.5 Hz, 4H	C-4, C-5, C-10	7.48
11	111.8 (d)[c]	7.27 (dd, *J* = 2 Hz, 2H)	C-1/C-2, C-3, C-7a, C-9	
12	35.1 (s)	-	-	
13	31.7 (q)	1.34 (s), 18 H	-	
1'	102.4 (d)[d]	-	-	
	NH	10.2 (br s), 2H	-	

[a] correlations obtained from HSQC data

[b] interchangeable signals

[c] overlapped signals

[d] data obtained from DEPT135

Likewise the H-8 and H-9 protons (which integrate to 2H each), have a coupling constant of *J* = 8.2 Hz, which indicates that these two protons are coupled. Additionally, the proton H-9 has a doublet of doublet multiplicity, and thus long range coupling (*J* = 2 Hz) is shown between H-9 and H-11 (at 7.27 ppm), although these two signals are almost considered to be overlapped. A singlet at 1.34 ppm integrating to 18H corresponding to the *t*-butyl methyl protons is also observed. NOESY (nuclear Overhauser effect spectroscopy) data confirmed the coupling of H-10 to H-7, and H-8 to H-9 (Fig. 3.6). No other correlations were observed. The molecule has two isomers, but there were no differences in the NMR spectra probably due to isomerization.

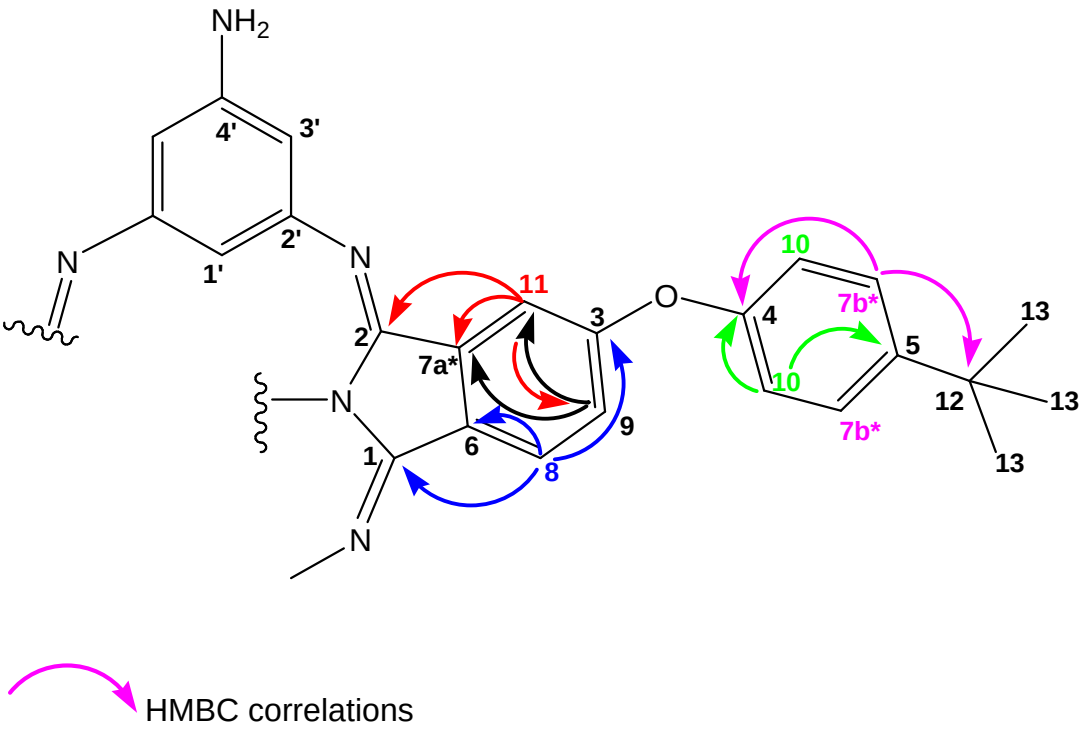

Fig. 3.4: Hp substructure with HMBC correlations observed and carbon numbers.*overlapped peaks. $^{+}$no clear correlation.

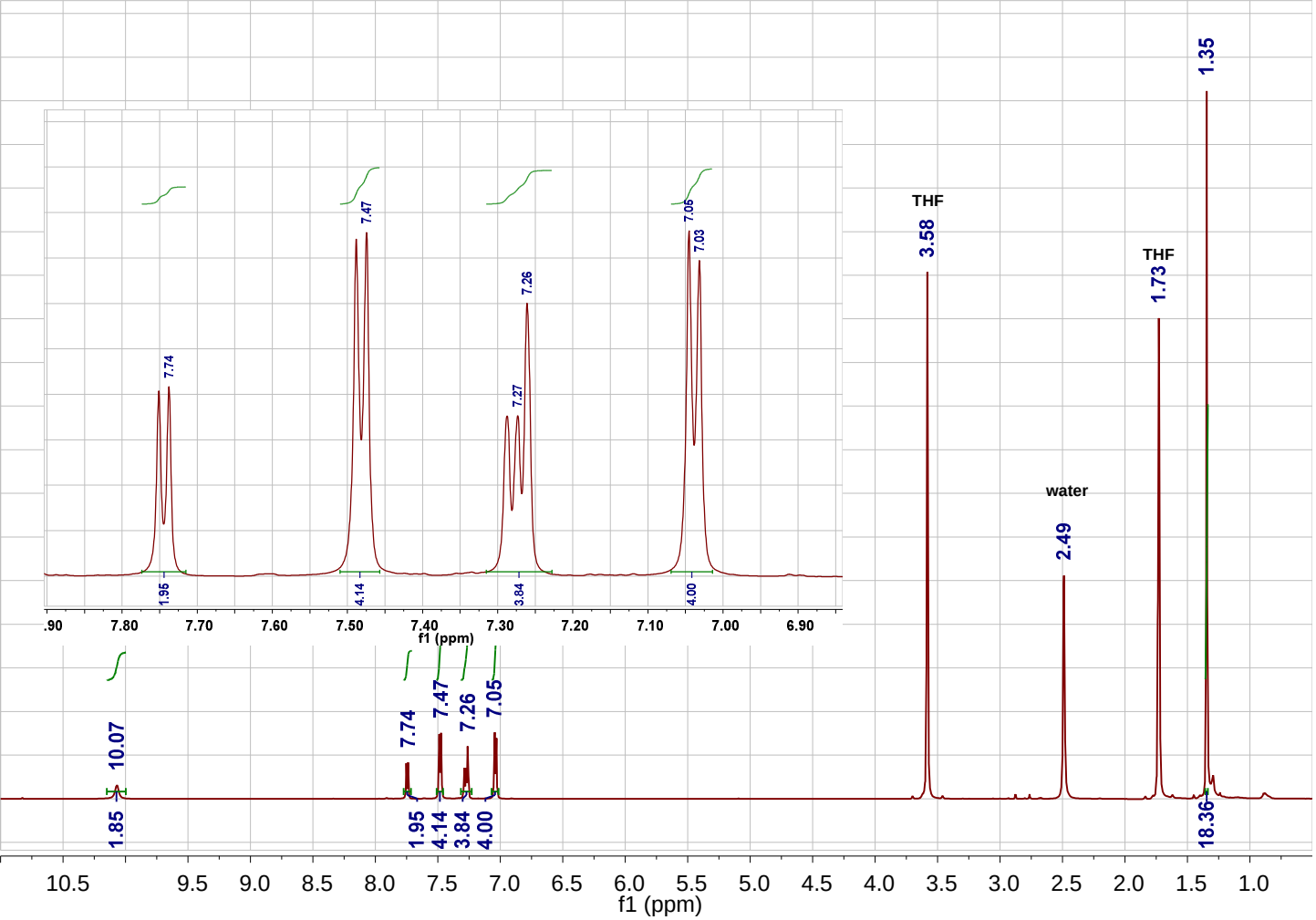

Fig. 3.5: Proton NMR of ClInHp in THF-d_8

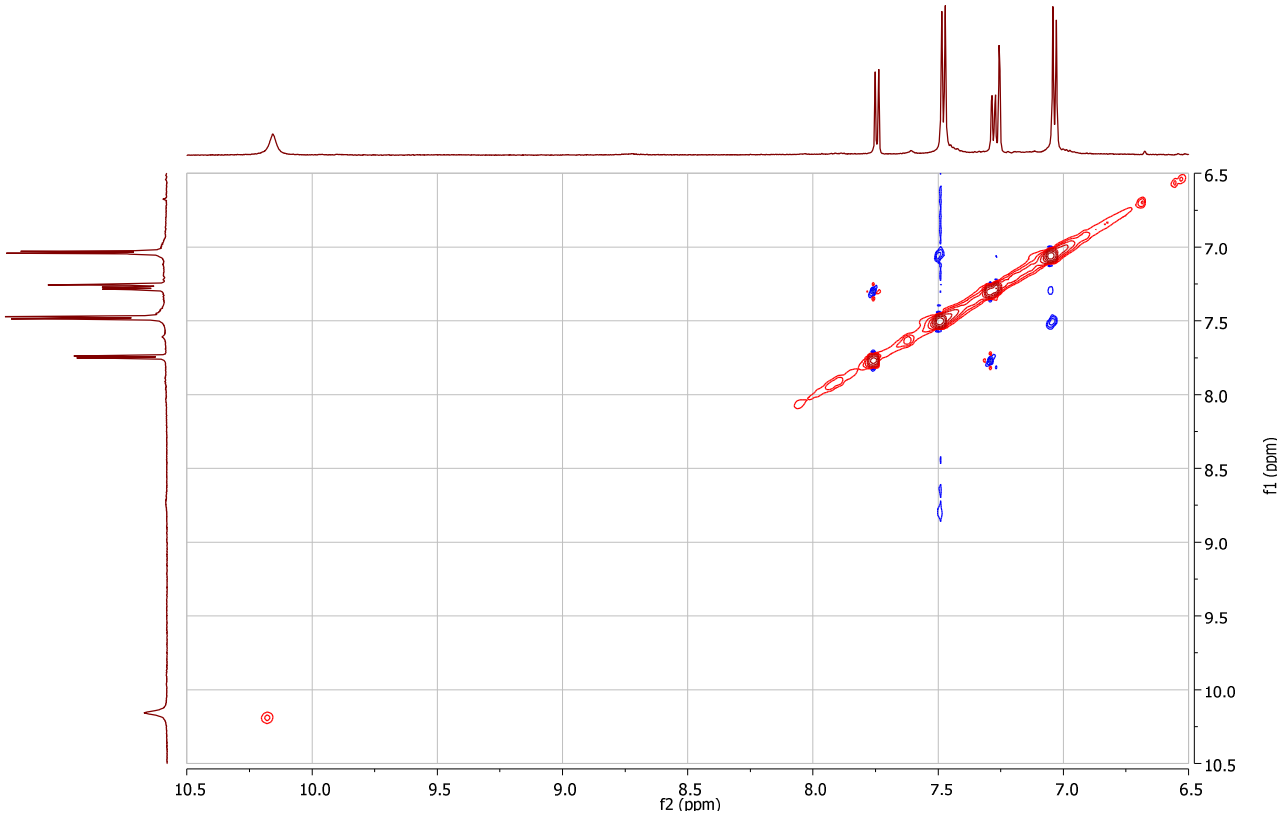

Fig. 3.6: NOESY spectrum of ClInHp in THF-d_8

1D ^{13}C (Fig. 3.7A) and DEPT135 (Distortionless Enhancement by Polarization Transfer) (Fig. 3.7B) NMR data were acquired for the ClInHp, Table 3.2. The ^{13}C data clearly shows the presence of five quarternary (4^{o}) carbons, with four highly deshielded signals. These were assigned to two -*C*=N (168.6, 168.8 ppm) and two aromatic =*C*-O (164.3, 154.0 ppm) and two aromatic =*C*- carbon signals at 148.8 and 136.8 ppm. The DEPT135 spectrum revealed the signal at 35.1 ppm (C-12) to be the 4^{o} carbon belonging to the *t*-butyl moiety, as well as the presence of an additional, protonated, carbon signal at 102.4 ppm not observed in the ^{13}C spectrum, surprisingly. This shielded signal may be due to one of the carbons of the aniline moiety (C-1').

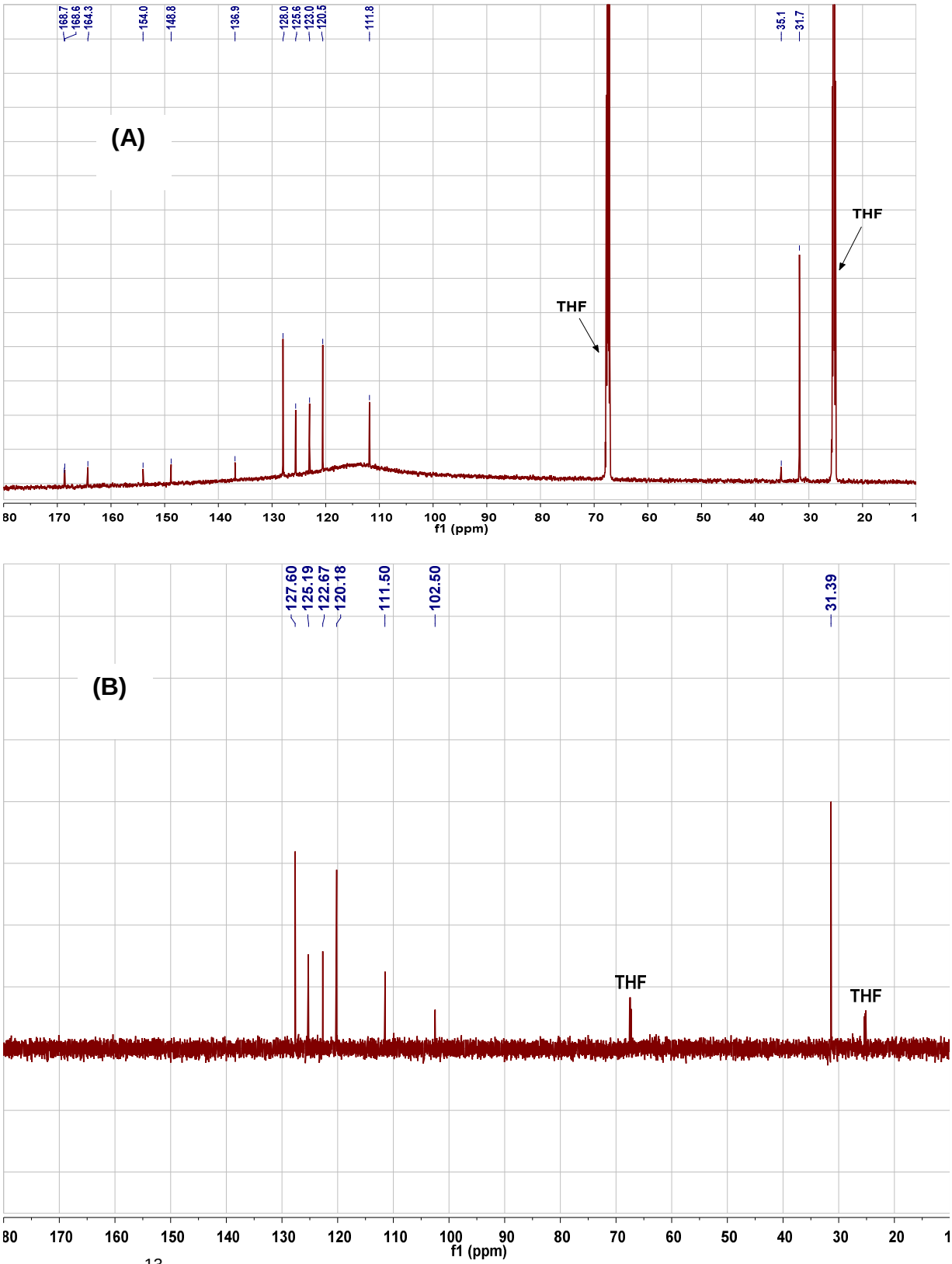

Fig. 3.7: (A) ^{13}C NMR spectrum and (B) DEPT135 spectrum of ClInHp in THF-d_8

The carbons corresponding to each of these proton signals were assigned by using an HSQC NMR (HSQC = Heteronuclear Single Quantum Coherence) (Fig. 3.8A) pulse program and the correlations are listed in Table 3.2. The HMBC (heteronuclear multiple-bond correlation) spectroscopy (Fig. 3.8B) data confirmed that several carbon signals including the signal at 128.0 (C-7) and 111.8 (C-11) ppm were overlapped, as for both H-11 and H-8, which are unequivocally assigned to a different ring system, and showed correlations to a signal at 128 ppm (assigned as C-7a for the 4^{o} carbon and C-7b for the protonated aromatic carbon). HMBC correlations can be seen in Fig. 3.4. H-7b was assigned using HSQC to 128.0 ppm and showed HMBC correlations to the 4^{o} *t*-butyl carbon at C-13, while both H-7b and H-10 showed correlations to the aromatic C=O at C-4. On the other hand, H-11 showed additional correlations to C-7a and C-2 (at 168.6 ppm), H-8 revealed connections to C-6 (136.8 ppm), C-1 (168.8 ppm) as well as to a carbon at 164.3 ppm (C-3), completing the isoindoline substructure. The three shifts observed in the ^{13}C for complex at ~170 generally correspond to N–C=N- and have been reported previously [12], but the shift at 164.3 ppm has been assigned to C-3 since H-8, H-9 and H-11 all show correlations to it [12]. Surprisingly, no correlations were unambiguously observed for the aniline subunit. The carbon at 102.4 ppm observed in the DEPT135 spectrum corresponds to a shift expected for C-1', while literature has reported identical shifts for C-1 and C-2. This may point to the fact that one of the correlations observed for H-8 and H-11 to 168.8 and 168.6 ppm may in fact be to the aniline carbon assigned as C-2'. A ^{13}C signal shift at δ 148.8 ppm as observed for C-5 also corresponds to the expected shift for C-4' on the aniline moiety. This brings the possibility that the carbon at δ 148.8 ppm may be an overlapped signal. The signal for C-3', however is not accounted for in the ^{1}H or ^{13}C spectra.

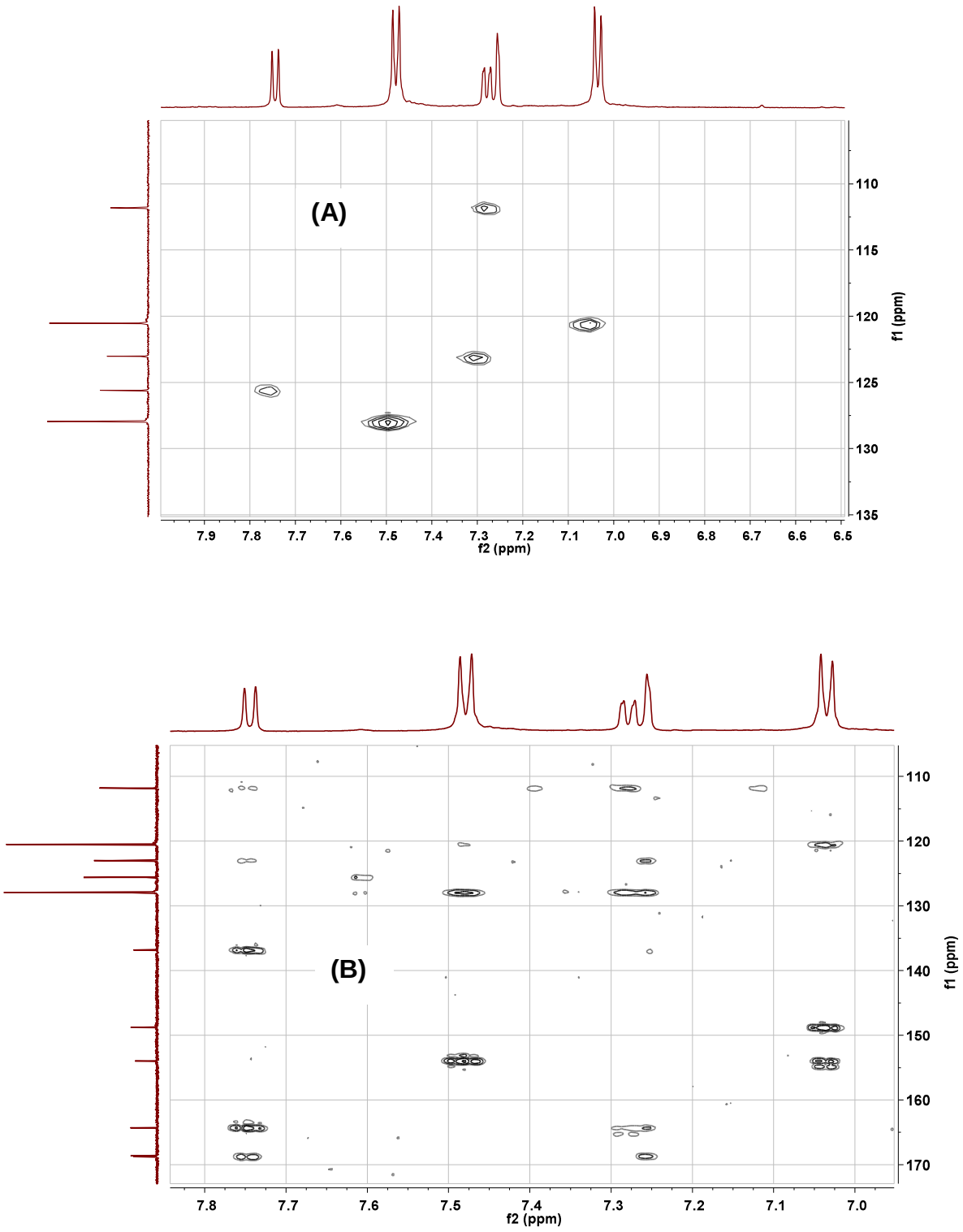

Fig. 3.8: (A) HSQC and (B) HMBC of ClInHp in THF-d_8

While the NMR data does not obviously account for the aniline moiety because the NH_2 groups are difficult to discern on the proton NMR, the evidence is provided by the FT-IR and mass spectral data.

3.2.3 Absorbance and Fluorescence spectra

Fig. 3.9 shows the absorption spectrum of InHp. One of the interesting aspects of Hps is a nearly complete absence of absorptions in the visible and near-infrared spectrum. The presence in Hps of an extended aromatic ring and C_{2V} symmetry determines transitions only in the near UV [175 - 177]. The absorbance bands for InHp are centered around 410 nm and consist of 3 bands. The fluorescence emission spectrum is broad for InHp as has been reported before [12]. The peculiar aspect of this graph is the fact that the excitation spectrum does not match up with the absorbance and is in fact blue-shifted and fairly broad, Fig. 3.9. Part of the reason for this could be the difference in instruments used to take either measurement, but this would not account for so large a shift which seems to indicate that some form of structural or conformational change has occurred to cause the blue-shift upon excitation.

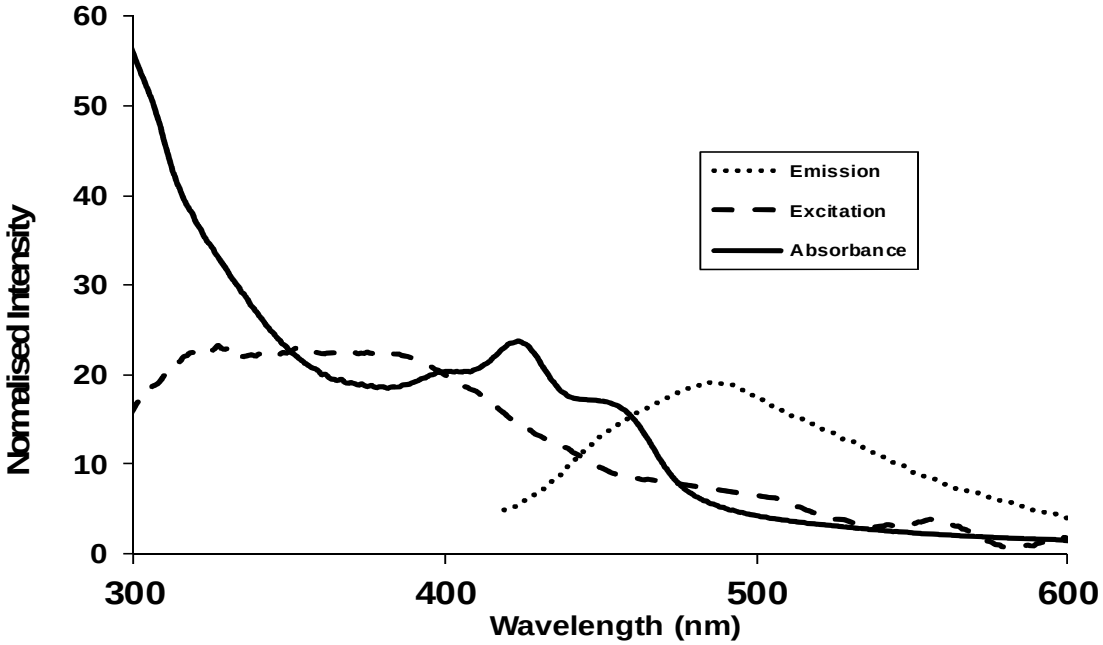

Fig. 3.9: Absorbance, Excitation and Emission Spectra of ClInHp in THF.

3.3 Nanomaterials

In this work H_2S, H_2Te and H_2Se gases were employed together with $CdCl_2$ for the synthesis of QDs. The H_2Te and H_2Se gases were formed in a heavily de-aerated reaction system that entailed adding a small amount of H_2SO_4 to tellurium or selenium powder and sodium borohydride in a small reaction vessel connected via a pipe to the setup described earlier until the grey tellurium or selenium powder reacted completely with the sodium borohydride. The gas produced is the desired reactant, and can then be introduced into the de-aerated cadmium solution to cause nucleation. Hydrogen sulphide was obtained as a gas already and was just injected into the cadmium solution. Once the gas is added to the cadmium solution, the reaction flask is brought to the boil to initiate Ostwald ripening.

3.3.1 X-ray Diffraction (XRD)

The X-ray diffraction patterns of the TGA capped CdTe and CdSe QDs (as examples) in solid nanocrystal form employed in this work are shown in Fig. 3.10. The diffraction pattern shows three characteristic peaks for bulk CdTe structure and two for the CdSe structure. Size determinations using the XRD peak at 2θ = 24 (Fig.

3.10 and equation 1.2), gave 3.4 nm for CdTe (Table 3.3), with the CdSe being 1.8 nm and CdS being 2.3 nm. The peak choice for use in the equation is based upon which of the peaks is the most intense.

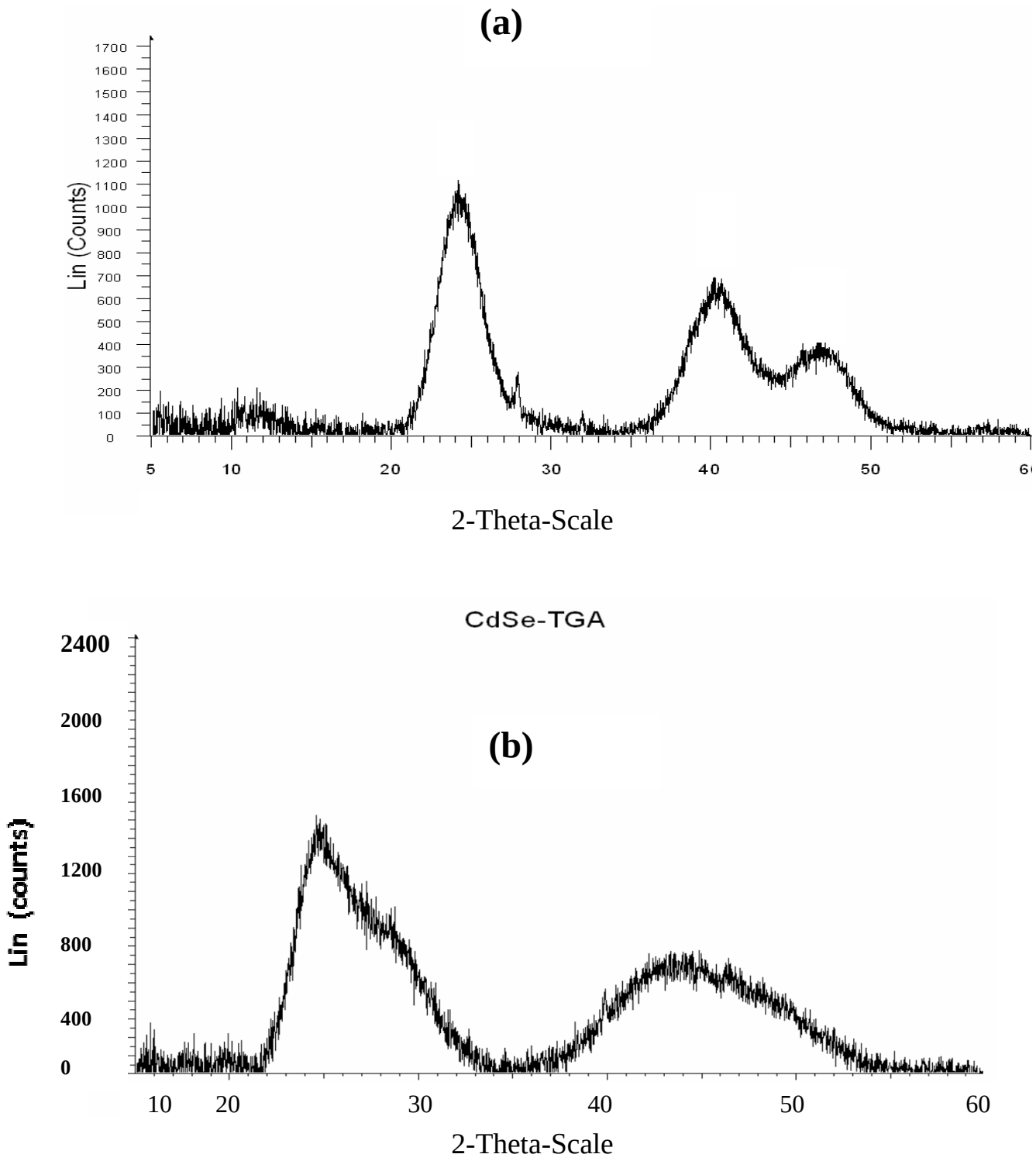

Fig. 3.10: X-ray diffraction spectra for (a) CdTe-TGA and (b) CdSe-TGA

Table 3.3: Size Determination and Fluorescence Data for Synthesized TGA-capped QDs in water.

QD	Emission (nm)	XRD Size (nm)
CdS	540	2.3
CdSe	634	1.8
CdTe	570	3.4

3.3.2 UV/Vis and emission spectra of QDs

Fig. 3.11A overlays the absorbance and emission spectra of CdTe-TGA. The emission peak is observed at 570 nm, with an absorption around 540 nm, which overlaps the 532 nm region of laser excitation, which may interfere with optical limiting ability of a quantum dot. However, it is the effects of the QDs on the OL behavior of the Pc complexes that is explored in the next chapter. Fig. 3.11B overlays the absorbance and emission spectra of CdSe-TGA and CdS-TGA. The CdSe-TGA possesses an absorbance spectrum that is below 532 nm, see also Fig. 3.11B and Fig. 3.12A, and its emission peak is more red-shifted and broad than the CdS-TGA. The broad emission peak could be because the CdSe-TGA is very close to becoming bulk material. The CdS-TGA shows no absorbance at 532 nm region (see Fig.3.12A). This is beneficial because the CdTe-TGA shows fairly strong absorption in this region, while CdS and CdSe do not. This will offer a point of comparison to see the effect of 532 nm absorption.

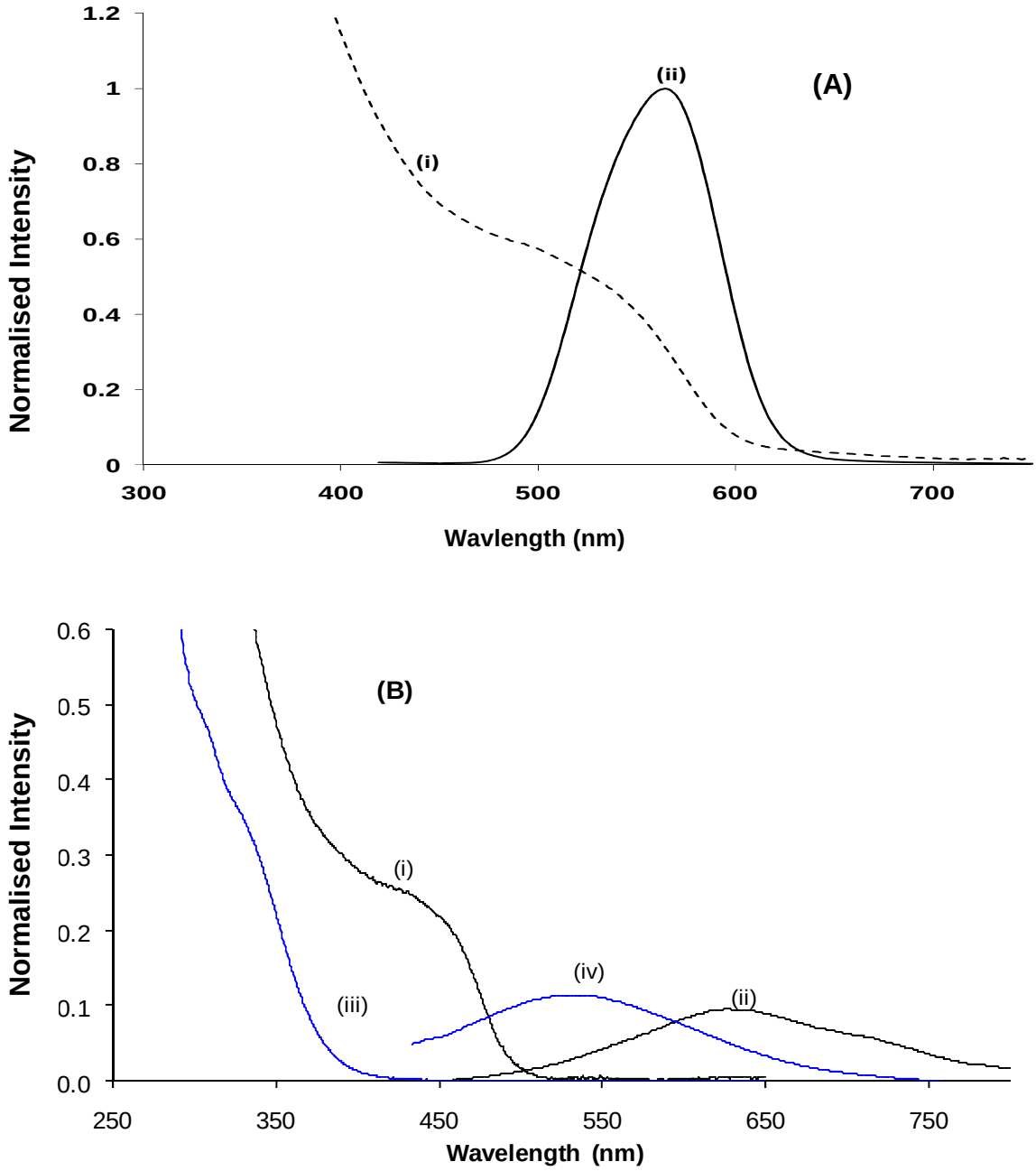

Fig. 3.11: (A) Overlaid and normalized absorbance (i) and emission (ii) spectra for CdTe-TGA in water, and (B) Overlaid and normalized absorbance and emission spectra CdSe-TGA ((i) absorbance and (ii) emission) and CdS-TGA ((iii) absorbance and (iv) emission).

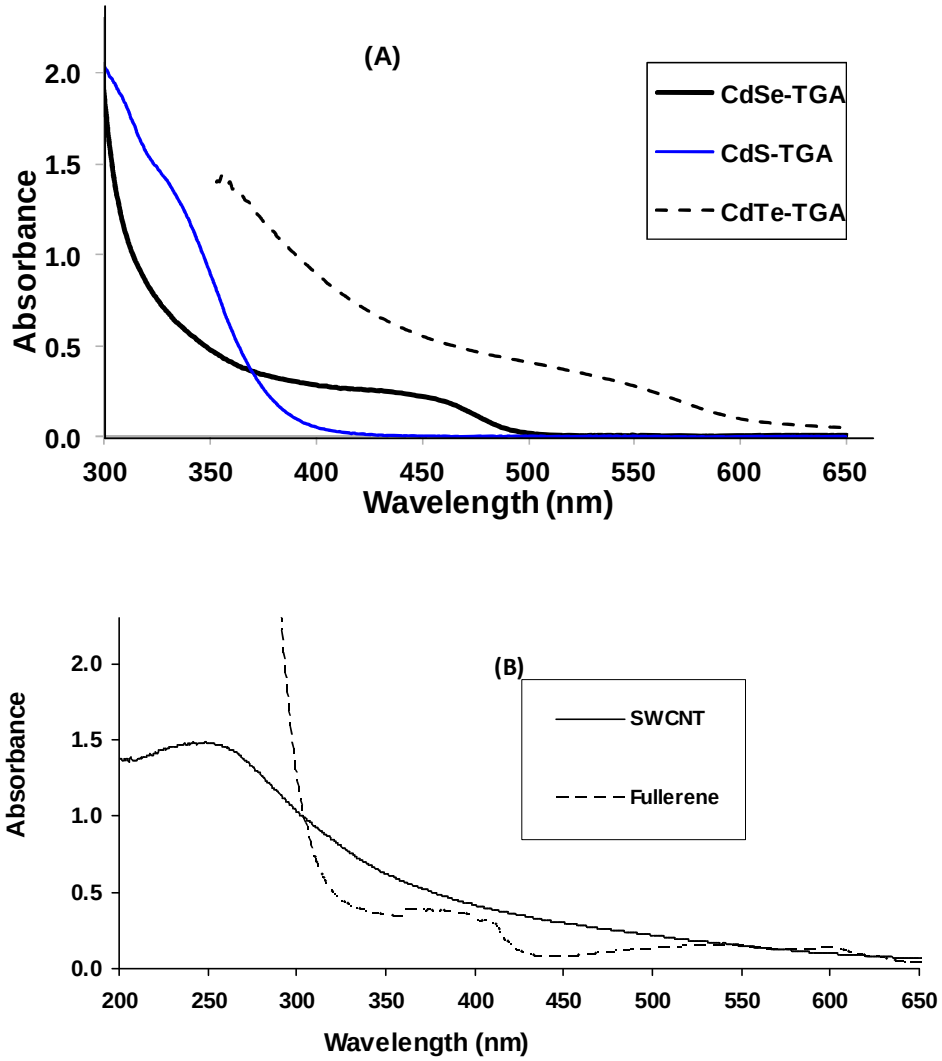

Fig. 3.12: UV-Visible spectra of (A) QDs CdTe-TGA, CdS-TGA and CdSe-TGA, and (B) SWCNT and fullerenes.

Fig. 3.12B shows the UV-Visible spectra of fullerenes and SWCNTs, which show absorption around the 532 nm region. In the case of the fullerene in particular which does have a very strong Z-scan signal, a comparison between using a NM which is not a good optical limiter which is then combined with a phthalocyanine versus one which is, can be made.

3.4 Characterization of phthalocyanines-polymer linked conjugates

The conjugation of Pcs with the polymers took place through an amide bond formation between the NH_2 group of $ZnPc(NH_2)_4$ (**14**) and the COOH group of the PMAA (Scheme 3.2), or the COOH groups of $MPc(COOH)_8$ complexes (**15, 16**) and the NH group of PEI (Scheme 3.3). EDC and NHS were employed as complexing agents. It has been shown [178] that both are required for the formation of an amide bond between two substances.

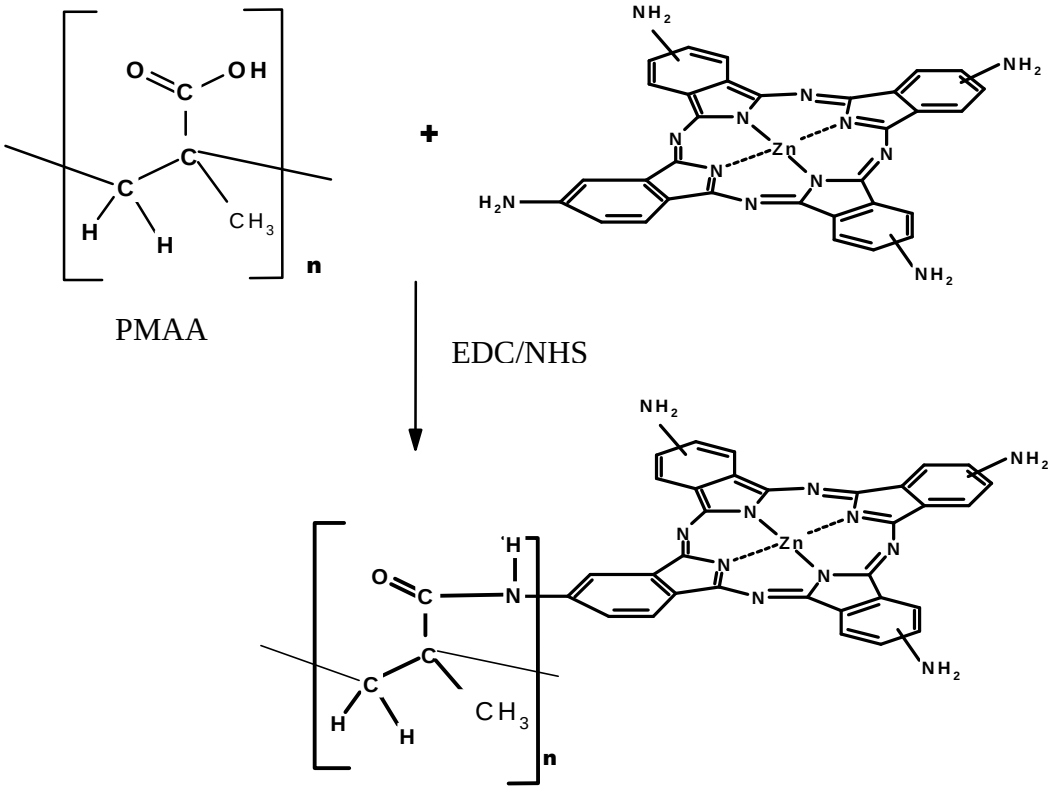

Scheme 3.2: Formation of the amide linkage between $ZnPc(NH_2)_4$ (**14**) and poly (methyl acrylic acid) (PMAA). EDC = N-(3-dimethylaminopropyl)-N'-ethylcarbodiimide hydrochloride, NHS = N-hydroxysuccinimide

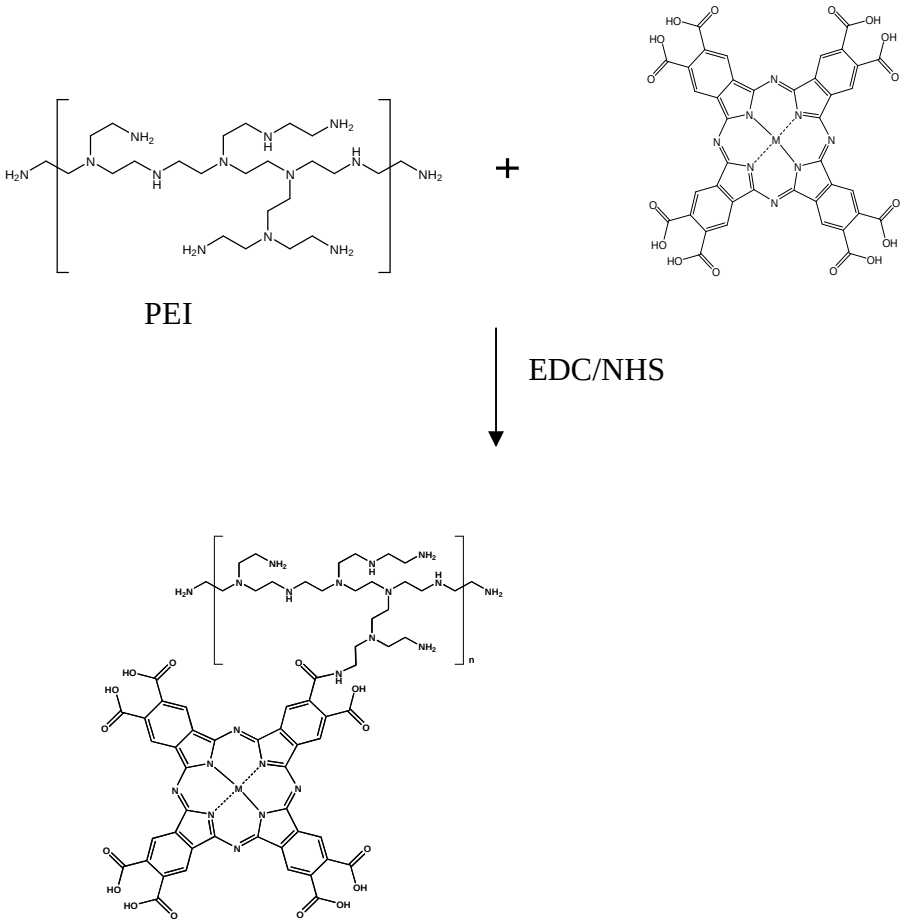

Scheme 3.3: Formation of the amide linkage between $MPc(COOH)_8$ (**15**, **16**) and polyethylenimine (PEI).

3.4.1 IR and Raman spectra

In the IR spectra (Table 3.4), the amide bond is observed at 1652 cm^{-1} for the conjugate of PMAA with $ZnPc(NH_2)_4$, which is shifted from C=O vibration of PMAA alone at 1666 cm^{-1}, confirming amide bond formation. There is also a shift of the N-H peak position from 3331 cm^{-1} (for $ZnPc(NH_2)_4$) to 3371 cm^{-1} for the conjugate. For conjugates of PEI with phthalocyanines **15** and **16**, the IR spectra showed an amide vibrational band near 1640 cm^{-1}, which was not observed with Pc or PEI alone, confirming amide bond formation.

Table 3.4: Infrared data of Pcs linked to polymers.

Compound	Wavenumber (cm^{-1})	Functionality
PMAA	1666	C=O vibration
$ZnPc(NH_2)_4$ (**14**)	3331	N-H stretch
$ZnPc(NH_2)_4$-PMAA	1652 3371	C=O amide vibration N-H stretch
PEI	3400 – 3300 3330 - 3250	Primary N–H stretch
$ZnPc(COOH)_8$ (**15**)	1760 - 1690	C=O COOH stretch
$AlPc(COOH)_8$ (**16**)	1760 - 1690	C=O COOH stretch
15/**16**-PEI	1640	C=O amide vibration

The covalent linkage of $ZnPc(COOH)_8$ (**15**) to PEI through an amide bond was further ascertained using Raman spectroscopy. Raman bands were observed in the amide [179] region 1200 to 1600 cm^{-1}, Fig. 3.13. The bands are weak, however, the amide bonds I, II and III are clearly visible in Fig. 3.13.

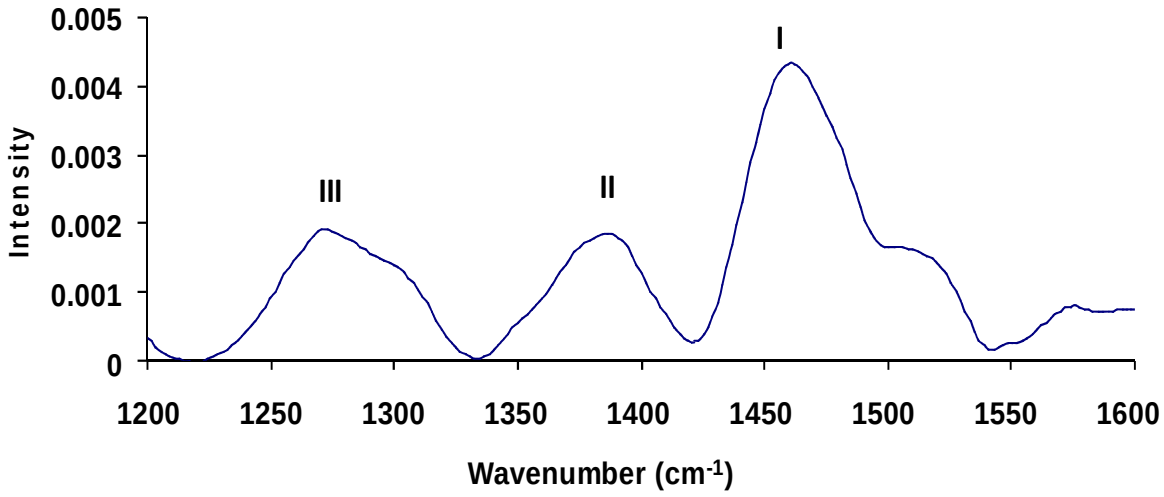

Fig. 3.13: Raman spectra of $ZnPc(COOH)_8$ (**15**) linked to PEI

3.4.2 XRD

Figure 3.14 shows the XRD patterns of **15** or **16** when mixed or linked with PEI and **14** when mixed or linked with PMAA. The XRD spectrum of **16** mixed and linked with PEI is shown in Fig. 3.14A. The peak at 2θ = 22° was the only pronounced peak on the XRD spectrum of PEI alone (Fig. 3.14A(i)) and it is close to the (002) reflection of carbon [180]. The broad nature of this peak underlines the substantial amorphous nature of PEI. The peak for the Pc alone was observed near 25° for complexes **14**-**16**, as is typical of phthalocyanines [181] (insert in Fig. 3.14A). Thus the peaks for the conjugate (or mixture) of Pc and PEI in the 24 to 25° region are expected to be an overlap of these two peaks. The XRD of the Pc alone shows some degree of crystallinity in this case as well.

The peak at 22° for the PEI alone is slightly shifted in the **16**/PEI covalently linked conjugate due to the possible binding interaction between **16** and PEI, along with the emergence of four relatively sharp peaks of crystalline nature (Fig. 3.14A (ii)). A similar XRD shift was observed for **15/**PEI, Fig. 3.14B, but no new sharp peaks emerged. When mixed (without a chemical bond) the spectra of **15**/PEI and **16**/PEI are similar to that of complexes **15** or **16** linked to PEI, (Fig. 3.14A and B (iii)) except the sharp peaks were less intense for **16** and there was a shoulder near 40° for **15**. There was also shifting in peaks. It has been reported that both the degree of crystallization and the interplanar space changes, imply a new crystal form or a new compound in phthalocyanines [182]. The theory behind the use of XRD was that due to the potential cross linking between the polymer strands caused by the phthalocyanines, that there may be an alteration in the crystallinity of the polymer, as observed in Fig. 3.14A and B. The XRD trace for $ZnPc(NH_2)_4$ (**14**) and PMAA shows

that the two amorphous peaks for PMAA alone (at 15 and 29°) form into a singular amorphous peak when **14** was mixed into or linked to PMAA.

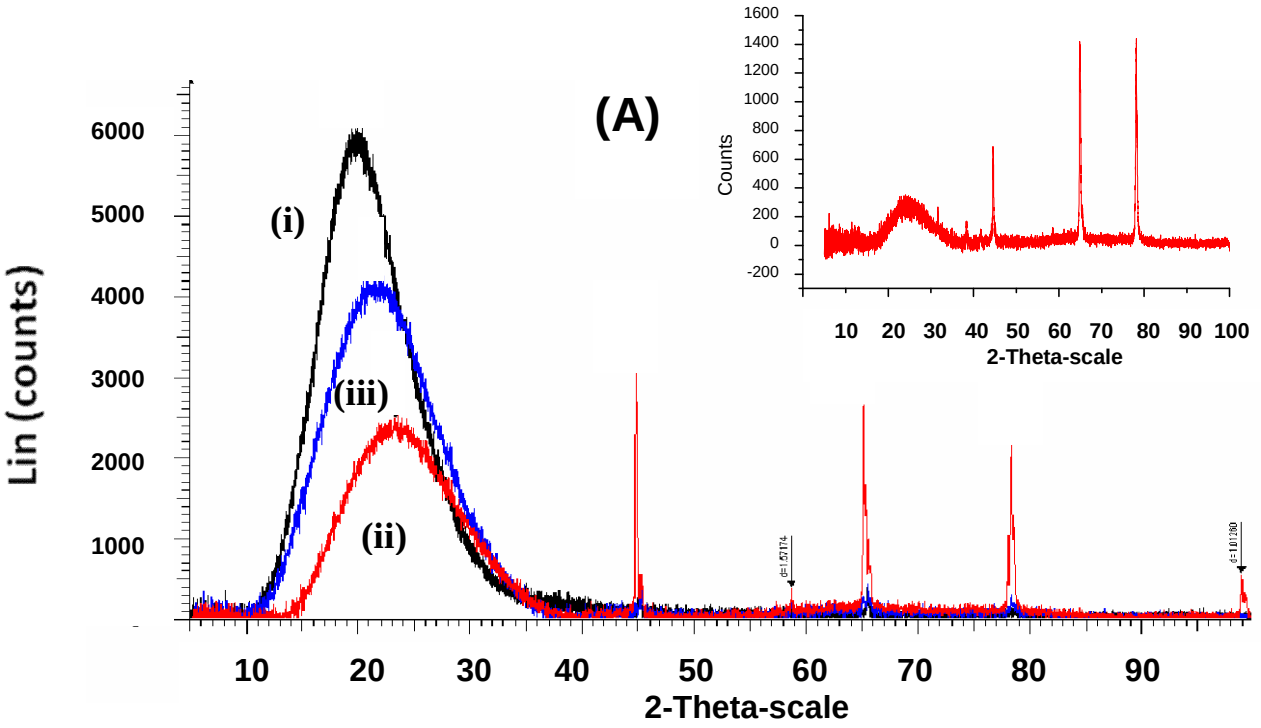
(A)
(i)
(iii)
(ii)
Lin (counts)
2-Theta-scale
Counts
2-Theta-scale

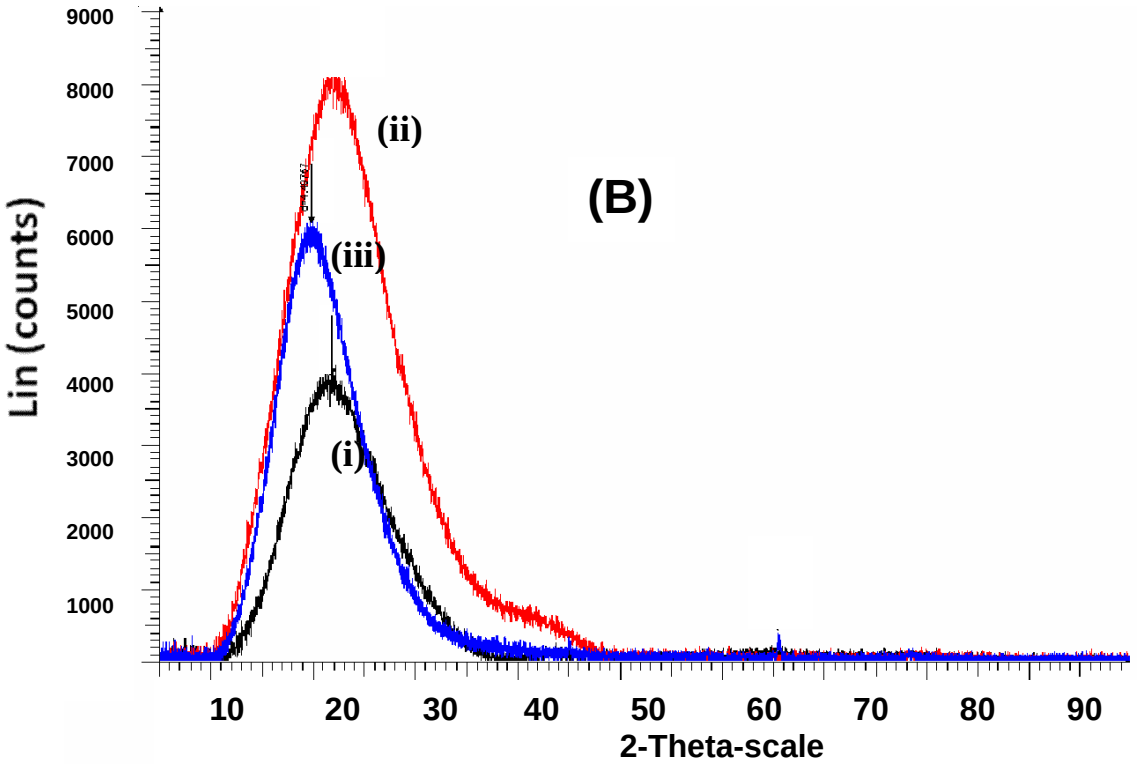
(B)
(ii)
(iii)
(i)
Lin (counts)
2-Theta-scale

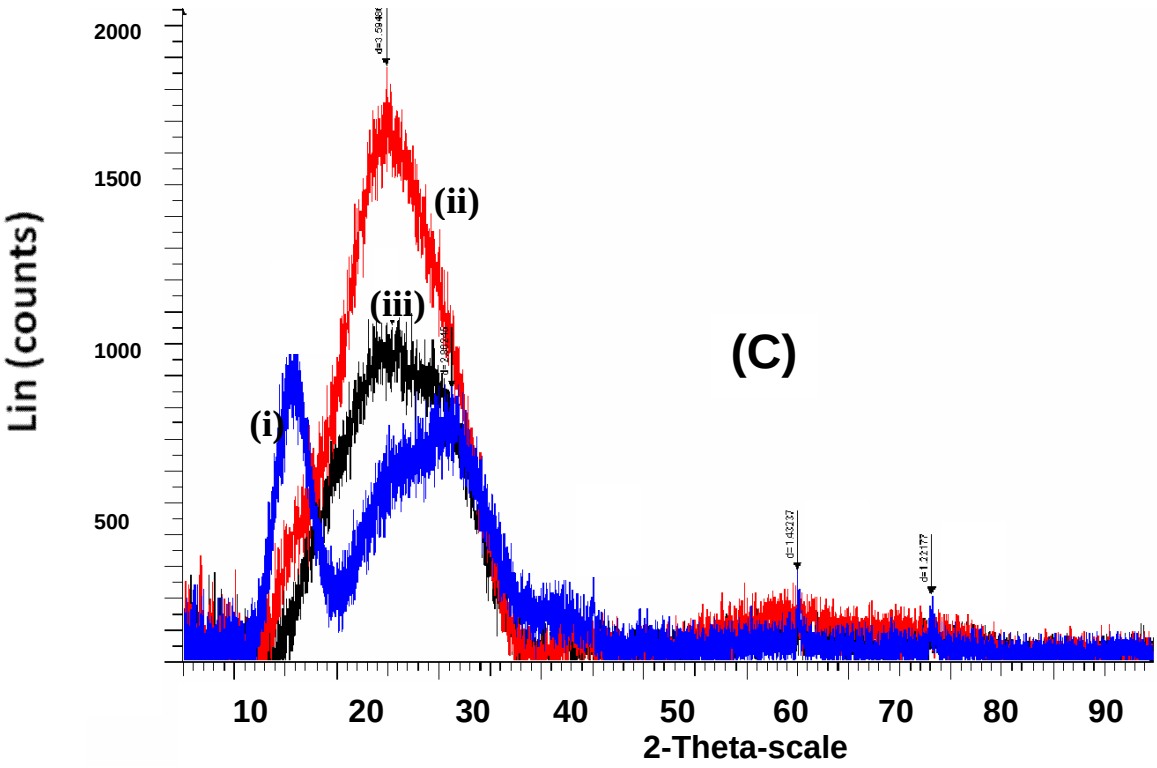

Fig. 3.14: XRD spectra of (A) $AlPc(COOH)_8$ (**16**) in PEI, (B) $ZnPc(COOH)_8$ (**15**) in PEI and (C) $ZnPc(NH_2)_4$ (**14**) in PMAA. (i) polymers alone, (ii) Pcs linked to the polymers and (iii) Pcs mixed into the polymers. Insert in (A) is Pc alone.

3.4.3. TGA

As stated above, cross linking is a possibility when $ZnPc(NH_2)_4$ is linked to PMAA or $MPc(COOH)_8$ are linked to PEI. Thermogravimetric analysis has been successfully employed to determine the extent of cross linking in polymers [183]. A completely cross linked polymer does not show a loss of mass in TGA traces. Fig 3.15 shows the TGA profiles of PMAA, $ZnPc(NH_2)_4$ and the latter mixed or chemically linked to PMAA. The initial mass loss (Fig. 3.15A and B) experienced around 100 °C may be attributed to solvent losses (e.g. water). PMAA alone shows two decomposition steps at 260 °C and then at 450 °C, while $ZnPc(NH_2)_4$ alone shows a single step at 285 °C (Fig. 3.15A(iii)). Upon mixing the PMAA and $ZnPc(NH_2)_4$, the mass losses

due to PMAA are still evident, Fig. 3.15A(ii). However, when the two are covalently linked there is a significant decrease in mass loss which is attributable to cross linking, Fig. 3.15B(ii) [183], in the $ZnPc(NH_2)_4$-PMAA conjugate. Cross linking results in the restriction of the flexibility of the polymer chain. An explanation for the increased rigidity could be that the linked phthalocyanine is sterically hindering the movement of the PMAA strands when the Pc is linked. This could then potentially result in an increase in the temperature at which mass loss occurs at within the Pc-polymer conjugate. The TGA data shows clearly that the polymer has changed markedly.

The rigidity of Pc environment has been shown to decrease the probability of non radiative relaxation, increasing the population of the singlet excited state and subsequently intersystem crossing to the triplet state [184]. This results in the improvement of optical limiting properties. Thus cross linking of the Pc-polymer conjugates may lead to improved optical limiting behaviour due to reduction in flexibility of the chain.

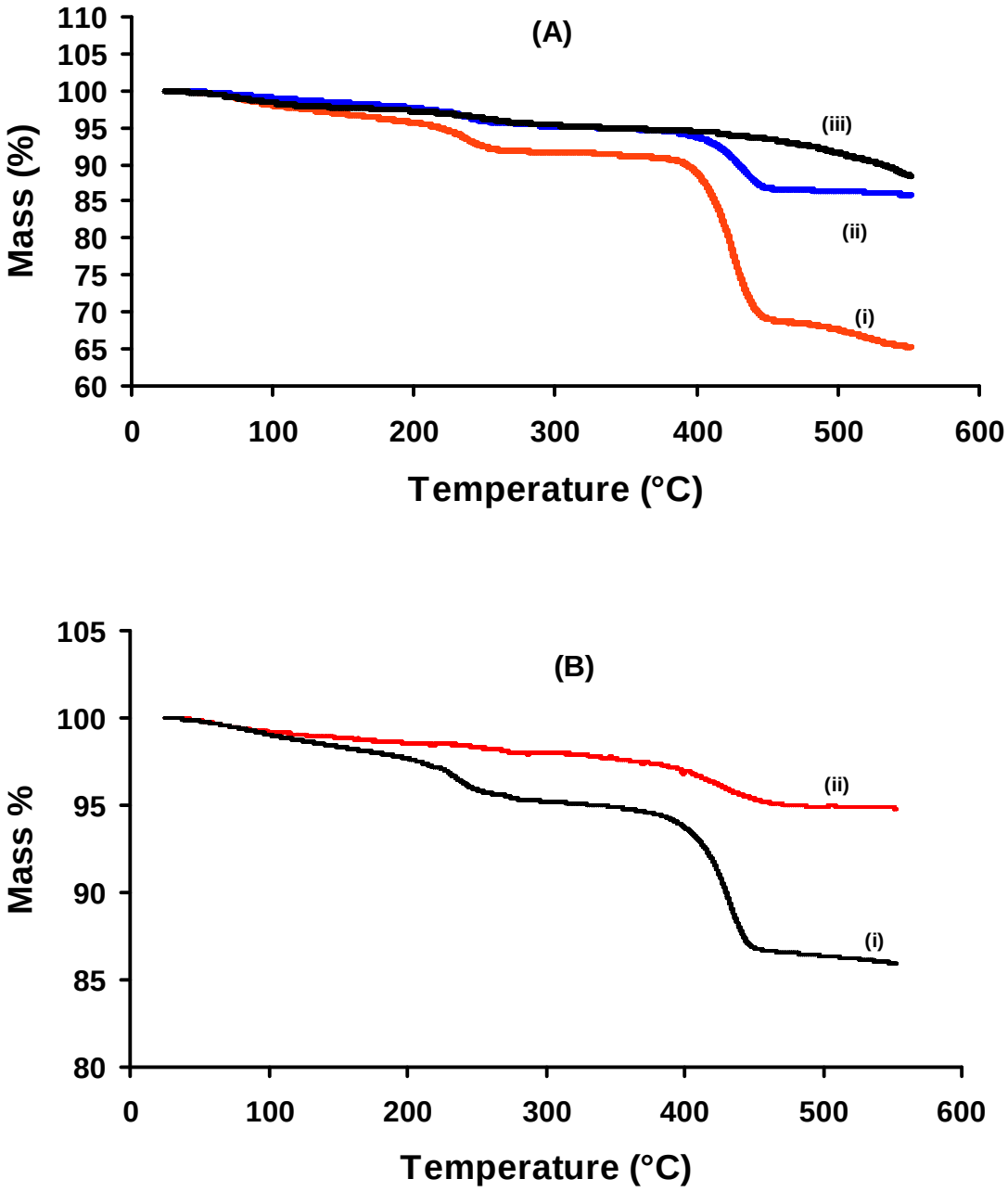

Fig. 3.15: TGA profiles of (A) (i) PMAA alone, (ii) PMAA mixed with $ZnPc(NH_2)_4$ and (iii) $ZnPc(NH_2)_4$ alone; (B) (i) PMAA mixed with $ZnPc(NH_2)_4$ and (ii) PMAA linked to $ZnPc(NH_2)_4$.

3.4.4 Mass Spectra

Mass spectra were employed to estimate the number of phthalocyanines coordinated to the polymer. PMAA and $ZnPc(NH_2)_4$ conjugate was again used as an example. The MALDI-TOF MS data of the PMAA alone shows peaks corresponding to 8 (675 amu), 10 (889 amu) and 13 (1124 amu) monomer units (Fig. 3.16A), with the mixture showing the same set of peaks, though with some enhanced (Fig. 3.16B). However, upon comparison of the mass spectra of the PMAA alone (Fig. 3.16A), the mixture (Fig. 3.16B) and the covalently linked Pc (Fig. 3.16C), additional peaks corresponding to the 8, 10 and 13 monomer units plus a Pc (M+Na) moiety (at 1347, 1560 and 1795 amu respectively) are observed. This may suggest that there is one Pc unit per every 2 or 3 polymer units. The increase in mass of the polymer was not observed when phthalocyanines were simply mixed (i.e. without formation of a chemical bond). The mass spectral results seem to reinforce the explanation provided by the TGA results, i.e. some carboxylic acid groups on the polymer chain remain unlinked and intact.

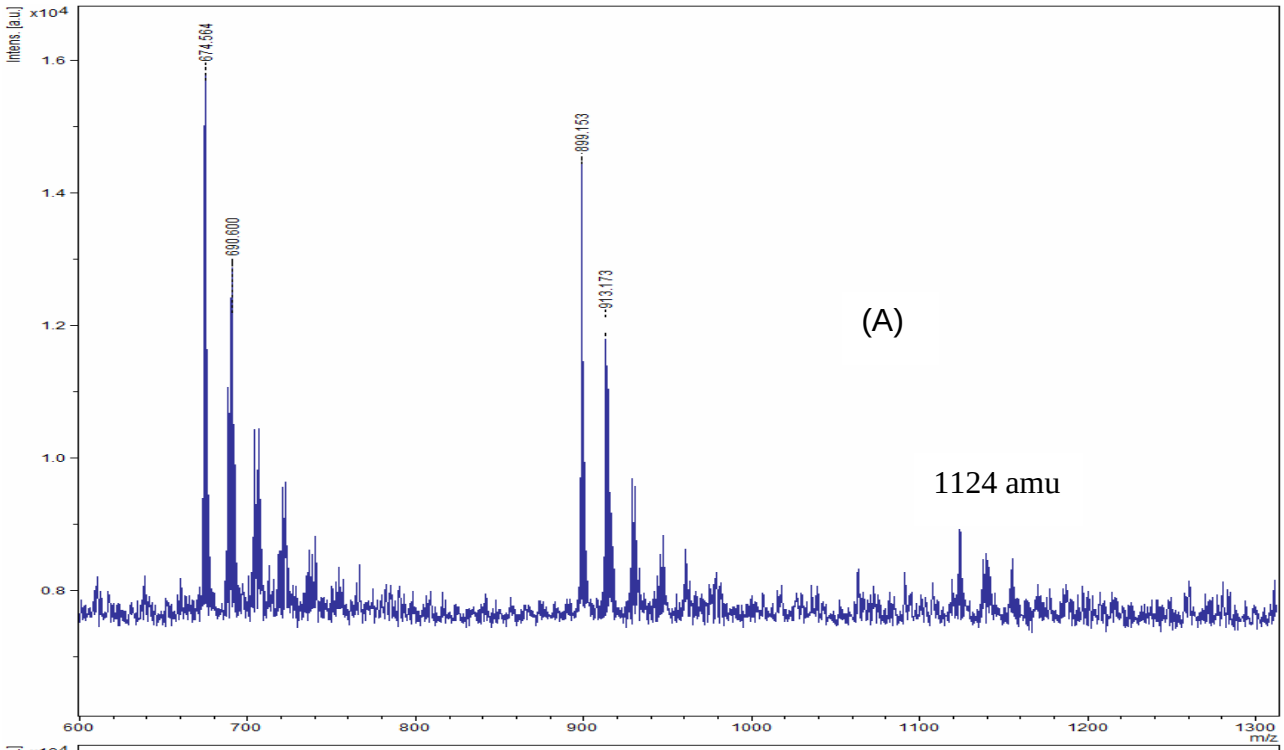
Intens. [a.u.]
x10⁴
1.6
1.4
1.2
1.0
0.8
674.564
690.600
899.153
913.173
(A)
1124 amu
600
700
800
900
1000
1100
1200
1300
m/z

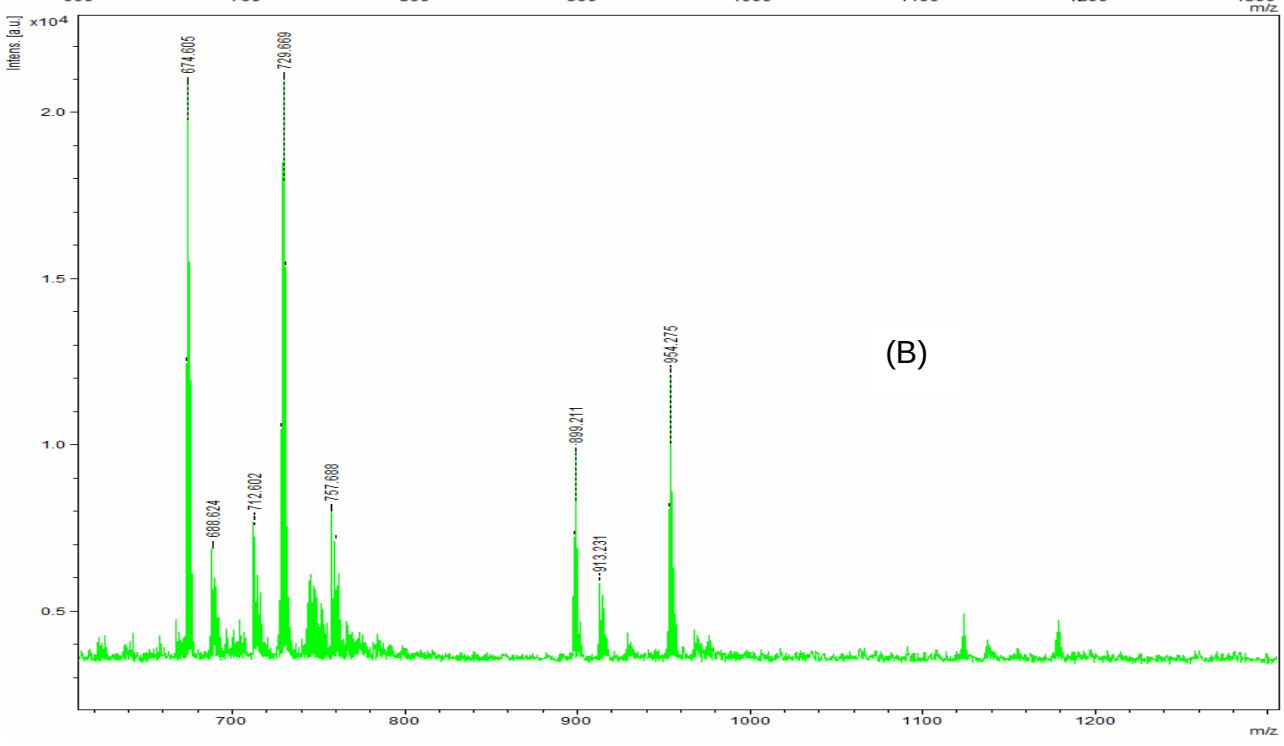
Intens. [a.u.]
x10⁴
2.0
1.5
1.0
0.5
674.605
688.624
712.602
729.669
757.688
899.211
913.231
954.275
(B)
700
800
900
1000
1100
1200
m/z

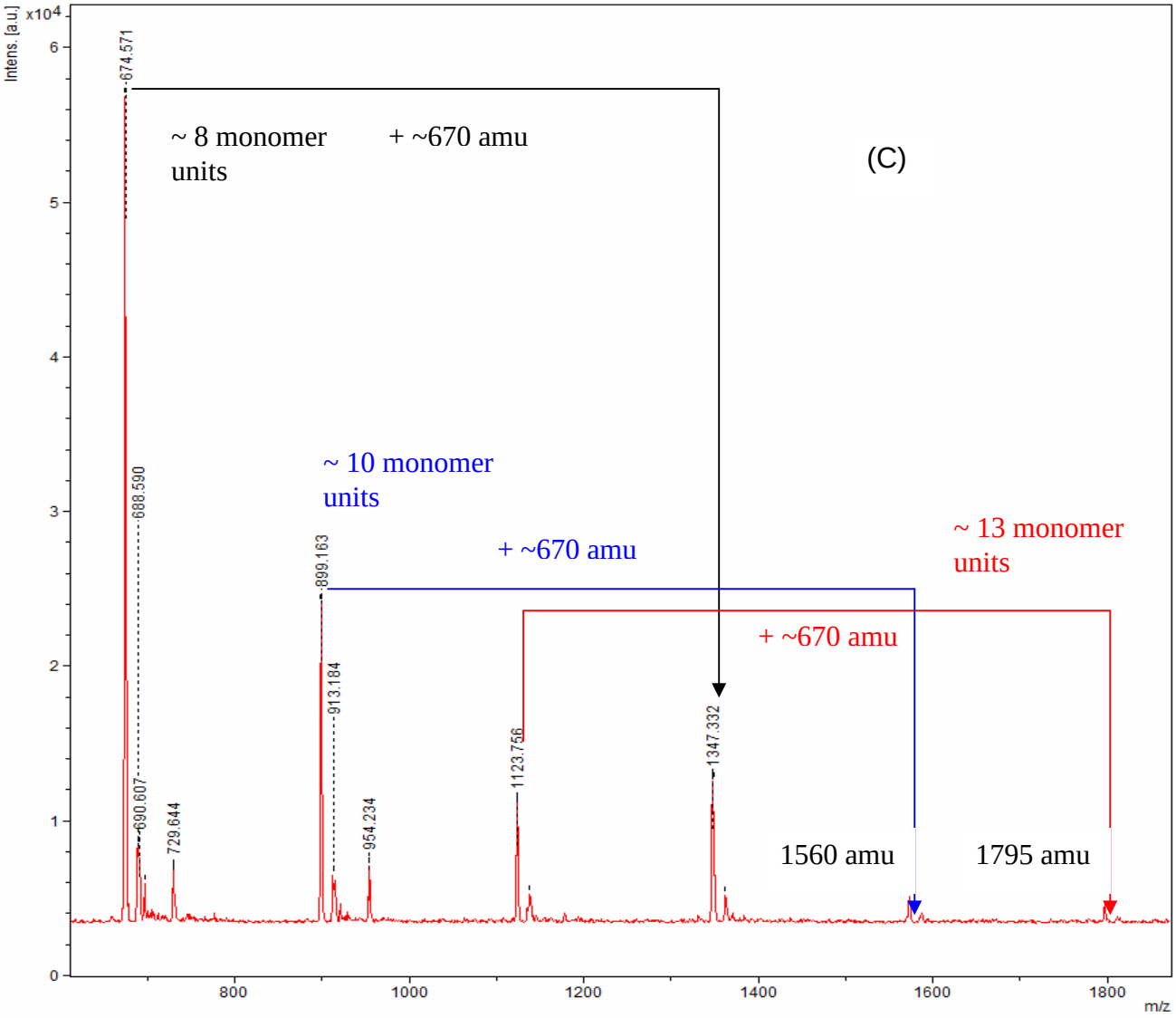

Fig. 3.16: Mass spectra of (A) PMAA alone, (B) $ZnPc(NH_2)_4$ mixed with PMAA and (C) $ZnPc(NH_2)_4$ linked to PMAA.

3.4.5 UV/Vis spectra of polymer films of Pc-polymer conjugates

Film thickness was determined by utilization of the knife-edge attachment of the XRD to physically measure the thickness of the films that were removed from the glass slides. Several measurements were taken of various films, and an average film thickness of each Pc/Polymer on glass was 95 μm.

Complexes **15** and **16** showed no aggregation when linked or mixed with the polymer, as evidenced by UV/Vis spectra, Fig. 3.17 (A and B). Both of these

complexes are octasubstituted with COOH and are known not to aggregate in solution [185]. Fig. 3.17A and B shows that the spectra of polymer mixed and linked complexes **15** and **16** are red shifted compared to solution spectra as is typical for solid state [186]. Complex **14** showed extensive aggregation when linked or mixed with the PMAA, compared to the DMSO solution (insert), Fig. 3.17C.

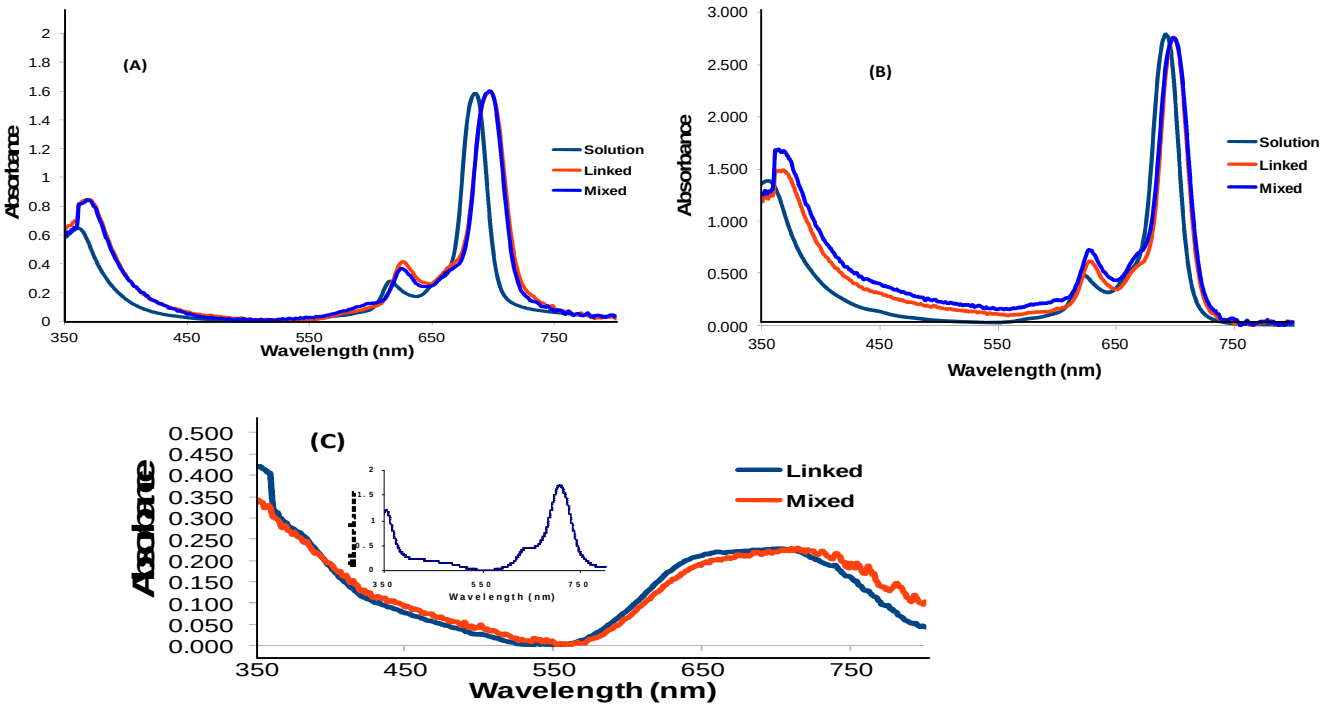

Fig. 3.17: UV-Visible spectra of phthalocyanines (A) **16**, (B) **15** and (C) **14** mixed and linked to polymers (PMAA for **15** and **16**, and PEI for **14**). Solution spectra for **15** and **16** were recorded in water, (pH 10). The spectra of mixed or linked complexes were of films (therefore solid state). Insert in C is the spectrum of **14** in a DMSO solution.

3.5 Characterisation of Pcs in the presence of NMs in solution

3.5.1 Pcs and CdTe-TGA QDs

Fig. 3.18 shows the effects on the UV-Vis spectra of Pcs on addition of CdTe-TGA QDs in DMSO:water (see Table 3.1). The ratio of MPc: QDs (97:1 mole ratio) was chosen due to the good OL properties after a series of ratios were tested. Complexes **6**, **7**, **12** and **14** still show monomeric behavior in the presence of QDs. Aggregation of phthalocyanines in the presence of QDs has been reported for quaternized derivatives [187, 188]. Aggregation is judged by broadening or splitting of the Q-band. Complexes **5**, **9**, **10** and **13** show considerable aggregation on addition of QDs, whereas aggregation for **11** is less severe in the presence of QDs. Complex **8** shows no spectral alteration on the addition of QDs. Aggregates could be broken on addition of Triton X 100. There is no change in the Q-band maxima of the monomeric Pcs **6**, **7**, **12** and **14** in the presence of CdTe-TGA QDs, Table 3.1, in DMSO:water.

The ratio of Pcs to QDs (97:1) were the same for all the spectra in Fig. 3.18, hence the observed aggregation in DMSO:water in the presence of QDs cannot be related to the differences in the concentration of the QDs. It is known that addition of salts to phthalocyanine solution results in increased aggregation [189]. The observed effects of QDs on the spectra of Pcs could be related to the salting effect of QDs, which could be substituent dependent.

When CdTe QDs were added to positively charged MPc complexes, the reduction of the latter was observed [188]. It was also reported that it was the capping agent that was involved in the reduction [188]. Since the MPc complexes in the reported work [188] were positively charged, and on addition of QDs showed spectra which was not

typical of ring reduction in MPc complexes, it was suggested that reduction occurs on the quaternized nitrogens. In the current work, the MPcs are neutral, and the spectral changes observed are typical of aggregated Pcs [30], we assign the observed spectral changes to formation of aggregates. Interestingly, it was determined that it was not the QDs' capping agent responsible for the aggregation, but the capped QDs themselves. Aggregates between Zn porphyrins and CdSe QDs have been reported through pyridyl linker groups [190]. The nature of the aggregates obtained in this work is not clear. The small changes in the Q band wavelength for some complexes could be attributed to change in the environment in the presence of QDs.

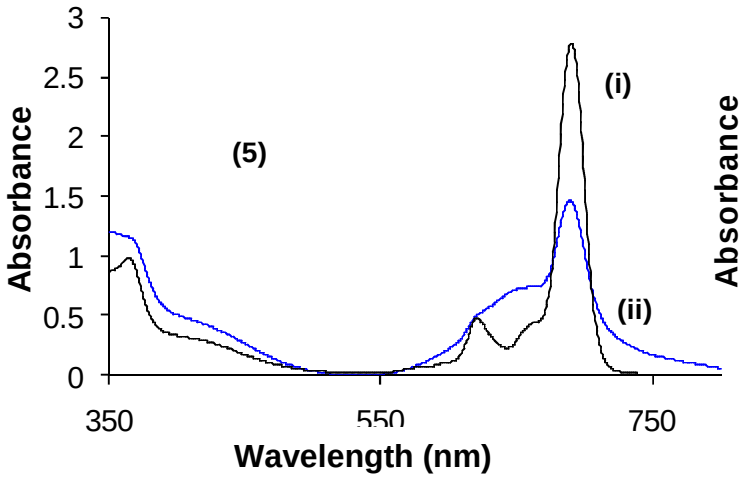
(5)
(i)
(ii)
Absorbance
Wavelength (nm)
0
0.5
1
1.5
2
2.5
3
350
550
750

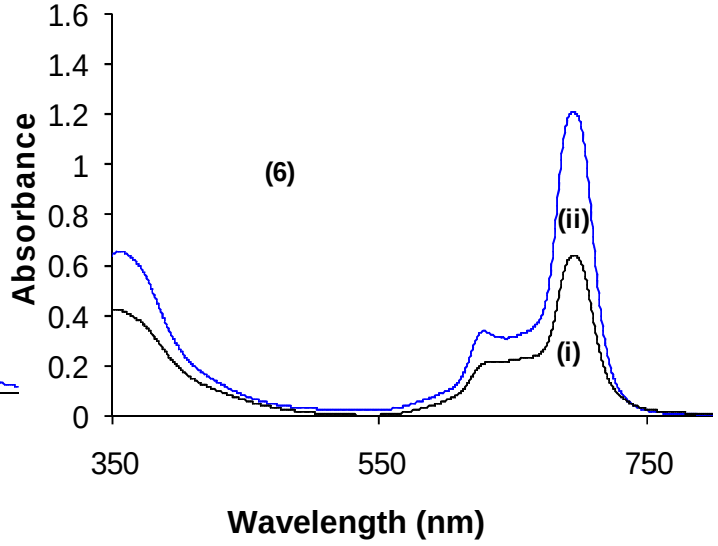
(6)
(ii)
(i)
Absorbance
Wavelength (nm)
0
0.2
0.4
0.6
0.8
1
1.2
1.4
1.6
350
550
750

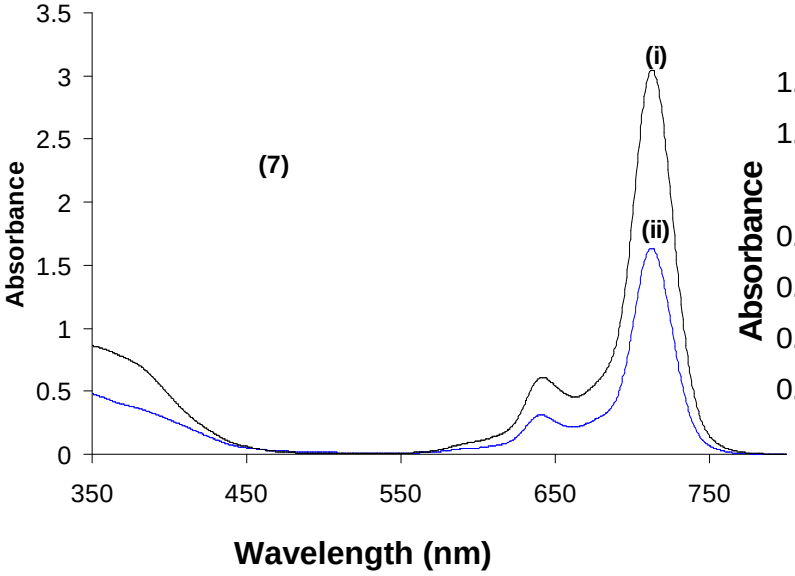
(7)
(i)
(ii)
Absorbance
Wavelength (nm)
0
0.5
1
1.5
2
2.5
3
3.5
350
450
550
650
750

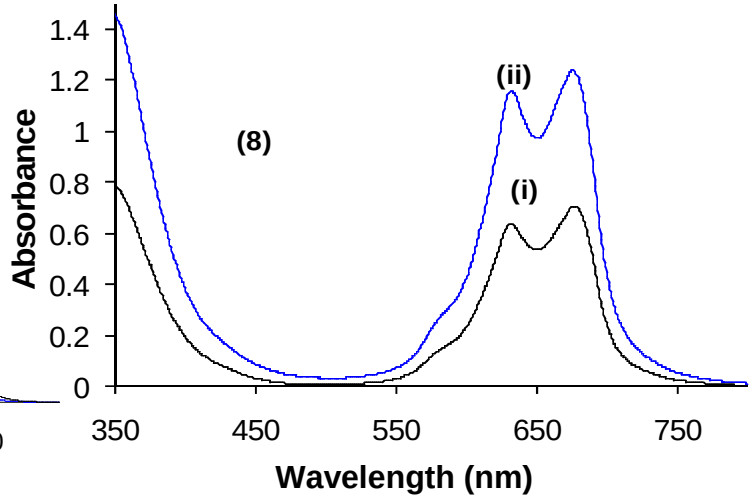
(8)
(ii)
(i)
Absorbance
Wavelength (nm)
0
0.2
0.4
0.6
0.8
1
1.2
1.4
350
450
550
650
750

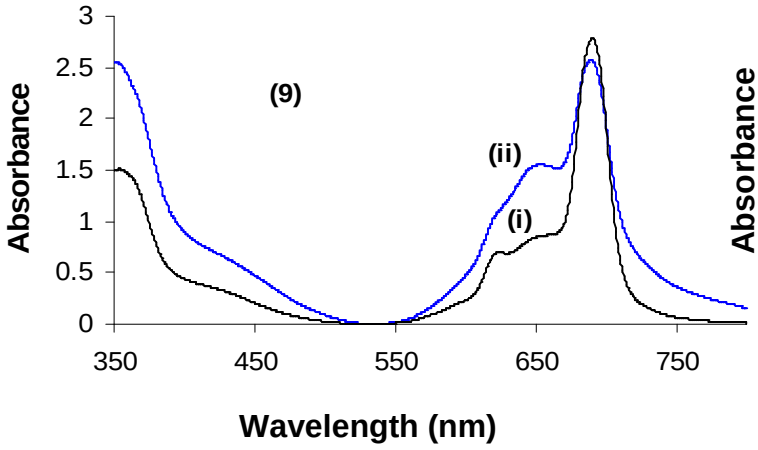
(9)
(ii)
(i)
Absorbance
Wavelength (nm)
0
0.5
1
1.5
2
2.5
3
350
450
550
650
750

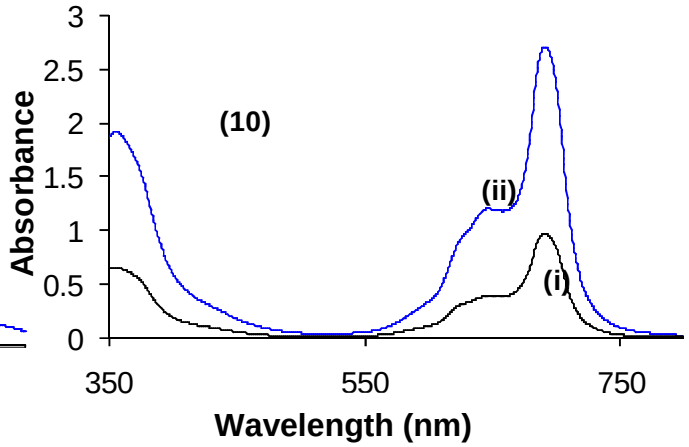
(10)
(ii)
(i)
Absorbance
Wavelength (nm)
0
0.5
1
1.5
2
2.5
3
350
550
750

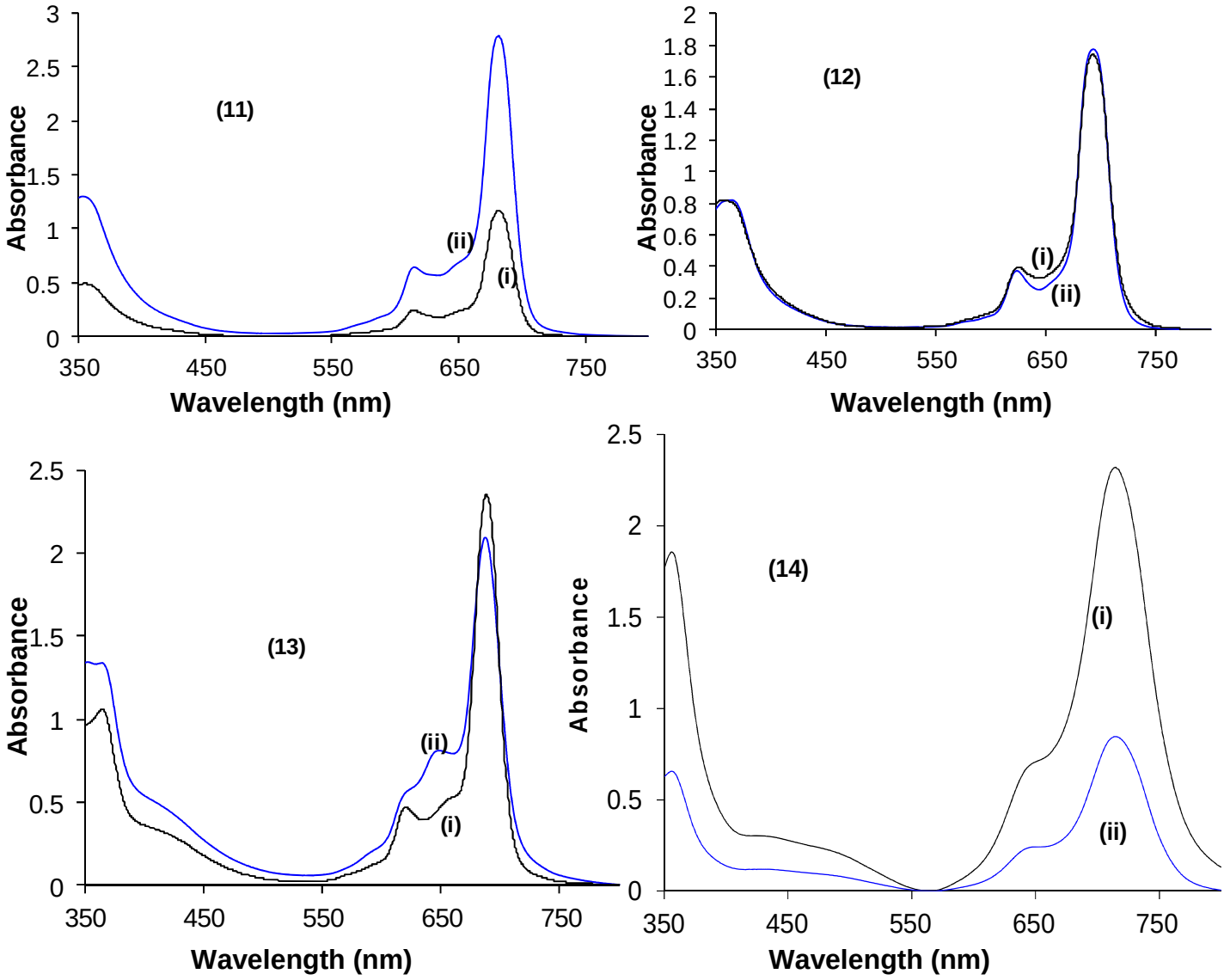

Fig. 3.18: Absorption Spectra of the studied phthalocyanines (**5**-**14**) with and without CdTe-TGA (97:1 mol ratio). Concentration: 7.16 x 10^{-6} to 3.26 x 10^{-5} M. Spectra of MPc without (i) and with (ii) QDs in DMSO:water.

*3.5.2 Complex **7** with fullerenes, SWCNTs, CdSe-TGA and CdS-TGA spectra.*

Figure 3.19 shows the spectrum of complex **7** in solution (DMSO) alone and in the presence of the other NMs {either DMF:water (9:1) or DMF:toluene (9:1) depending on the NM}. There is slight but significant blue shifting of the spectrum of **7** in the presence of the NMs in solution (Fig. 3.19A and B), Table 3.5. The spectra were run three times and consistently gave a similar results. The data in Table 3.5 was obtained from UV-visible spectra.

The blue-shifting of the Pc monomer band when the NMs are present is most likely due to the NMs behaving like electron acceptors to the Pcs and causing an increase in highest occupied molecular orbital (HOMO) to lowest unoccupied molecular orbital (LUMO) gap. Both CdTe QDs and SWCNT are known electron acceptors [191, 192]. Electron withdrawing groups increase the HOMO-LUMO gap resulting in blue shifting of the Q band [193].

Table 3.5: Spectral data of complex **7** in the presence of nanomaterials

Complex or mixture	$\lambda_{Q\ band}$ (nm)	
	DMF:water (9:1)	PMMA film
7 alone	710	713
7 + CdS-TGA	706	710
7+CdSe-TGA	708	710
7 + Fullerene	704	709
7+ SWCNT	704	709

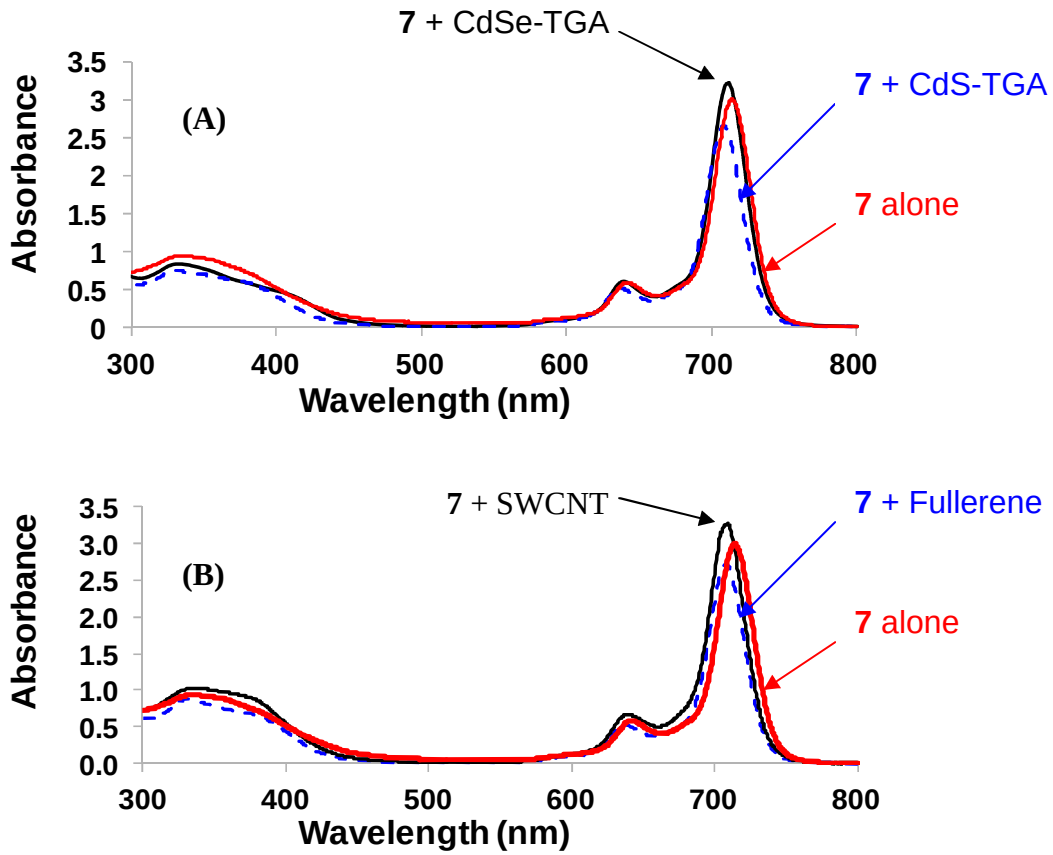

Fig. 3.19: UV-Visible spectra of complex **7** and QDs (A) and complex **7** and other NMs (B) in solution (DMF:water (9:1) for all except **7** + fullerenes which are in DMF:toluene (9:1)).

3.6 Pcs and NMs embedded in polymer films

3.6.1 Characterization of polymer films of Pcs alone

The UV-Visible spectra of the phthalocyanines alone in PMMA films (see Fig. 3.20) show aggregation.

Complexes **6**, **7**, **11**, **12**, **13** and **14** showed a monomer peak (lower energy) which was more intense than the aggregate (higher energy), Fig. 3.20. Complexes **8**, **9**, **10** all octa substituted with benzyloxy phenoxy groups shows the aggregate peak to

either be slightly less intense, or more intense than, the monomer peak, Fig. 3.20, suggesting that octasubstitution with this substituent encourages a greater amount aggregation especially in the solid state.

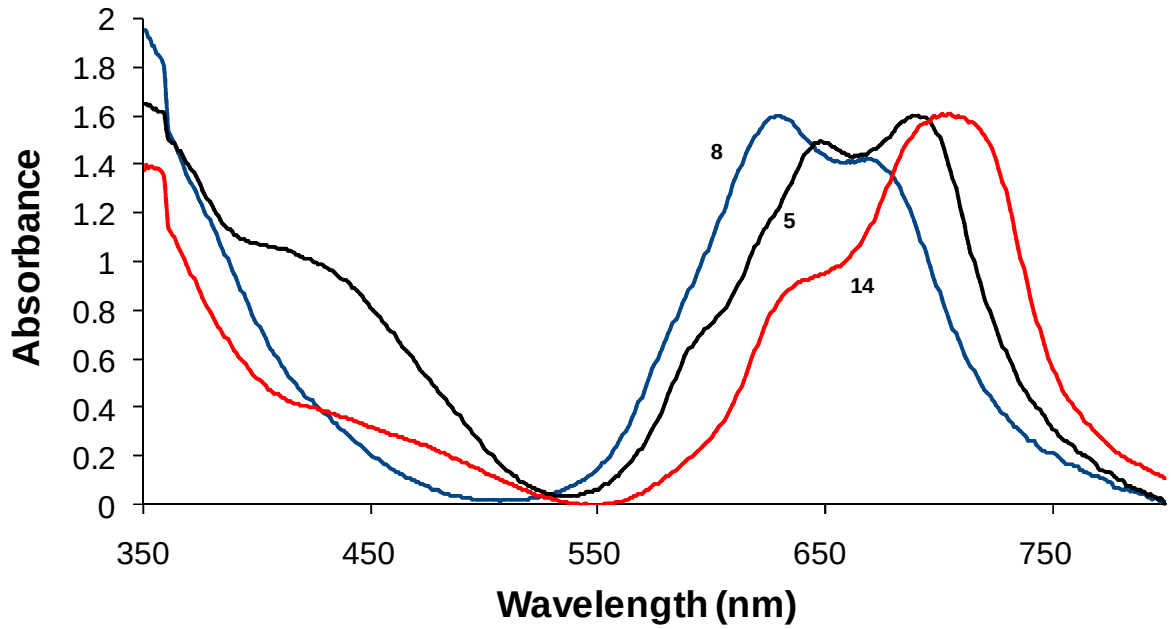

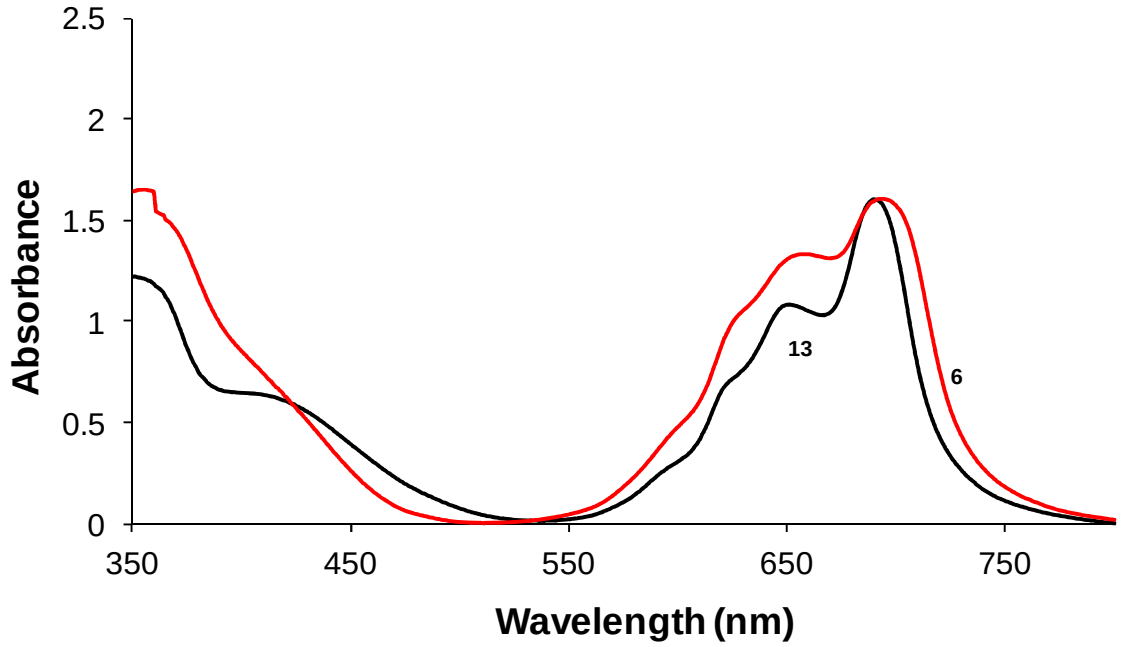

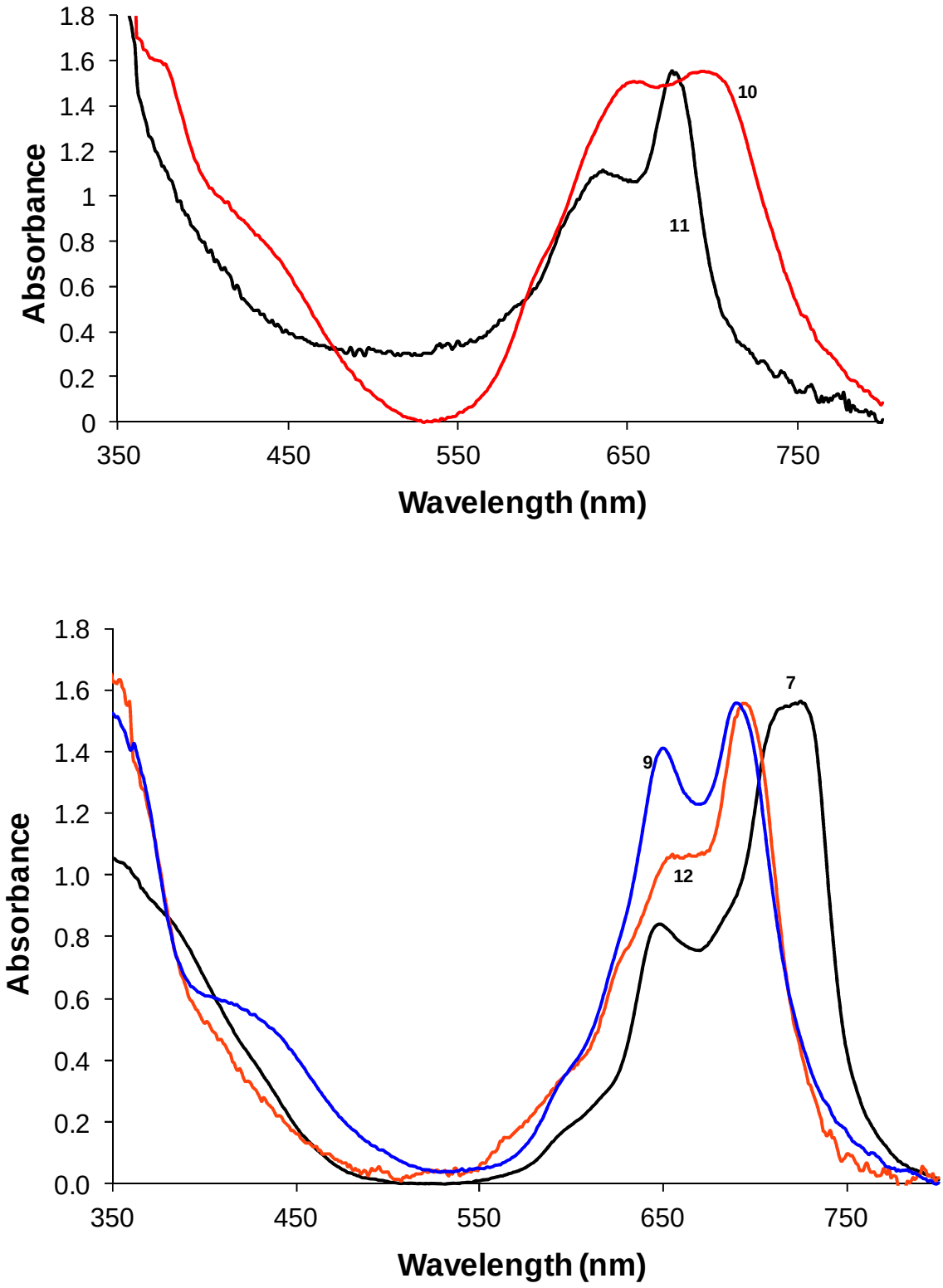

Fig. 3.20: UV-Visible spectra of phthalocyanines **5**-**14** in PMMA thin films.

3.6.2 Pcs combined with CdTe-TGA in PMMA films.

Compared to when alone in the polymer, Pcs are less aggregated in the presence of CdTe QDs, Fig. 3.21 (using **6**, **7**, **9**, **11**, **13** and **14** as examples). The presence of QDs and Pcs within the polymer seems to reduce the co-planar association of the rings. In solution, there was enhanced aggregation for some complexes (**5**, **8**, **9**, **10** and **13**), as discussed above (Fig. 3.18).

Complexes **8**, **9** and **10** (all containing benzyloxy phenoxy substituents) showed extensive aggregation compared to the rest of the complexes in PMMA films and in the absence of CdTe QDs, only **9** shown in Fig. 3.21. However, Fig. 3.22 comparing the spectra these MPc complexes in the presence CdTe-TGA QDs and in PMMA films, shows complex **9** to be less aggregated compared to **8** and **10**. This is not to say that complex **9** has no aggregation, just significantly less aggregation than the other two complexes. The most aggregated complex in Fig. 3.22 is **8**, with a high energy band (due to the aggregate) being about the same height as the low energy band (due to the monomer). The extensive aggregation for complex **8** could be a result of the lack of axial ligand coordinated to the central metal zinc, unlike in the case of complexes **9** and **10**.

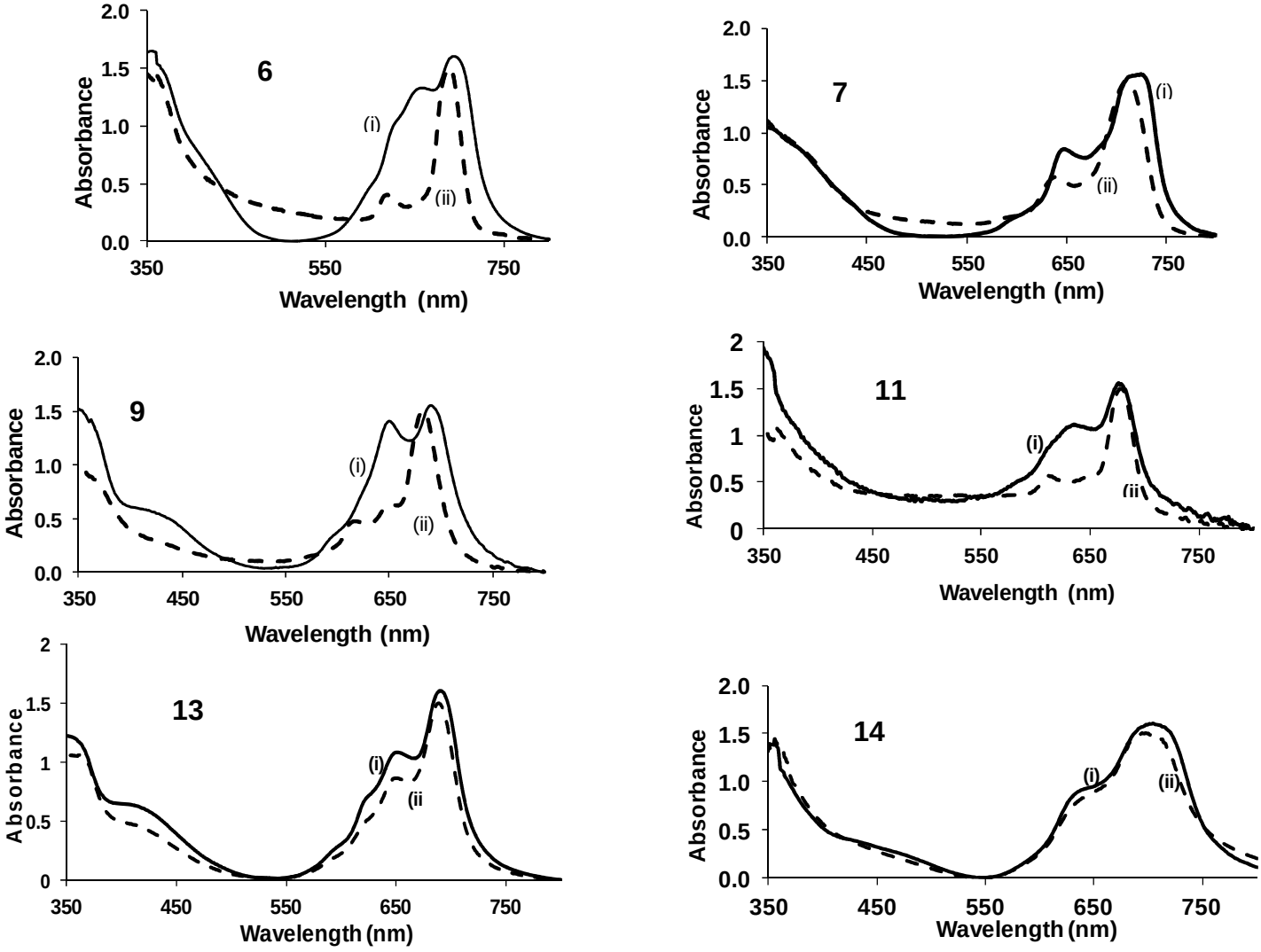

Fig. 3.21: UV-Visible spectra of complexes **6**,**7**,**9**,**11**,**13**,**14** as thin films in the absence (i) and presence (ii) of CdTe QDs.

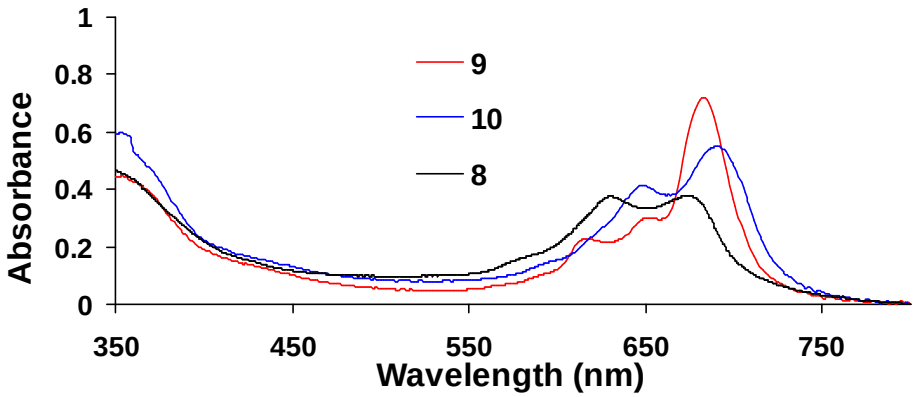

Fig. 3.22: UV-Visible spectra of phthalocyanines **8,9,10** combined with CdTe-TGA in PMMA thin films.

*3.6.3 Phthalocyanine **7** combined with other NMs in PMMA films.*

Fig. 3.23 indicates that no significant aggregation or shifting of Q-bands occurs when the complex **7**/NM mixtures are placed within PMMA films, though there does seem to be a slight broadening of the Q-band.

Figure 3.23 shows that there is less aggregation for Pc in polymer and in the presence of fullerenes, SWCNT and CdS-TGA QDs. For CdSe-TGA the aggregation is still evident. For **7** in the presence of CdTe-TGA QDs, the narrowing of spectra was discussed above, Fig. 3.21. Blue-shifting occurs in polymer films compared to **7** alone as was the case in solution, Table 3.5.

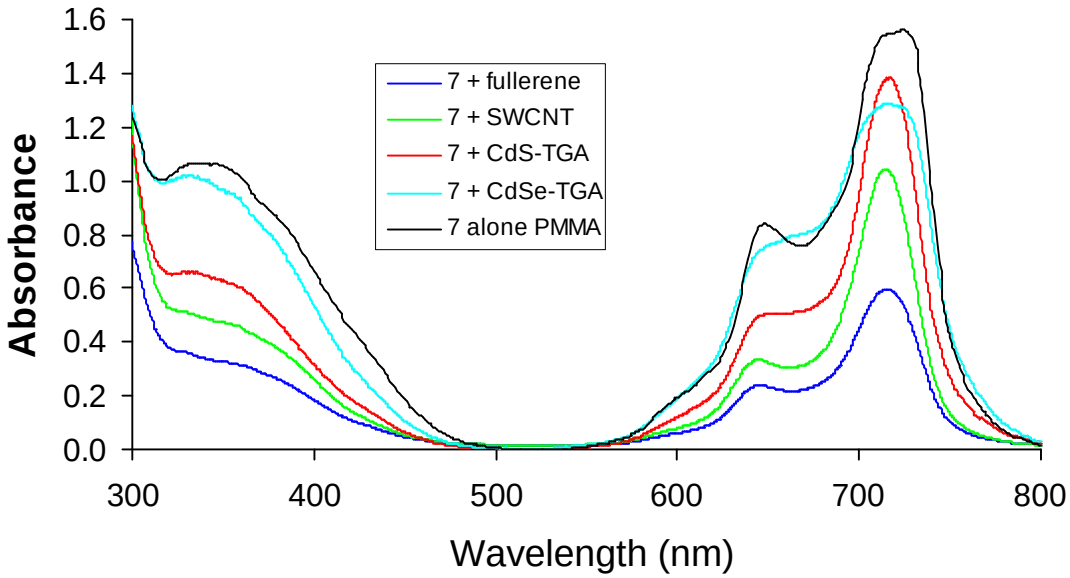

Fig. 3.23: Phthalocyanine **7** in the presence of the rest of the NMs embedded in PMMA film.

3.7 Triplet state studies of phthalocyanines in the absence and presence of quantum dots.

Fig. 3.24 shows the triplet decay curves of complex **8** in the presence and absence of QDs. Both curves obeyed first order kinetics. This is typical of Pc complexes that are pure and not at very high concentrations, as opposed to second order kinetics which occur at high concentrations (>1 $\times$ 10^{-5} M) [194, 195] due to triplet–triplet recombination. Φ_T values in DMSO: water are smaller than in DMSO alone for Pcs alone, Table 3.6. Water is known to quench the triplet state of the Pc complexes, hence the observation of low Φ_T values in the presence of water [196] is not surprising. τ_T values generally decreased in DMSO:water with the exception of **5**, **6**, **13** and **14**. In general the Φ_T values are larger for MPc complexes containing heavier

metals (In and Ga) in DMSO, which can be seen in Table 3.6. QDs are known to increase Φ_T values of Pcs due to the heavy atom effect [197], and this is observed in Table 3.6 in general with the exception of complex **5** in DMSO:water. Aggregation of the complexes in the presence of QDs is expected to reduce Φ_T values, however this turned out not to be the case in Table 3.6. For example complexes that are aggregated in the presence of QDs (**5**, **8**, **9**, **10** and **13**) show larger Φ_T values compared to **6** and **7** which are not aggregated in the presence of QDs. τ_T values have been reported to increase in the presence of QDs depending on the solvent [171, 188]. In Table 3.6, there is a decrease (in the presence of QDs) in τ_T values for complexes **5**, **8**, **11** and **13**, which are aggregated, there is no change in τ_T values for **7**, **10** and **12**, and there is an increase for **6**, **9** and **14**, Table 3.6.

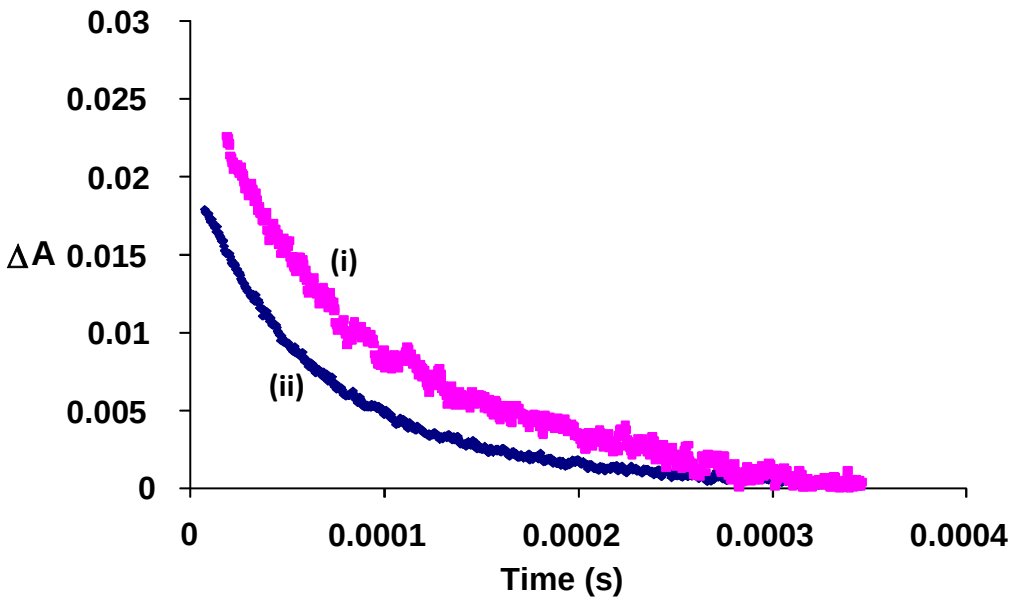

Fig. 3.24: Triplet decay curve of compound **8** in the absence (i) and presence (ii) of QDs in DMSO:water (9:1).

Table 3.6: Phthalocyanines **5** – **14** photophysical parameters in presence and absence of CdTe-TGA QDs.

Substance	Solvent	Φ_T	τ_T (μs) ± 1
5	DMSO DMSO:water (9:1)	0.70 0.38	50 420
5 + CdTe-TGA	DMSO:water (9:1)	0.34	320
6	DMSO DMSO:water (9:1)	0.59 0.032	40 50
6 + CdTe-TGA	DMSO:water (9:1)	0.079	60
7	DMSO DMSO:water (9:1)	0.60 0.063	50 40
7 + CdTe-TGA	DMSO:water (9:1)	0.12	40
8	DMSO DMSO:water (9:1)	0.47 0.055	200 130
8 + CdTe-TGA	DMSO:water (9:1)	0.21	80
9	DMSO DMSO:water (9:1)	0.74 0.22	200 150
9 + CdTe-TGA	DMSO:water (9:1)	0.24	180

10	DMSO DMSO:water (9:1)	0.89 0.011	70 50
10 + CdTe-TGA	DMSO:water (9:1)	0.094	50
11	DMSO DMSO:water (9:1)	0.60 0.31	210 190
11 +CdTe-TGA	DMSO:water (9:1)	0.46	110
12	DMSO DMSO:water (9:1)	0.69 0.052	50 40
12 + CdTe-TGA	DMSO:water (9:1)	0.075	40
13	DMSO DMSO:water (9:1)	0.84 0.59	60 340
13 + CdTe-TGA	DMSO:water (9:1)	0.70	220
14	DMSO DMSO:water (9:1)	0.47 0.27	5 5
14 +CdTe-TGA	DMSO:water (9:1)	0.66	20

Chapter 4

Nonlinear Parameters

4. NLO studies

Obtained experimental data were best fitted to two photon absorption. It is expected that the sequential two-photon absorption mechanism which is typical of phthalocyanines and has been especially effective at producing large nonlinear absorption, occurs [123].

It has been reported that nonlinear absorption coefficients can give rise to varied signals depending on the repetition rate of the laser and on the experimental conditions [198]. Thermal heating effects have been reported at high repetition rates [199]. In this work, by changing the repetition rate, very weak new peaks occasionally appeared at the lower repetition rates, probably due to localized heating resulting in formation of bubbles and hence scattering. The fitting program generally overlooks these small peaks when creating the fitting curve; hence the reported results were not affected. It was noted that as the repetition rate was lowered for the laser, the average energy detected by the Z-scan setup increased from ~15 μJ to ~18 μJ. It may be this increase in the energy that can account for the thermal heating. All comparative Z-scan analysis were done at ~15 μJ and 20 Hz repetition rate, thus lowering the likelihood of thermal heating. Three measurements were taken for each sample and the reported results are the averaged values obtained.

4.1 Solution studies.

4.1.1 Pcs alone.

Open aperture Z-scan spectra (see Fig. 4.1, using complexes **9** and **10** as examples) were collected for a single pulse energy for each compound and showed RSA [200, 201]. A Z-scan measures the compounds' transmittance at a certain wavelength, in this case 532 nm, as the compound is moved along the path of a laser which has been focused by a lens. The theory of Sheikh-Bahae et al. [150, 202] was used to fit the open aperture data, and the imaginary third-order susceptibilities, $Im[\chi^{(3)}]$ (esu) and the second molecular hyperpolarizabilities, γ (esu) were calculated from the fits. The waist radius (ω_0) of the beam was treated as a free parameter in the fitting algorithm because of the fluctuating nature of the laser employed and the effect that the nonlinear material has on the light's refraction. Complexes **5**-**14** exhibited on average ω_0 = 25.55 μm in all cases. For complex **14**, $ZnPc(NH_2)_4$, SA was observed when it was linked to PMAA.

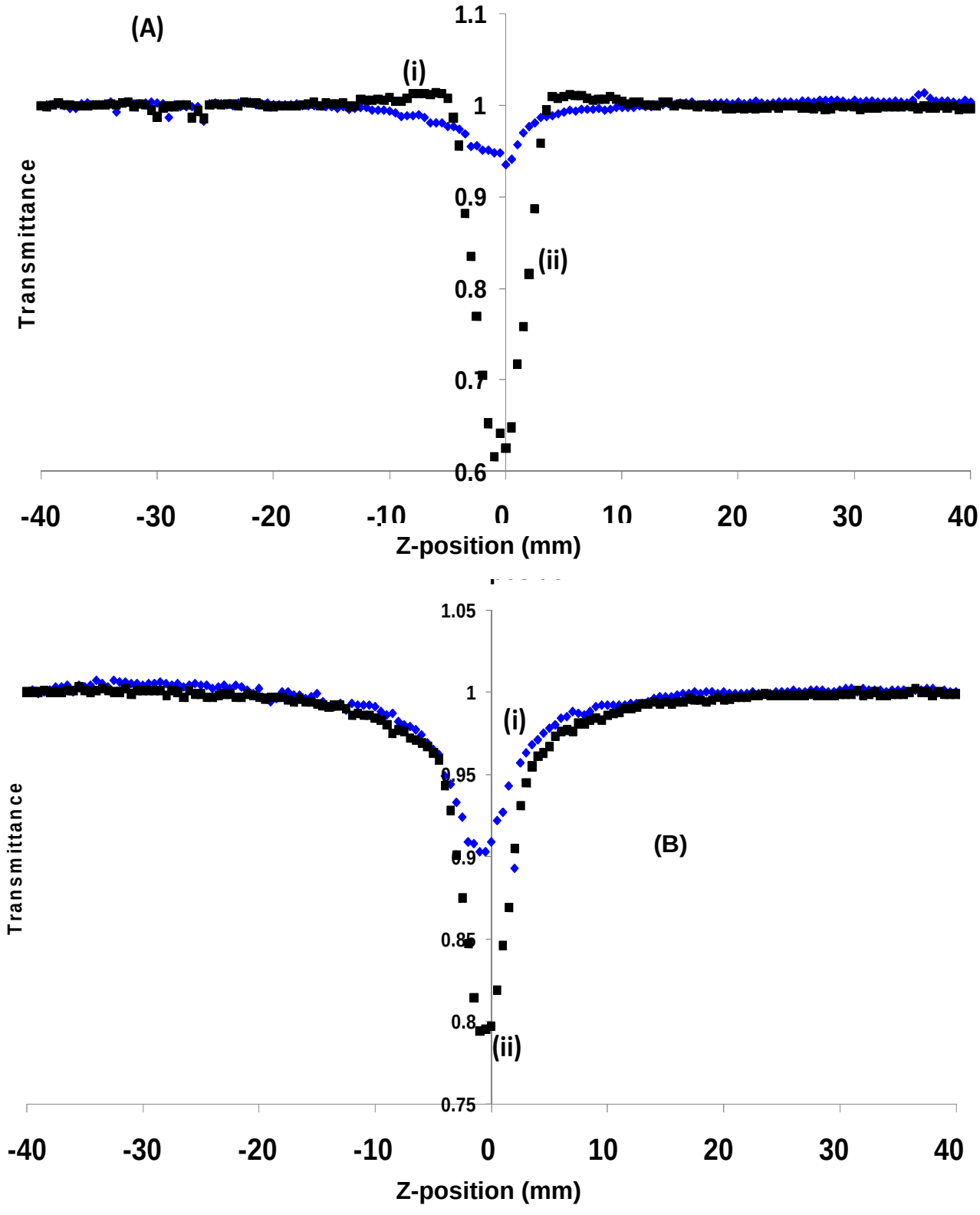

Fig. 4.1: Z-scan spectra of complexes **9** (A) and **10** (B) without (i) and with (ii) CdTe-TGA. Solvent: DMSO:water 9:1.

The $Im[\chi^{(3)}]$ and γ were calculated using equations 1.10 and 1.12 respectively. Table 4.1 summarizes the third-order susceptibility data in solution for the compounds analyzed with the Z-scan. A decent range for imaginary third-order susceptibilities ($Im[\chi^{(3)}]$) is generally 10^{-11} to 10^{-9} esu [203]. The values Table 4.1 for Pcs in the absence of QDs are in the lower end of this range. For hyperpolarizability (γ) the reported range is 10^{-34}-10^{-29} esu.L [151] and the values in Table 4.1 fall within the upper portion of this range, ranging from 10^{-31}-10^{-29} esu.L for Pcs in the absence of QDs. The possible reason why the $Im[\chi^{(3)}]/\alpha$ values trend deviates form the β values trend could be because of either aggregation of the sample, scattering caused by the sample or nonlinear refraction caused by the sample (or any combination of these three). Any of these three phenomena could could cause significant deviation of the nonlinear behaviour of the sample in comparison to the nonlinear behaviour a monomeric, non-scattering sample may produce without it being accounted for by the α value. This would mean that the constants calculated from $(Im[\chi^{(3)}]/\alpha)/\beta$ for these samples would be different to the monomeric samples. Also, the $(Im[\chi^{(3)}]/\alpha)/\beta$ constants would be different for a pure DMSO solution compared to a DMSO-water solution because of a slight difference existing between their refractive indexes and the introduction of QDs may also influence this constant, though these differences may also be because certain solvent systems cause aggregation whilst others don't.

Let us consider the optimal ranges of γ and $Im[\chi^{(3)}]$. If the values of either of them are of a magnitude smaller than the optimal range, then the optical limiting effect will be too small to significantly reduce the light's intensity and the light will still have the possibility to damage the eye. If the magnitudes are higher than the optimal region then the optical limiter would probably start to behave more like a filter and potentially cut off a wavelength in the linear absorption region from being observed.

Whilst this may save one's eye, it would prove to be problematic in terms of viewing a particular wavelength.

Nonlinear absorption is known to increase with triplet state yield [126]. High triplet lifetimes should also improve on the nonlinear absorption properties of the MPc complexes. The third-order susceptibility values in Table 4.1 are generally larger in DMSO than in DMSO:water due to the larger Φ_T values in the former. Low Φ_T (<0.1) values in DMSO:water and in the absence of QDs are observed for half of the complexes except **5**, **9**, **11**, **13** and **14**, hence the latter complexes will be expected to give increased third-order susceptibility parameters in DMSO:water.

Table 4.2 summarizes F_{sat} and I_{lim} values in solution for Pcs in the absence and presence of QDs. I_{lim} values were calculated using equation 1.9 and Fig. 4.2 shows the plots from which I_{lim} and F_{sat} were obtained. Trends in these values are discussed below.

Table 4.1: Third-order susceptibility values of studied phthalocyanines and Pc:QD (97:1 mole ratios) mixtures.

Substance	Solvent	Im[$\chi^{(3)}$] (esu)	Im[$\chi^{(3)}$]/α (esu.cm)	γ (esu.L)	Φ_T	τ_T (μs)	β (cm/MW)
5	DMSO	8.54×10^{-11}	2.67×10^{-11}	2.39×10^{-30}	0.70	50	2.46×10^{-2}
	DMSO:water (9:1)	4.12×10^{-12}	2.79×10^{-12}	2.49×10^{-31}	0.38	420	1.17×10^{-2}
5 + CdTe-TGA	DMSO:water (9:1)	3.80×10^{-10}	2.60×10^{-10}	2.32×10^{-29}	0.34	320	1.09×10^{-1}
6	DMSO	8.97×10^{-11}	3.46×10^{-11}	2.09×10^{-30}	0.59	40	2.58×10^{-2}
	DMSO:water (9:1)	2.01×10^{-11}	1.64×10^{-11}	9.92×10^{-31}	0.032	50	5.70×10^{-2}

Substance	Solvent	Im[$\chi^{(3)}$] (esu)	Im[$\chi^{(3)}$]/α (esu.cm)	γ (esu.L)	Φ_T	τ_T (μs)	β (cm/MW)
6 + CdTe-TGA	DMSO:water (9:1)	2.39×10^{-11}	1.97×10^{-11}	1.19×10^{-30}	0.079	60	6.87×10^{-3}
7	DMSO	4.37×10^{-11}	1.46×10^{-11}	1.02×10^{-30}	0.60	50	1.26×10^{-2}
	DMSO:water (9:1)	3.75×10^{-12}	1.44×10^{-12}	1.00×10^{-31}	0.063	40	1.06×10^{-2}
7 + CdTe-TGA	DMSO:water (9:1)	1.21×10^{-11}	7.40×10^{-12}	5.14×10^{-31}	0.12	40	3.49×10^{-3}
8	DMSO	2.88×10^{-11}	3.28×10^{-11}	2.17×10^{-30}	0.47	200	8.29×10^{-3}
	DMSO:water (9:1)	1.29×10^{-11}	7.18×10^{-12}	4.76×10^{-31}	0.055	130	3.67×10^{-2}
8 + CdTe-TGA	DMSO:water (9:1)	6.18×10^{-11}	4.99×10^{-11}	3.31×10^{-30}	0.21	80	1.78×10^{-2}
9	DMSO	3.95×10^{-11}	1.44×10^{-11}	1.69×10^{-30}	0.74	200	1.14×10^{-2}
	DMSO:water (9:1)	1.12×10^{-11}	1.44×10^{-11}	1.69×10^{-30}	0.22	150	3.17×10^{-2}
9 + CdTe-TGA	DMSO:water (9:1)	3.34×10^{-10}	1.30×10^{-10}	1.53×10^{-29}	0.24	180	9.61×10^{-2}
10	DMSO	9.21×10^{-11}	3.50×10^{-11}	4.12×10^{-30}	0.89	70	2.65×10^{-2}
	DMSO:water (9:1)	4.14×10^{-12}	4.17×10^{-12}	4.91×10^{-31}	0.011	50	1.18×10^{-2}
10 + CdTe-TGA	DMSO:water (9:1)	1.50×10^{-10}	5.56×10^{-11}	6.55×10^{-30}	0.094	50	4.33×10^{-2}
11	DMSO	4.81×10^{-11}	1.74×10^{-11}	1.30×10^{-30}	0.60	210	1.39×10^{-2}
	DMSO:water (9:1)	5.42×10^{-12}	1.98×10^{-12}	1.47×10^{-31}	0.31	190	1.54×10^{-2}
11 +CdTe-TGA	DMSO:water (9:1)	5.04×10^{-11}	1.81×10^{-11}	1.34×10^{-30}	0.46	110	1.45×10^{-2}

Substance	Solvent	Im[$\chi^{(3)}$] (esu)	Im[$\chi^{(3)}$]/α (esu.cm)	γ (esu.L)	Φ_T	τ_T (μs)	β (cm/MW)
12	DMSO	5.62×10^{-11}	2.09×10^{-11}	1.78×10^{-30}	0.69	50	1.62×10^{-2}
	DMSO:water (9:1)	3.22×10^{-12}	2.33×10^{-12}	1.99×10^{-31}	0.052	40	9.14×10^{-3}
12 + CdTe-TGA	DMSO:water (9:1)	2.41×10^{-11}	1.36×10^{-11}	1.16×10^{-30}	0.075	40	6.94×10^{-3}
13	DMSO	4.53×10^{-11}	2.08×10^{-11}	1.15×10^{-30}	0.84	60	1.31×10^{-2}
	DMSO:water (9:1)	4.00×10^{-12}	3.11×10^{-12}	1.71×10^{-31}	0.59	340	1.14×10^{-2}
13 + CdTe-TGA	DMSO:water (9:1)	4.93×10^{-11}	2.36×10^{-11}	1.30×10^{-30}	0.70	220	1.42×10^{-2}
14	DMSO	7.82×10^{-11}	5.41×10^{-11}	1.82×10^{-30}	0.47	5	2.40×10^{-2}
	DMSO:water (9:1)	1.35×10^{-11}	7.44×10^{-12}	2.18×10^{-31}	0.27	5	3.82×10^{-2}
14 +CdTe-TGA	DMSO:water (9:1)	4.12×10^{-12}	5.06×10^{-12}	1.49×10^{-31}	0.66	20	1.17×10^{-2}

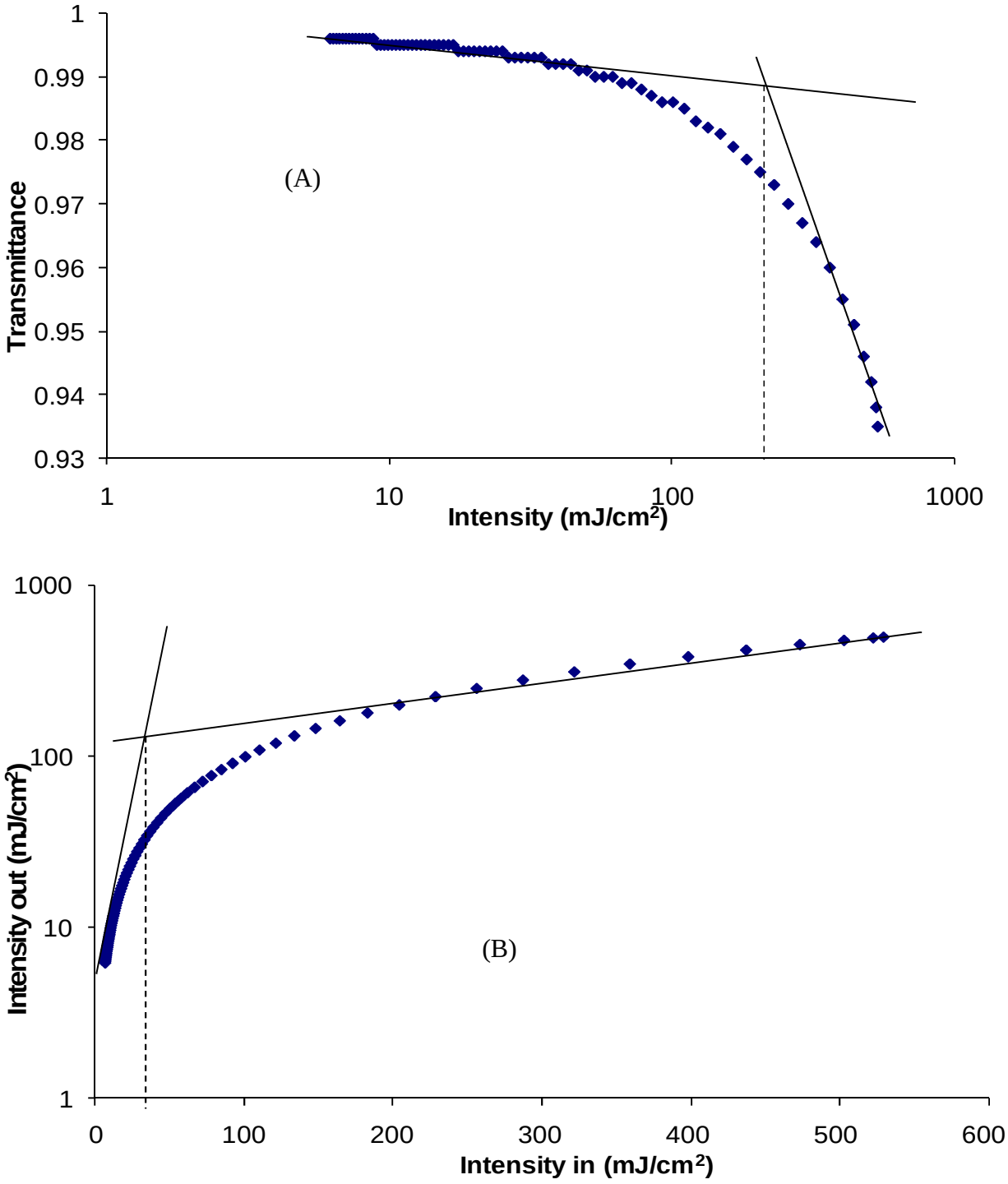

Fig. 4.2: Plots of (A) transmittance against intensity and (B) output intensity against input intensity for complex **14** alone in DMF:water solution.

*4.1.1.1 Trends in terms of imaginary third-order susceptibility (Im[$\chi^{(3)}$]/α) of complexes **5-14** in the absence of QDs*

The values for Im[$\chi^{(3)}$] normalized for absorption (Im[$\chi^{(3)}$]/α) Table 4.1, will be employed for the discussion below. There is an increase in Im[$\chi^{(3)}$]/α (Table 4.1) in DMSO on going from Ga (complex **9**) to In (complex **10**), both containing the same substituent, showing the effects of the heavy atom effect. However there is a decrease in Im[$\chi^{(3)}$]/α in going from **9** to **10** in DMSO:water, showing the effects of the solvent. This could be due to reduced Φ_T and τ_T values in **10** compared to **9** in DMSO:water, whilst Φ_T values in DMSO are larger for **10** than for **9**. Comparing peripherally tetrasubstitution (complex **11**) with peripherally octasubstitution (complex **8**) with the same substituent (benzyloxyphenoxy) and central metal (Zn), there is a slight decrease in Im[$\chi^{(3)}$]/α for tetrasubstituted complex **11** compared to **8** in both DMSO and DMSO:water. This is unusual because the tetrasubstituted complex **11** is less symmetrical than the octasubstituted complex **8** and so should have greater third-order susceptibility [204]. Also, based on Φ_T values, **11** would be expected to show larger Im[$\chi^{(3)}$]/α values since it has a larger Φ_T value than **8**. **11** also has a slightly larger τ_T value than **8**. Comparing complexes **6** and **7** both containing In central metal and the same substituents, but one peripherally (**6**) and the other non-peripherally (**7**) substituted, shows that non-peripheral substitution reduces the Im[$\chi^{(3)}$]/α value in both DMSO and DMSO:water. Both **6** and **7** have Φ_T < 0.01 in DMSO:water and have similar values in DMSO. Their τ_T values are also similar. Comparing **5**, **9** and **13** (all containing Ga central metal) but octasubstituted with different groups, shows an decrease in Im[$\chi^{(3)}$]/α in DMSO for **9** and **13** substituted with benzyloxyphenoxy or phenoxy groups in comparison to **5** which is

substituted with *tert* –butylphenoxy groups. Thus, *tert* –butylphenoxy improves Im[$\chi^{(3)}$] parameter compared to benzyloxyphenoxy or phenoxy substituents. Due to their bulky nature, *tert*–butylphenoxy substituents are expected to increase solubility and to reduce aggregation more than benzyloxyphenoxy or phenoxy groups. Decrease in aggregation could explain the improved value for Im[$\chi^{(3)}$]/α in the presence of *tert*–butylphenoxy. There could possibly also be a slight alteration of symmetry of the phthalocyanine when *tert*-butylphenoxy is used as the substituents and this could account for the improvement in Im[$\chi^{(3)}$]/α for complex **5**. In terms of Φ_T, **13** has a larger value than **5** and **9**. In DMSO:water, complex **9** showed higher Im[$\chi^{(3)}$]/α values compared to **5** or **13**. Complex **9** shows aggregation in DMSO:water but not in DMSO, this would affect the Im[$\chi^{(3)}$]/α values. **9** also showed the lowest Φ_T in DMSO:water compared to **5** and **13**.

Comparing **6** and **12** containing In and tetrasubstituted at the peripheral positions there is an decrease in Im[$\chi^{(3)}$]/α in DMSO and DMSO:water for **12** compared to **6**, the latter is substituted with *tert*-butylphenoxy groups, showing improvement with this substituent when compared to phenoxy (for complex **12**). Complex **14** containing amino groups shows the Im[$\chi^{(3)}$]/α value which is comparable to all of the other complexes before addition of QDs. Amino groups are known to quench excited states. For example, the corresponding $ZnPc^{\alpha}(NH_2)_4$ substituted at non-peripheral positions with amino groups, does not show triplet-triplet absorption [205]. Thus the decent value of Im[$\chi^{(3)}$] for **14** is surprising. In summary, *tert*–butylphenoxy improves Im[$\chi^{(3)}$]/α values (depending on the solvent) compared to benzyloxyphenoxy and phenoxy, and the heavy central metals increase the Im[$\chi^{(3)}$]/α value and non-peripheral substitution reduces the value of this parameter.

*4.1.1.2 Trends in terms of hyperpolarizability (γ) of complexes **5-14** in the absence of QDs*

In terms of hyperpolarizability (γ), Table 4.1, the heavy atom effect is clear on going from Ga (complex **9**) to In (complex **10**), both containing the same substituent and in DMSO and not in DMSO:water. The larger value for **9** in DMSO:water could be related to increased Φ_T and τ_T values for **9** compared to **10**. Comparing tetrasubstituted (complex **11**) with octasubstituted (complex **8**) complexes containing the same substituent (benzyloxyphenoxy) and Zn central metal, there is a decrease in γ for tetrasubstitution (**11**) in DMSO and DMSO:water as observed for $Im[\chi^{(3)}]/\alpha$, even though **11** has an improved Φ_T. Comparing complexes **6** and **7** both containing In central metal and the same substituent (*tert*–butylphenoxy), but one peripherally (**6**) and the other non-peripherally (**7**) substituted, shows that non-peripheral substitution reduces the γ value in both DMSO and DMSO:water as also occurred with $Im[\chi^{(3)}]/\alpha$. Comparing **5**, **9** and **13** (all containing Ga central metal) but octasubstituted with different groups, shows an increase in γ for **5** substituted with *tert*–butylphenoxy, and low values (in DMSO) for **9** and **13** containing benzyloxyphenoxy and phenoxy groups, respectively as was the case for the $Im[\chi^{(3)}]/\alpha$ values. Again complex **9** gives a larger value for γ in DMSO:water compared to **5** and **13** as discussed above for $Im[\chi^{(3)}]/\alpha$. Comparing **6** and **12** containing In and tetrasubstituted at the peripheral positions a decrease in γ for **12** compared to **6** is observed, perhaps because the *tert* –butylphenoxy which tends to improve solubility and hence third-order susceptibility parameters. Complex **14** containing amino groups shows the γ value which is similar to other complexes.

4.1.1.3 Trends in I_{lim} and F_{sat}.

For the best optical limiters F_{sat} and I_{lim} values must be sufficiently low as to aid in limiting the transmitted light to a less dangerous level, but not so low as to practically make it an optical filter. Fig. 4.2 shows the plots used to obtain the F_{sat} and I_{lim} values in DMF: water. DMF: water and DMSO: water have similar behaviours in regards to optics and DMF was more readily available for these examinations. Table 4.2 shows that the I_{lim} values in solution are lowest (< 40 $mJcm^{-2}$) for Pcs in the absence of CdTe-TGA QDs for **5**, **8**, **10**, **12**, **13** and **14**, whilst higher values were obtained for **6**, **7**, **9** and **11**. The trend is not clear in terms of substituents or central metal. However complexes **6** and **7**, which gave the largest I_{lim} values in the absence of QDs, contain indium as a central metal, suggesting that perhaps the gallium lowers these values further than indium (compare **6** and **7** to **5**). The two complexes also contain tert-butyl substituents, showing the importance of these substituents in NLO. These values need to be taken in context with third-order susceptibility and hyperpolarizability values. What is meant here is that whilst these two complexes may have the largest I_{lim} values, they may also possess some of the largest $Im[\chi^{(3)}]/\alpha$ and γ values of the examined complexes and are therefore still viable optical limiting complexes.

In terms of F_{sat} in the absence of QDs, the largest value was obtained for **9** containing gallium and the lowest for **6** and **12** containing indium. The substituent effects are unclear here.

From a series of studies [124, 126, 155, 156, 157, 159], F_{sat} values in solution were found to range from 2 to 27 Jcm^{-2} and I_{lim} range in solution from 0.09 to 10.1 Jcm^{-2}, hence the values reported here in solution fall within the lower part of the I_{lim} range

and are thus comparable, and are well below the F_{sat} range. This indicates an improvement in NLO behaviour.

Table 4.2: F_{sat} and I_{lim} Parameters for Phthalocyanine/CdTe-TGA Complexes in DMF:water solutions.

DMF:water solutions	**F_{sat} (mJ/cm^2)**	**I_{lim} (mJ/cm^2)**
(**5**)	205	37
(**5**)+QD	278	30
(**6**)	100	48
(**6**)+QD	109	49
(**7**)	225	47
(**7**)+QD	280	51
(**8**)	262	36
(**8**)+QD	230	34
(**9**)	324	43
(**9**)+QD	231	33
(**10**)	198	36
(**10**)+QD	410	47
(**11**)	292	42
(**11**)+QD	386	39
(**12**)	170	36
(**12**)+QD	540	62
(**13**)	222	39
(**13**)+QD	233	36

(**14**)	212	38
(**14**)+QD	112	43

*4.1.2 Pcs **5-14** in the presence of CdTe-TGA QDs in solution.*

Fig. 4.1 shows the Z-scan traces for **9** and **10** in the presence of CdTe-TGA QDs in DMSO:water.

4.1.2.1 Third-order susceptibility studies.

For these studies, several ratios of Pcs to QDs were tested and 97:1 was found to be the best ratio in terms of the increase in third-order susceptibility it brought. The changes in third-order susceptibility on the addition of QDs are more likely due to a combination of an increase in the amount of intersystem crossing occurring in the Pc and hence increase the triplet quantum yield. A general (except for **5**) increase in triplet quantum yield of phthalocyanines on addition of QDs is observed in DMSO:water, as shown in Table 4.1. For complex **5** there was a decrease in the Φ_T and τ_T values upon the addition of CdTe-TGA. In all cases (except for **14**), there is an increase in both $Im[\chi^{(3)}]/\alpha$ and γ in the presence of QDs (Table 4.1), for all complexes corresponding to increased intersystem crossing due to the heavy atom effect of the QDs. Increase in Pc $Im[\chi^{(3)}]/\alpha$ has been also be associated with increase of the molecule's dimension by incorporating it within a liquid crystal [206]. It was proposed that this was caused by the increase of the charge transfer effects and change of the dipole moments of the molecule with the increase of either molecular dimension or electrical properties [206].

The complexes **5, 8**, **9**, **10** and **13**, are aggregated but showed large increases in γ values in the presence of QDs. Complexes **6**, **7** and **12** which were not aggregated in the presence of QDs, also showed an increase in their γ values in the presence of QDs, but not as large as the increase observed for **5** and **9**. Thus it is becoming apparent that the complexes which showed aggregation in the presence of QDs do not have their γ values affected detrimentally.

4.1.2.2 Trends in I_{lim} and F_{sat} in the presence of CdTe-TGA QDs

F_{sat} values in solution generally increased in the presence of QDs except for **8**, **9** and **14** where there is a decrease (Table 4.2). It is observed however that complexes **8** and **9** improved in $Im[\chi^{(3)}]$ and γ in the presence of QDs whilst **14** decreased for these values (Table 4.1), meaning that if the F_{sat} decrease is not too large as to make the mixture limit the transmitted light too much, then there is improvement with these complexes in the presence of QDs. The changes in I_{lim} are minor and therefore should not impact things too significantly.

A possible trend is that **8** and **14**, which contain zinc as the central metal, have improved F_{sat} and I_{lim} values in the presence of QDs, and hence give them potential as optical limiters.

*4.1.3 Third-order susceptibility and NLO studies of Pc **7** and other NMs*

The Z-scan traces were similar to those shown in Fig. 4.1 and the traces for F_{sat} and I_{lim} were similar to Fig. 4.2. Tables 4.3 and 4.4 give the $Im[\chi^{(3)}]$, γ, k, I_{lim} and F_{sat}

values for complex **7** in the presence of CdSe-TGA, CdS-TGA, SWCNTs and fullerenes. Complex **7** was chosen as an example Pc to study with the various NMs. Comparison of Im[$\chi^{(3)}$] and γ between all NMs except SWCNTs is possible because proper molar concentration could be determined and proper ratios of 9:1 Pc:NM could be employed. This is because a method exists to determine QD molar concentrations and the fullerenes employed were a fixed size and hence fixed molar mass. For the SWCNTs no molar mass was obtainable because SWCNTs are generally a collection of sizes and therefore a concentration based upon weight was employed to ensure that the solutions and films containing SWCNTs were comparable with each other, but are not comparable to the other NMs.

As stated above, factors such as the particle size, the surface morphology, and the defect concentration affect the nonlinear optical properties of quantum dots [207]. The β term measured by the Z scan increases with increase in the size of nanomaterials [208, 209]. Also for CNTs, the solutions are in the form of a dispersion, and it has been reported that their optical limiting is due to scattering combined with possible electronic absorption contributions [210]. However, the aim in this work was to carry out a preliminary assessment of the different NM on the NLO behavior of MPc complexes, without directly comparing the NM. Such a comparison will be difficult due to the factors stated above.

Table 4.3 shows that the parameters, Im[$\chi^{(3)}$]/α and γ for all nanomaterials alone in solution are higher than for complex **7** alone. In solution, the reported hyperpolarizability (γ) value range from 10^{-34} to 10^{-29} esu.L for phthalocyanines [151] and the values for **7** in Table 4.3 are within the general trend. Comparison of Im[$\chi^{(3)}$]/α and γ values of the CdTe-TGA QDs alone in water at 8.13×10^{-6} and 7.28×

10^{-25} esu. L, respectively, Table 4.3, and those for complex **7** alone (1.44×10^{-12} and 1.00×10^{-31} esu. L, respectively) with those of the mixture (at 7.40×10^{-12} and 5.14×10^{-31} esu. L, respectively) shows that the values for the mixture are closer to the value of **7** alone. This suggests that QDs enhance the NLO behavior of the phthalocyanine complex. Fig. 4.3 (same as Fig. 3.12A) shows that CdTe-TGA QDs absorb at 532 nm where NLO behavior was determined, whereas CdS-TGA and CdSe-TGA do not absorb. The higher values of $Im[\chi^{(3)}]/\alpha$ and γ parameters for **7** in the presence of CdSe-TGA or CdS-TGA QDs compared to CdTe-TGA suggests that absorption at 532 nm is prominent in determining NLO. For SWCNT and fullerenes, enhancements in $Im[\chi^{(3)}]/\alpha$ and γ parameters of complex **7** are observed in Table 4.3.

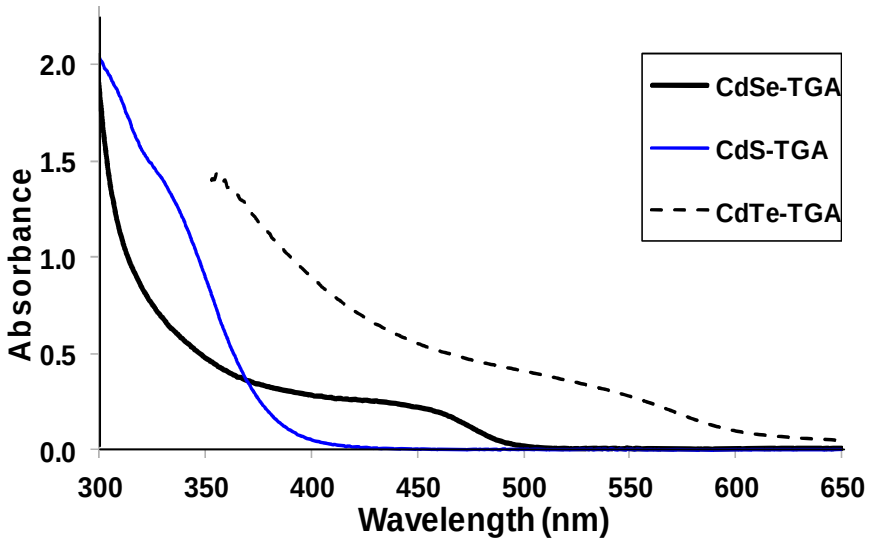

Fig. 4.3: Absorbance spectra of QDs.

The absorbance of CdTe at 532 nm is important because it would mean poorer k values for the CdTe-TGA than the other two QDs and that the absorbance of the CdTe-TGA may interfere with the phthalocyanine nonlinear absorbance.

k values should be above one and as high as possible give a good indication that a compound should have strong optical limiting ability. The k values in Table 4.4 are unfortunately below one, thus indicating that the compounds have a greater tendency to remain in the singlet state. In terms of trends, there is an increase in k value when the Pc is in the presence of QDs and a decrease in the presence of the other two NMs. This seems to mirror the trend observed in the I_{lim} values and perhaps indicates a correlation between I_{lim} and k values. I_{lim} values increase for the Pc in the presence of QDs but decrease in the presence of fullerenes and SWCNTs. For the F_{sat} values, adding CdTe-TGA to the Pc solution caused an increase in F_{sat} value in comparison to the Pc alone, but the other NMs decreased the F_{sat} value. Again, these values cannot be considered alone and the third-order susceptibility parameters must be considered in conjunction with these in order to determine whether a compound/mixture is a viable optical limiter.

Table 4.3: Third-order susceptibilities for phthalocyanine **7**/NM complexes and NM alone in solutions.

State/Solvent	**Compound**	**γ (esu.L)**	**Im[$\chi^{(3)}$]/α**
water	CdSe-TGA	4.45×10^{-27}	2.41×10^{-7}
water	CdS-TGA	1.57×10^{-26}	1.61×10^{-7}
water	SWCNT	6.32×10^{-29}	9.21×10^{-7}
toluene	Fullerene	5.37×10^{-28}	1.45×10^{-6}
water	CdTe-TGA	7.28×10^{-25}	8.13×10^{-6}
DMSO:water	(**7**)+CdSe-TGA	1.09×10^{-26}	1.37×10^{-7}
DMSO:water	(**7**)+CdS-TGA	9.79×10^{-27}	1.23×10^{-7}

DMSO:water	(**7**)+SWCNT	1.16×10^{-26}	1.46×10^{-7}
DMSO:toluene	(**7**)+fullerene	1.06×10^{-26}	1.33×10^{-7}
DMSO:water	(**7**) alone	1.00×10^{-31}	1.44×10^{-12}
DMSO:water	(**7**) + CdTe-TGA	5.14×10^{-31}	7.40×10^{-12}

Table 4.4: k values, F_{sat} and I_{lim} parameters for phthalocyanine **7**/NM complexes in solutions (either DMF:water (9:1) or DMF:toluene (9:1)).

Compound	k value	I_{lim} (mJ/cm^2)	F_{sat} (mJ/cm^2)
7 alone	0.24	47	225
7 + CdTe-TGA	0.5	51	280
7 + CdSe-TGA	0.5	56	107
7 + CdS-TGA	0.729	52	131
7 + Fullerene	0.0996	27	49
7 + SWCNT	0.0181	42	102

4.1.4 Chloroindium hemiporphyrazine NLO

Fig. 4.4 shows the Z scan trace for ClInHp. The shape of the Z scan trace with a valley is typical of two photon absorption (TPA) following SA [201]. The phenomenon occurring in Fig. 4.4 is not uncommon to see. It occurs quite often with QDs. Some explanations about why this occurs in QDs include higher-order susceptibilities becoming larger than the third-order susceptibility, scattering, refractive index alterations or alterations in polarisation of the QD. Any of these could also be an explanation for what occurred in Fig. 4.4. Also, the optical setup alignment was always checked before use and multiple runs were done, all of which generate very similar graphs to Fig. 4.4.

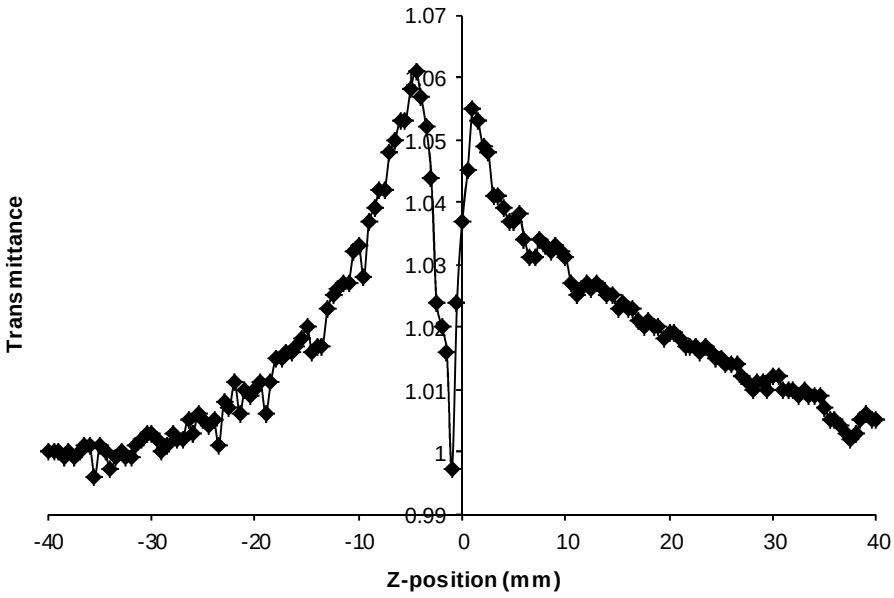

Fig. 4.4: Z-scan of ClInHp in DMF.

The determined third order susceptibility and hyperpolarizability values (Table 4.5) for the ClInHp are larger than most of the previously analyzed Pcs in solution, but

smaller than the same Pcs in poly-methylmethacrylate (PMMA) films to be discussed below. The differences in solvents (DMF vs DMSO) in Table 4.5 are not expected to have a significant effect on the NLO parameters. This would imply that ClInHp is a superior optical limiter in solution and has the added benefit of being yellow in color. Yellow is a lot less obtrusive a color than green, meaning that a polymer film made from the ClInHp would not have a green tint but rather a slightly yellow one.

As already stated, a good optical limiter must have, low I_{lim} and low F_{Sat} values. Table 4.5 contains the F_{sat} and I_{lim} values for ClInHp, and Fig 4.5 shows the relevant curves used to obtain these values. The I_{lim} value is comparable to those obtained for previously analyzed Pcs in solution and the F_{sat} value is much larger than what was obtained for the Pcs. This would imply that the ClInHp and the Pcs begin nonlinear processes at a similar intensity, but the former needs much higher intensities/fluences for the absorber to become saturated. No k value was obtainable because of the high emission signal observed during laser flash photolysis at 532 nm, which obscured any triplet absorption signal. This may also be the reason for the shape of the z-scan curve.

Table 4.5: Nonlinear parameters of ClInHp in DMF.

Compound	$Im[\chi^{(3)}]$	$Im[\chi^{(3)}]/\alpha$	γ	F_{sat} (mJ/ cm^2)	I_{lim} (mJ/ cm^2)
ClInHp	1.13×10^{-7}	3.32×10^{-7}	3.23×10^{-28}	1000	54
6[a]	4.37×10^{-11}	1.46×10^{-11}	1.02×10^{-30}	225	47
7[a]	8.97×10^{-11}	3.46×10^{-11}	2.09×10^{-30}	100	48
10[a]	9.21×10^{-11}	3.50×10^{-11}	4.12×10^{-30}	198	36
12[a]	5.62×10^{-11}	2.09×10^{-11}	1.78×10^{-30}	170	36

[a] = Data in DMSO.

The ClInHp's third-order susceptibility is 10000x greater than Pcs in solution featured in Table 4.3 and 100x greater hyperpolarizability. This indicates a great improvement in third-order susceptibility ability. The significantly higher F_{sat} value of the ClInHp is not desirable, but the I_{lim} value is in line with the Pcs in solution.

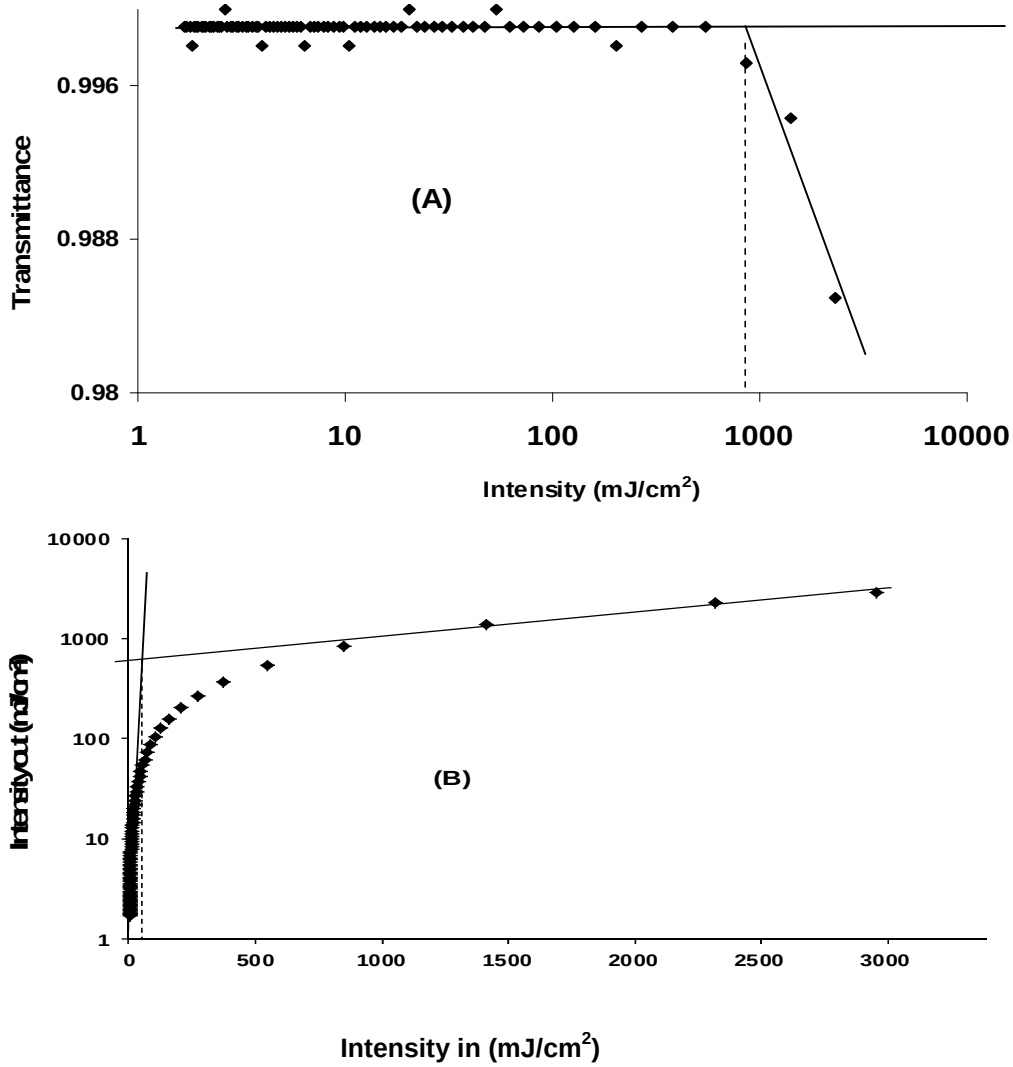

Fig. 4.5: Plot of (A) transmittance against incident intensity and (B) output intensity against input intenisty at 532 nm for ClInHp**.** Solvent DMF.

4.2 Polymer films.

*4.2.1 Phthalocyanines **5**-**14** in the absence of NMs in PMMA Thin Film*

Fig. 4.6A shows the Z scan plot of complex **12** in a PMMA thin film as a representative for all films. Table 4.6 gives the third-order susceptibility values calculated for the different thin films. Hyperpolarizability (γ), which is generally regarded as a better parameter to use for comparison purposes, exhibited values (10^{-26} to 10^{-25}) which are much larger than those found in DMSO solutions (10^{-30}) for the same complexes, Table 4.6. The values of $Im[\chi^{(3)}]/\alpha$ were also larger than in solution. Thus Pcs in thin films are considered to have better third-order susceptibilities than Pcs in solutions. Part of the reason for this could be due to contribution of the polymer to a reduction in transmission, or it could be the greater amount of aggregation that the phthalocyanines experience in thin films, which in turn leads to greater optical limiting. Liu *et al.* [211] examined indium phthalocyanine, both in solution and in a PMMA polymer film, and observed a significant increase in optical limiting ability, along with observations of phthalocyanine aggregation in the polymer film. It was also mentioned [211] that PMMA has no optical limiting ability of its own as can be seen from the data plotted in Fig. 4.6C, but that the crystallization and morphology of the polymer could not be discounted to contribute towards the improvement in γ and $Im[\chi^{(3)}]$ values.

Comparing complexes **6** and **7** which both contain In central metal and the same substituents, but one peripherally (**6**) and the other non-peripherally (**7**) substituted (and embedded in PMMA polymer), shows that peripheral substitution results in larger values of both $Im[\chi^{(3)}]/\alpha$ and γ as was the case for the solution studies, Table 4.6. Comparing **5**, **9** and **13** (all containing Ga central metal) but octasubstituted with

different groups (and embedded in PMMA), shows an decrease in Im[$\chi^{(3)}$]/α and γ for **9** and **13** substituted with benzyloxyphenoxy or phenoxy groups in comparison to **5** which is substituted with *tert* –butylphenoxy groups. Thus, *tert*–butylphenoxy improves these parameters compared to benzyloxyphenoxy or phenoxy substituents. There could possibly be a slight alteration of symmetry of the phthalocyanine when *tert*-butylphenoxy is used as a _ubstituents due to its bulkiness. This could account for the improvement in Im[$\chi^{(3)}$]/α and γ for complex **5**. However comparing complex **6** and **12** in PMMA, containing In central metal and tetrasubstituted with *tert*–butylphenoxy and phenoxy substituents, respectively, larger values of Im[$\chi^{(3)}$]/α and γ are obtained for complex **12** containing the phenoxy _ubstituents. Thus the effects of the substituents on the optical limiting parameters could also depend on the central metal and on the number of substituents.

Comparing peripheral tetrasubstitution (complex **11**) with peripheral octasubstitution (complex **8**) with the same _ubstituents (benzyloxyphenoxy) and central metal (Zn), there is a slight decrease in Im[$\chi^{(3)}$]/α and γ for tetrasubstituted complex **11** compared to **8.** It has previously been shown that octasubtitution gives better optical limiting behaviour than tetrasubstitution [155]. Complex **14** containing amino groups shows the Im[$\chi^{(3)}$]/α and γ values which are comparable to all of the other complexes even though amino groups are known to quench excited states [205].

Complex **14** behaved like a saturable absorber instead of a reverse saturable absorber (figure not shown). This means that the linked complex becomes utterly saturated by the intense laser light and can no longer absorb any more light.

k values (Table 4.7) for Pcs alone in polymer films are greater than 1 except for **8**, **9** and **11**, unlike in solution where k < 1 for **7** alone or in the presence of NMs. This confirms that Pcs are better OL in polymer films. **8** and **9** are highly aggregated in

PMMA films (as discussed in Chp. 3 Fig. 3.20); and **11** has a large absorbance at 532 nm. These factors may affect the observed k values. F_{sat} for Pcs alone are much lower in polymer films than in solution (Table 4.7), confirming that polymer films are superior compared to solutions. Complex **9** gave the largest F_{sat} value in solution and polymer, making it the worst performing in terms of this parameter. The lowest F_{sat} for polymer films was obtained for **10**, even though it was not the lowest in solution. In terms of I_{lim}, the lowest values in solution were **5**, **8**, **10**, **12**, **13** and **14**, but only **8** and **14** give the lowest values in polymer films. Both **8** and **14** contain zinc as the central metal, showing that in terms of this parameter ZnPcs show promise as OL materials. An estimation of the uncertainty of the F_{sat} and I_{lim} values is about 2 mJ/cm^2.

No damage was detected due to running the Z-scan on the polymer films, thus limiting the probability of erroneous scattering developing. A possible reason for this is that the point of focus was altered between each repeat run on the Z-scan and the polymer film was never subjected to high intensities long enough to be destroyed.

As for the asymmetrical Z-scans which occasionally emerge, it is believed that some form of strong refraction is occurring to cause this, possibly due to an inconsistency in the thickness of the polymer film. There is also the possibility that the refraction could be nonlinear.

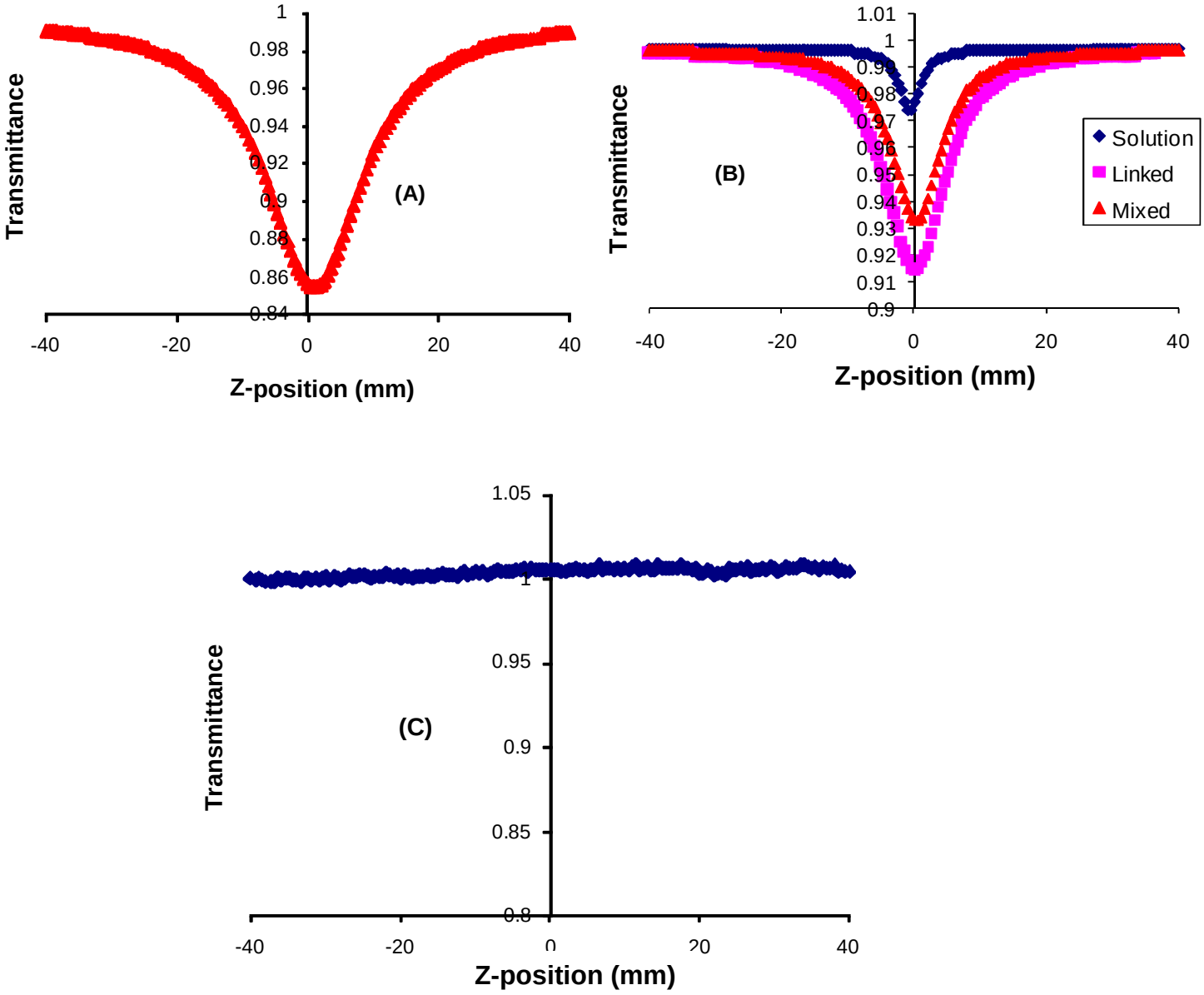

Fig. 4.6: Z-scan spectra of (A) **12** in PMMA thin film, (B) **16** mixed and linked to PEI as thin films, as well as in solution (water) and (C) PMMA alone.

Table 4.6: Third-order susceptbilities for phthalocyanine complexes in the absence of NMs as PMMA polymer films.

Thick Films	**Im[$\chi^{(3)}$]^{a} (esu)**	**Im[$\chi^{(3)}$]/α**	**γ (esu.L)**
(**5**) PMMA	6.21×10^{-4} (8.54×10^{-11})	7.53×10^{-6} (2.67×10^{-11})	6.49×10^{-25} (2.39×10^{-30})
(**6**) PMMA	1.17×10^{-4} (8.97×10^{-11})	1.18×10^{-6} (3.46×10^{-11})	9.64×10^{-26} (2.09×10^{-30})
(**7**) PMMA	1.12×10^{-4} (4.37×10^{-11})	6.78×10^{-7} (1.46×10^{-11})	4.54×10^{-26} (1.02×10^{-30})
(**8**) PMMA	4.70×10^{-4} (2.88×10^{-11})	5.67×10^{-6} (3.28×10^{-11})	3.63×10^{-25} (2.17×10^{-30})
(**9**) PMMA	6.22×10^{-5} (3.95×10^{-11})	6.92×10^{-7} (1.44×10^{-11})	7.87×10^{-26} (1.69×10^{-30})
(**10**) PMMA	4.01×10^{-4} (9.21×10^{-11})	8.18×10^{-6} (3.50×10^{-11})	9.31×10^{-25} (4.12×10^{-30})
(**11**) PMMA	3.70×10^{-5} (4.81×10^{-11})	1.95×10^{-6} (1.74×10^{-11})	1.40×10^{-25} (1.30×10^{-30})
(**12**) PMMA	8.18×10^{-5}	2.93×10^{-6}	1.71×10^{-25}

	(5.62×10^{-11})	(2.09×10^{-11})	(1.78×10^{-30})
(**13**) PMMA	1.28×10^{-4} (4.53×10^{-11})	1.61×10^{-6} (2.08×10^{-11})	8.53×10^{-26} (1.15×10^{-30})
(**14**) PMMA	8.84×10^{-4} (7.82×10^{-11})	5.19×10^{-6} (5.41×10^{-11})	1.47×10^{-25} (1.82×10^{-30})

[a] Values in brackets are for Pcs alone in DMSO solution.

Table 4.7: F_{sat} and I_{lim} Parameters for Phthalocyanine/CdTe-TGA Complexes as PMMA polymer films. The values in parentheses are for the solutions (DMF:water).

PMMA Films	**F_{sat} (mJ/cm^2)**	**I_{lim} (mJ/cm^2)**	**k**
(**5**)	34 (205)	38 (37)	2.806
(**5**)+QD	4 (278)	52 (30)	1.052
(**6**)	36 (100)	26 (48)	2.593
(**6**)+QD	169 (109)	132 (49)	0.139
(**7**)	58 (225)	43 (47)	8.473
(**7**)+QD	52 (280)	117 (51)	0.144
(**8**)	30 (262)	17 (36)	0.602
(**8**)+QD	64 (230)	132 (34)	0.016
(**9**)	79 (324)	47 (43)	0.695
(**9**)+QD	249 (231)	23 (33)	0.470
(**10**)	23 (198)	14 (36)	5.491
(**10**)+QD	39 (410)	19 (47)	0.299
(**11**)	54 (292)	30 (42)	0.413
(**11**)+QD	288 (386)	38 (39)	0.071
(**12**)	67 (170)	46 (36)	2.579
(**12**)+QD	87 (540)	14 (62)	0.655
(**13**)	34 (222)	27 (39)	2.422
(**13**)+QD	92 (233)	50 (36)	1.492
(**14**)	32 (212)	31 (38)	-
(**14**)+QD	17 (112)	10 (43)	-

*4.2.2 Phthalocyanines **5-14** in the presence of QDs in PMMA Thin Film*

4.2.2.1 CdTe-TGA QDs

Table 4.8 shows the OL parameters of the Pcs in the absence and presence of CdTe-TGA QDs within PMMA. There is a general increase in $Im[\chi^{(3)}]/\alpha$ and γ for the Pcs in the presence of CdTe-TGA, with the exception of complexes **9**, **10**, **11** and **12**, where there is a decrease in these values. An increase in these values is expected due to the heavy atom effect of the QDs. It is known that factors such as the particle size, the surface morphology, and the defect concentration affect the nonlinear optical properties of quantum dots [207]. It is expected that these factors will also influence the third-order susceptibility behaviour when Pcs are mixed with QDs. Different Pc complexes will interact with defects on the QDs differently, hence observed differences in Table 4.8. Φ_T and τ_T values were determined using equation 1.11 and the Origin fitting program respectively. These values were obtained on films as explained in the experimental. The Φ_T values are used for comparison purposes only since no standard could be used in their calculation.

There is a general increase in the triplet quantum yield when CdTe-TGA was added, except for **6**, **9**, **11** and **12**, and an increase (except for **11**) in triplet lifetime values, Table 4.8. No triplet lifetime or triplet quantum yield values were obtained for $ZnPc(NH_2)_4$ (**14**) because no measurable signal was obtainable from the laser flash photolysis. The $Im[\chi^{(3)}]/\alpha$ and γ do increase when there are increases in Φ_T on the addition of QDs. This was observed for all complexes except for **9** – **12**, where there was a decrease in $Im[\chi^{(3)}]/\alpha$ and γ on addition of QDs even though the Φ_T increased for **10** (though marginally). For **9**, **11** and **12**, where there is a decrease in Φ_T there is also a decrease in $Im[\chi^{(3)}]/\alpha$ and γ. Thus there is a correlation between Φ_T and third-

order susceptibility. In terms of τ_T there is a decrease for **11** only on the addition of QDs, which also corresponds to the decrease in $Im[\chi^{(3)}]/\alpha$ and γ. The Φ_T values obtained in Table 4.8 came from the usual flash photolysis setup used for solution, but the polymer film was placed at a 45° angle in the sample holder so as to have the laser and xenon lamp light able to strike it. The values are so low due to the thin nature of the polymer films.

In terms of the k values (Table 4.7), they decreased with the addition of the QDs to Pcs, but this was expected because the QDs enhanced singlet absorption in the polymer film far more than triplet absorption.

Interestingly, there appears to be a general increase in F_{sat} and I_{lim} values, with a few exceptions, when the QDs were added to them. Whether these values fall within useful ranges depends on the application of the optical limiters.

Table 4.8: Third-order susceptibilities for phthalocyanine/CdTe-TGA complexes as PMMA polymer films.

PMMA Films	**γ (esu.L)**	**$Im[\chi^{(3)}]/\alpha$**	**Φ_T**	**τ_T (μs)**
(**5**)	6.49×10^{-25}	7.53×10^{-6}	4.43×10^{-4}	290
(**5**)+QD	1.23×10^{-23}	1.43×10^{-4}	1.09×10^{-2}	420
(**6**)	9.64×10^{-26}	1.18×10^{-6}	1.61×10^{-4}	40
(**6**)+QD	2.16×10^{-25}	2.63×10^{-6}	3.83×10^{-5}	70
(**7**)	4.54×10^{-26}	6.78×10^{-7}	4.79×10^{-5}	30
(**7**)+QD	2.34×10^{-24}	3.50×10^{-5}	1.47×10^{-3}	50

(**8**)	3.63×10^{-25}	5.67×10^{-6}	7.48×10^{-5}	170
(**8**)+QD	6.60×10^{-25}	1.03×10^{-5}	3.14×10^{-4}	230
(**9**)	7.87×10^{-26}	6.92×10^{-7}	3.32×10^{-4}	230
(**9**)+QD	1.44×10^{-26}	1.26×10^{-7}	3.39×10^{-5}	240
(**10**)	9.31×10^{-25}	8.18×10^{-6}	7.48×10^{-4}	30
(**10**)+QD	7.83×10^{-25}	6.89×10^{-6}	7.83×10^{-4}	40
(**11**)	1.40×10^{-25}	1.95×10^{-6}	8.33×10^{-5}	340
(**11**)+QD	6.19×10^{-26}	8.62×10^{-7}	7.70×10^{-5}	210
(**12**)	1.71×10^{-25}	2.93×10^{-6}	2.22×10^{-4}	30
(**12**)+QD	1.57×10^{-25}	2.70×10^{-6}	1.82×10^{-4}	40
(**13**)	8.53×10^{-26}	1.61×10^{-6}	1.35×10^{-4}	170
(**13**)+QD	1.40×10^{-25}	2.63×10^{-6}	2.25×10^{-4}	310
(**14**)	1.47×10^{-25}	5.19×10^{-6}	-	-
(**14**)+QD	2.47×10^{-25}	8.70×10^{-6}	-	-

4.2.2.2 Other NMs (CdSe, CdS, SWCNT, fullerenes) and linked complexes.

Table 4.9 shows NLO parameters of phthalocyanine **7** with different nano-materials, along with phthalocyanine **14** – **16** linked to different polymers (polymers used indicated in table). The Z scans of the linked or mixed complex **16** are shown in Fig. 4.6B, together with the solution scan (in water). The same behaviour was observed for **14** and **15**.

In the case of other NMS (CdSe, CdS, SWCNT, fullerene) and in terms of $Im[\chi^{(3)}]/\alpha$ and γ, Table 4.9, none of the current polymer film Z-scan examinations of the alternative NMs in combination with phthalocyanine **7** seems to offered an

improvement over the phthalocyanine **7**/CdTe-TGA combination ($Im[\chi^{(3)}]/\alpha$ value is 3.50 x 10^{-5} esu; γ value is 2.34 x 10^{-24}, Table 4.9). The $Im[\chi^{(3)}]/\alpha$ values of the other NM combinations fell into a 10^{-6} to 10^{-8} range.

Table 4.9 shows that simply placing phthalocyanines in a PEI thin film has increased their optical limiting ability compared to that in aqueous solution. A slight increase in hyperpolarizability and $Im[\chi^{(3)}]/\alpha$ was observed for linked samples when compared with the mixed samples for **15**/PEI and only marginally for **16**/PEI, indicating that the link formation may have further improved the thin films as optical limiters. This cannot be taken as definitive however because there are too many variables (including different amounts of Pcs in the linked and mixed conjugates) that could exist between the mixed and linked thin films that could account for the difference.

Despite the low k values, there does seem to be a trend of decreased k values when the polymer film was formed in the presence of NMs compared to **7** alone. Coupled with this is the fact that the F_{sat} values decreased for the polymer films compared to **7** alone, showing an improvement. Excepting for **7**/CdTe and **7**/fullerene, the I_{lim} generally decreased for polymer films compared to solutions. The decreases were generally marginal and it might be concluded that forming the films did not significantly affect the I_{lim} values. The k value decreased for **7**/CdTe, **7**/CdSe, **7**/fullerenes and **7**/SWCNT compared to their solution values, indicating that these polymer films should perform badly as OL materials. The reason for the decrease is not fully understood, just that there was a decrease in the triplet-triplet absorption. An increase was observed however for **7**/CdS, meaning that it shows potential as an optical limiter.

Table 4.9: k values, F_{sat} and I_{lim} Parameters for Phthalocyanine **7**/NM Complexes as PMMA polymer films and solutions (either DMF:water (9:1) or DMF:toluene (9:1)), along with phthalocyanines **14** – **16** linked to various polymer films. Values in parentheses are for solutions.

Compound	k value	I_{lim} (mJ/cm^2)	F_{sat} (mJ/cm^2)	γ (esu.L)	$Im[\chi^{(3)}]/\alpha$
7 alone	8.473 (0.24)	43 (47)	58 (225)	4.54×10^{-26}	6.78×10^{-7}
7 + CdTe-TGA	0.144 (0.5)	117 (51)	52 (280)	2.34×10^{-24}	3.50×10^{-5}
7 + CdSe-TGA	0.0726 (0.5)	18 (56)	54 (107)	7.87×10^{-27}	1.18×10^{-7}
7 + CdS-TGA	1.723 (0.729)	31 (52)	53 (131)	1.66×10^{-25}	2.48×10^{-6}
7 + Fullerene	0.0220 (0.0996)	34 (27)	47 (49)	1.46×10^{-26}	2.18×10^{-7}
7 + SWCNT	0.0162 (0.0181)	32 (42)	54 (102)	4.89×10^{-27}	7.31×10^{-8}
14 PMAA linked	0.0404	-[a]	-[a]	-[a]	-[a]
14 PMAA mixed	-[b]	8.45	13.5	2.59×10^{-24} (2.18×10^{-31})	7.07×10^{-5} (7.44×10^{-12})
15 PEI linked	-[b]	12	44	4.31×10^{-26}	7.27×10^{-7}

				(1.18×10^{-26})	(1.41×10^{-7})
15 PEI mixed	-[b]	17.3	112	1.64×10^{-26} (1.18×10^{-26})	2.76×10^{-7} (1.41×10^{-7})
16 PEI linked	0.124	9.7	16	6.42×10^{-26} (8.20×10^{-27})	9.65×10^{-7} (8.8×10^{-8})
16 PEI mixed	-[b]	15	46.7	6.40×10^{-26} (8.20×10^{-27})	9.63×10^{-7} (8.8×10^{-8})

[a] = complex displayed SA.

[b] = no signal detected

4.3 Degradation Studies

These studies were performed to see if polymer films improve the photostability of Pcs and Pc/NM mixtures embedded in them. Fig. 4.7 shows the photodegradation of phthalocyanine film of **8** alone evaporated from solution on a slide (Fig. 4.7A) and within a PMMA thin film (Fig. 4.7B). In both figures, UV-Visible spectra show a decrease in absorption over time and the inserts show the linear decrease in absorption with time. Both samples were exposed to a quartz lamp with a water filter to absorb IR radiation from the lamp. The rate of degradation of the phthalocyanine on its own was observed to be slightly faster than when in a polymer matrix. Similar degradation behaviour was observed for the rest of the phthalocyanines embedded

in PMMA, with slight differences depending on the ring substituents. Photodegradation of phthalocyanines is through the singlet oxygen produced by them. This confirms that embedding the phthalocyanines in a polymer improves stability probably by limiting their interaction with atmospheric oxygen.

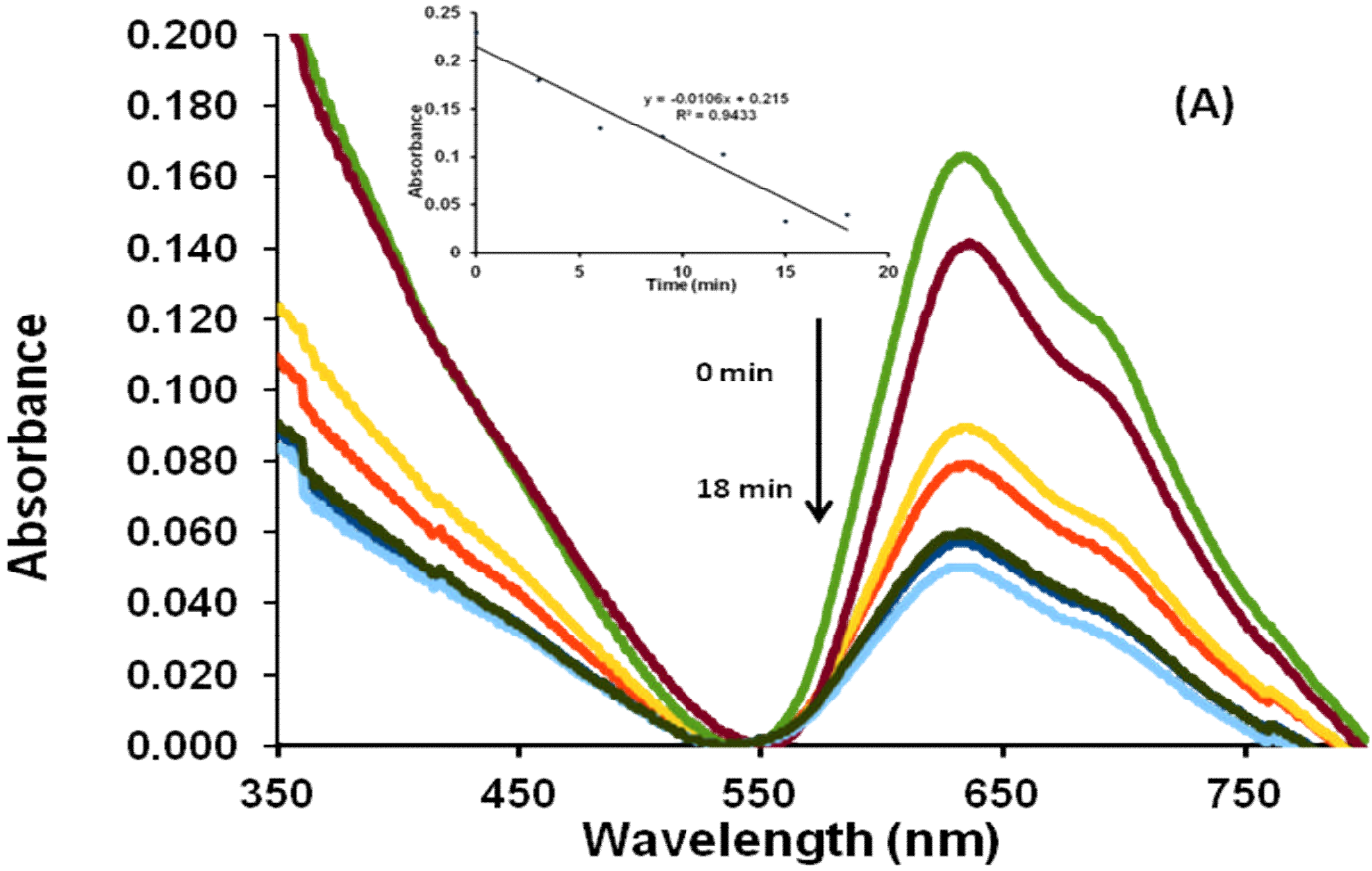

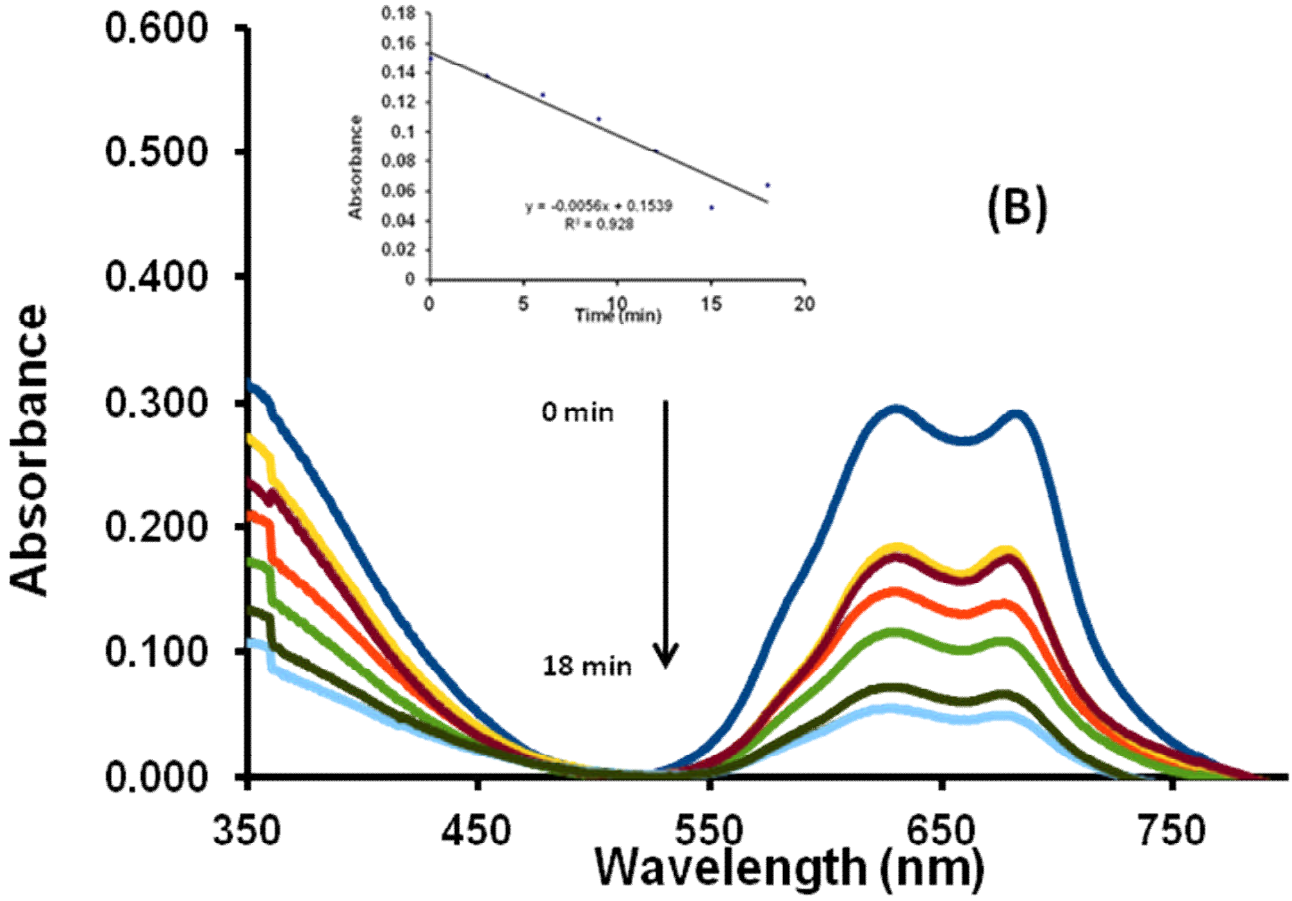

Fig. 4.7: UV-Visible spectra of phthalocyanine **8** (A) deposited on a glass slide from a DMSO solution and (B) in PMMA thin film exposed to white light. Insert: plot absorption alteration over time (in minutes) of **8** in PMMA thin film.

For SWCNT in the presence of complex **7** and in PMMA film, there was no degradation of the phthalocyanine as judged by the lack of decrease in the Q band intensity. What was observed was a change from aggregated state to monomeric state without any clear dependence on irradiation time, Fig. 4.8. Even though the third order susceptibility values are reduced for complex **7** in the presence of SWCNT, the film containing SWCNT and **7** show stability, which is part of the requirements for complexes which exhibit NLO (hence have possibility to be applied as OL materials).

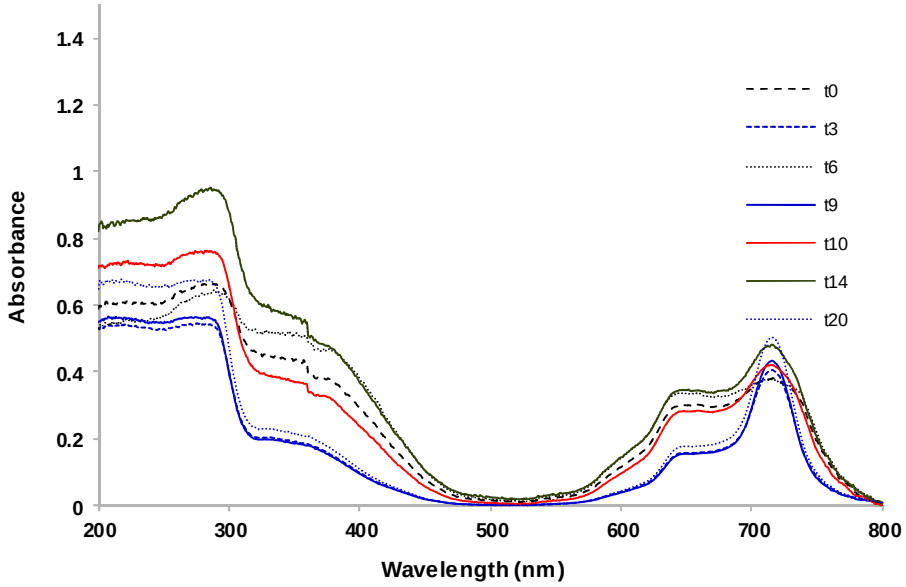

Fig. 4.8: UV-Visible spectra of phthalocyanine **7** in the presence of SWCNTs in PMMA film exposed to UV/visible lamp. T_0 to t_{20} refer to irradiation time in minutes.

Chapter 5

Conclusions and References

5. Conclusions

A range of phthalocyanine compounds and their mixtures with CdTe QDs were analyzed with the Z-scan and found to have optical limiting ability which improves in the presence of QDs. It has been determined that a Pc:QD ratio of around 97:1 yields improvements in optical limiting ability of the mixture when compared against the Pc alone. The optical limiting parameters of Pcs were larger when *tert*-butylphenoxy substituents were present compared to when benzyloxyphenoxy and phenoxy substituents were employed, depending on the solvent and aggregation state of the complexes. Non-peripheral substitution decreased the optical limiting parameters. The OL parameters improved in the presence of QDs.

Complexes **5-16** were studied for their optical limiting behavior as thin films when mixed, complexes **14-16** were also linked directly to the polymers. Covalent linking increased optical limiting behavior. Phthalocyanine **8** was employed to test whether a polymer matrix affords any protection against photodegradation of the phthalocyanine. Degradation studies indicate that placing a phthalocyanine within a polymer thin film reduces the rate of photodegradation.

Optical limiting parameters were determined for complexes **5-14** when embedded in PMMA polymer in the presence of QDs. The QDs employed were CdTe-TGA. k values decreased with the addition of the CdTe-TGA as triplet lifetimes increased. The F_{sat} values were smaller in the films when compared to the solutions. I_{lim} generally increased when QDs were added to the Pc polymer films, except for **9**, **12** and **14**. The same trend is observed for F_{sat}, except this time **5**, **7** and **14** do not follow the trend.

The Im[$\chi^{(3)}$]/α and γ parameters were also determined for complexes **5-14** when embedded in PMMA polymer in the presence of other nanomaterials. The nanomaterials employed were fullerenes, single walled carbon nanotubes as well as the quantum dots: CdS-TGA, CdSe-TGA and CdTe-TGA. Im[$\chi^{(3)}$]/α and γ values generally increase for Pcs in the presence of CdTe QDs. In PMMA films, the **7**/CdS and **7**/CdTe combinations resulted in the best Im[$\chi^{(3)}$]/α and γ values

ClInHp was successfully synthesized and characterized, along with determining its nonlinear parameters. It was shown to possess superior optical limiting ability, with a Im[$\chi^{(3)}$]/α value of 3.32 x 10^{-7} esu and a hyperpolarizability of 3.23 x 10^{-28} esu. In comparison, the previously analyzed Pcs have Im[$\chi^{(3)}$]/α values of the 10^{-11} esu range and hyperpolarizabilities of 10^{-30} esu range. Its I_{lim} is also of comparable magnitude to previously analyzed Pcs, but the F_{sat} was found to be much higher.

References

[1] R. Bonnett, *Chemical aspects of photodynamic therapy*, Gordon and Breach Science Publishers, Germany, 2000.

[2] A. Von Braun, J. Tscheniac, *Ber. Deut. Chem. Ges*., 40 (1907) 2709.

[3] H. de Diesbach, E. von der Weid, *Helv. Chim. Acta*, 10 (1927) 886.

[4] G.T. Byrne, R.P. Linstead, A.R. Lowe, *J. Chem. Soc*, (1934) 1017.

[5] R.P. Linstead, A.R. Lowe, *J. Chem. Soc*., (1934) 1022.

[6] C.E. Dent, R.P. Linstead, *J. Chem. Soc*., (1934) 1027.

[7] J.A. Elvidge, R.P. Linstead, *J. Chem. Soc*., (1955) 3526.

[8] J.M. Robertson, *J. Chem. Soc*., (1935) 615.

[9] J.M. Robertson, *J. Chem. Soc*., (1936) 1195.

[10] J.M. Robertson, I. Woodward, *J. Chem. Soc*., (1937) 3536.

[11] C.C. Leznoff, A. B. P. Lever, *Phthalocyanines: Properties and Applications*, VCH, New York, vol 1-4 (1989 – 1996).

[12] D. Dini, M.J.F. Calvete, M. Hanack, V. Amendola, M. Meneghetti. *J. Am. Chem. Soc.*, 130 (2008) 12290.

[13] B. Hauschel, D. Ruff, Michael Hanack, *J. Chem. Soc. Chem. Comm.*, (1995) 2449.

[14] M. G. Waltera, A. B. Rudine, C.C. Wamser, *J. Porphyrins Phthalocyanines*, 14 (2010) 759.

[15] S. Rajaputra, S. Vallurupalli, V. P. Singh, *J Mater Sci: Mater Electron* DOI 10.1007/s10854-007-9152-5.

[16] V.P. Singh, R.S. Singh, B. Parthasarathy, A. Aguilera, J. Anthony, M. Payne, *Appl. Phys. Lett.*, 86 (2005) 0821061.

[17] J. Nelson, J. Kirkpatrick, P. Ravirajan, *Phys. Rev. B*, 69 (2004) 035337.

[18] V.P. Singh, B. Parthasarathy, R.S. Singh, A. Aguilera, J. Anthony, M. Payne, *Sol. Energy. Mater. Sol. Cells*, 90 (2006) 798.

[19] P. Peumans, A. Yakimov, S.R. Forrest, *J. Appl. Phys.*, 93 (2003) 3693

[20] C.W. Tang, *Appl. Phys. Lett.*, 48 (1986) 183.

[21] P. Peumans, V. Bulovic, S.R. Forrest, *Appl. Phys. Lett.*, 76 (2000) 2650.

[22] A. Yakimov, S.R. Forrest, *Appl. Phys. Lett.*, 80 (2001) 1667.

[23] I.A. Levitsky, W. B. Euler, N. Tokranova, B. Xu, J. Castracane, *Appl. Phys. Lett.*, 85 (2004) 25.

[24] Peng, B.-X.; Gao, D.-T.; Yan, T.-T. *J.G.S.C.A.S.*, 17 (2000) 43.

[25] Xu, H.-T.; Chen, L.-J.; Gao, D.-T. et al. *J.G.S.C.A.S.*, 19 (2002) 399.

[26] D. Dini, M.J.F. Calvete, M. Hanack, V. Amendola, M. Meneghetti, *Chem. Commun.*, 22 (2006) 2394.

[27] M. Gouterman, In *The Porphyrins*, (Ed. D. Dolphin), Part A. Physical

Chemistry, Academic Press, New York, (1978).

[28] A.J. McHugh, M. Gouterman, C. Weiss, *Theoret. Chim. Acta,* 24 (1987) 246.

[29] A.M. Schaffer, M. Gouterman, E. R. Davidson, *Theoret. Chim. Acta,* 30

(1973) 9.

[30] M.J. Stillman, T. Nyokong, In Phthalocyanines*: Properties and Applications* (Eds. C. C. Leznoff, A. B. P. Lever, VCH, New York, (1989).

[31] C. Altucci, R. Borrelli, C. de Lisio, F. De Riccardis, V. Persico, A. Porzio, A. Peluso. *Chem. Phys.Lett.*, 354 (2002) 160.

[32] S. Couris, E. Koudoumas, A.A. Ruth, S. Leach *J. Phys. B: At. Mol. Opt. Phys.*, 8 (1995) 4537.

[33] J. Robertson *Mater. Today* 2004, 7, 46.

[34] N.V. Kamanina, A.I. Plekhanov *Opt. Spectrosc.*, 93 (2002) 408.

[35] N.V. Kamanina *Proceedings of the NATO Advanced Research Workshop on Organic Nanophotonics.*, II/100 (2003)177.

[36] N.V. Kamanina, E.F. Sheka *Opt. Spectrosc.*, 96 (2004) 599.

[37] N.V. Kamanina, N.A. Shurpo, S.V. Likhomanova, S.V. Serov, P.Ya. Vasilyev, V.G. Pogareva, V.I. Studenov, D.P. Uskokovic *Acta Phys. Pol.,* A, 120 (2011) 256.

[38] G. Galli, A. Puzder, A.J. Williamson, J.C. Grossman, L. Pizzagalli, *Nanotech*. 1 (2002) 470.

[39] R.E. Bailey, S.M. Nie, *J. Am. Chem. Soc.,* 125 (2003) 7100.

[40] S. Dayal, C. Burda, *J. Am. Chem. Soc.* 129 (2007) 7977.

[41] S. Moeno, T. Nyokong, *J. Photochem. Photobiol. A: Chem.* 201 (2009) 228.

[42] S. Moeno, T. Nyokong, *Polyhedron* 27 (2008) 1953.

[43] A.O. Orlova, V.G. Maslov, A.V. Baranov, I. Gounko, S. Byrne, *Opt. Spectrosc.*, 105 (2008) 726.

[44] P. Juzenas, W. Chen, Y-P. Sun, M.A.N. Coelho, R. Generalov, N. Generalova, I.L. Christensen, *Adv. Drug Deliv. Rev.*, 60 (2008) 1600.

[45] P. Holister, C. Román, T. Harper, *Quantum Dots: Technology White Papers nr. 13*, Cientifica, 2003, pg. 1-7

[46] S. Dayal, R. Krolicki, Y. Lou, X. Qiu, J.C. Berlin, M.E. Kenney, C. Burda, *Appl. Phys. B*, 84 (2006) 309.

[47] M.E. Wieder, D.C. Hone, M.J. Cook, M.M. Handsley, J. Gavrilovic, D.A. Russel, *Photochem. Photobiol Sci.*, 5 (2006) 727.

[48] A.R. Clapp, I.L. Medintz, H. Mattoussi, *Chem. Phys. Chem.* 7 (2006) 47

[49] A.C.S. Samia, S. Dayal, C. Burda *Photochem. Photobiol.*, 82 (2006) 617.

[50] A.C.S. Samia, X. Chen, C. Burda *J. Am. Chem. Soc.*, 125 (2003) 15736.

[51] R. Bakalova, H. Ohba, Z. Zhelev, M. Ishikawa, Y. Baba *Nat. Biotechnol.*, 22 (2004) 1360.

[52] R. Bakalova, H. Ohba, Z. Zhelev, T. Nagase, R. Jose, M. Ishikawa,

Y. Baba *Nano Lett.*, 4 (2004) 1567.

[53] W.W. Yu, E. Chang, R. Drezek, V.L. Colvin *Biochem. Biophys. Res. Commun*., 348 (2006) 781.

[54] A. K. Jeremiah, C. Netta, L. N. Jay, *J. Phys. Chem. B*, 108 (2004) 17042.

[55] J.-M. Hsieh, M.-L. Ho, P.-W. Wu, P.-T. Chou, T.-T. Tsai, Y. Chi, *Chem. Commun.*, 615 (2006) 615.

[56] S.S. Kim, Y.T. Lim, E.G. Soltesz, A.M. De Grand, J. Lee, A. Nakayama, J.A. Parker, T. Mihaljevic, R.G. Laurence, D.M. Dor, L.H. Cohn, M.G. Bawendi, J.V. Frangioni *Nat. Biotechnol.*, 22 (2004) 93.

[57] Z. Kaul, T. Yaguchi, S.C. Kaul, T. Hirano, R. Wadhwa, K. Taira *Cell Res*, 13 (2003) 503.

[58] H.Z. Wang, H.Y. Wang, R.Q. Liang, K.C. Ruan *Acta Biochim. Biophys. Sin. (Shanghai)*, 36 (2004) 681.

[59] H.M.E. Azzazy, M.M.H. Mansour, S.C. Kazmierczak *Clin. Biochem.*, 40 (2007) 917.

[60] A.M. Iga, J.H.P. Robertson, M.C.Winslet, A.M. Seifalian, *J. Biomed. Biotechnol.*, 2007 (2007) 1.

[61] D.B. Tada, L.L.R. Vono, E.L. Duarte, R. Itri, P.K. Kiyohara, M.S. Baptista, L.M. Rossi, *Langmuir*, 2 (2007) 8194.

[62] J.W. Arbogast, A.P. Darmanyan, C.S. Foote, F.N. Diederich, R.L. Whetten, Y. Rubin, M.M. Alvarez, S.J. Anz *J. Phys. Chem.*, 95 (1991) 11.

[63] J. W. Arbogast, C. S. Foote *J. Am. Chem. Soc.*, 113 (1991) 8886.

[64] H. Andreas *Angewandte Chemie International Edition in English*, 32 (1993) 1138.

[65] F. Diederich, C. Thilgen *Science*, 271 (1996) 317.

[66] M. Prato *J. Mater. Chem.*, 7 (1997) 1097.

[67] F.B. Kooistra, J. Knol, F. Kastenberg, L.M. Popescu, Wiljan J. H. Verhees, J.M. Kroon, J.C. Hummelen *Org. Lett.*, 9 (2007) 551.

[68] S. Guha, K. Nakamoto *Coordination Chemistry Reviews*, 249 (2005) 1111.

[69] S. Stevenson, G. Rice, T. Glass, K. Harich, F. Cromer, M.R. Jordan, J. Craft, E. Hadju, R. Bible, M.M. Olmstead, K. Maitra, A.J. Fisher, A.L. Balch, H.C. Dorn *Nature*, 401 (1999) 55.

[70] L. Dunsch, M. Krause, J. Noack, P. Georgi *J. Phys. Chem. Solids*, 65 (2004) 309.

[71] N. Chen, L-Z Fan, K. Tan, Y-Q Wu, C-Y Shu, X. Lu, C-R Wang *J. Phys. Chem. C*, 111 (2007) 11823.

[72] T. Cai, L. Xu, M.R. Anderson, Z. Ge, T. Zuo, X. Wang, M.M. Olmstead, A.L. Balch, H.W. Gibson, H.C. Dorn *J. Amer. Chem. Soc.*, 128 (2006) 8581.

[73] A. Huczko *Focus on Physical Chemistry Academia*, 2 (2006) 16.

[74] B.C. Thompson, J.M.J. Fréchet *Angew. Chem. Int. Ed.*, 47 (2008) 58.

[75] M. Cha, N.S. Sariciftci, A.J. Heeger, J.C. Hummelen, F. Wudl *Appl. Phys. Lett.*, 67 (1995) 3850.

[76] Q. Chen, L. Kuang, E.H. Sargent, Z.Y. Wang *Appl. Phys. Lett.*, 83 (2003) 2115.

[77] M.S. Dresselhaus, G. Dresselhaus, P.C. Eklund, *Science of Fullerenes and Carbon Nanotubes* (Academic, San Diego, 1996).

[78] J.W. Mintmire, B.I. Dunlap, C.T. White *Phys. Rev. Lett.*, 68 (1992) 631.

[79] N. Hamada, S. Sawada, A. Oshiyama *Phys. Rev. Lett.*, 68 (1992) 1579.

[80] R. Saito, M. Fujita, G. Dresselhaus, M.S. Dresselhaus *Appl. Phys. Lett.*, 60 (1992) 2204.

[81] R. Saito, M. Fujita, G. Dresselhaus, M.S. Dresselhaus *Phys. Rev. B*, 46 (1992) 1804.

[82] T.W. Odom, J-L Huang, P. Kim, C.M. Lieber *Nature*, 391 (1998) 62.

[83] C. Journet, W.K. Maser, P. Bernier, A. Loiseau, M. Lamyde la Chapelle, S. Lefrant, P. Deniard, R. Leek, J.E. Fischerk *Nature*, 388 (1997) 756.

[84] J. Chen, M.A. Hamon, H. Hu, Y. Chen, A.M. Rao, P.C. Eklund, R.C. Haddon *Science*, 282 (1998) 95.

[85] C. Liu, Y.Y. Fan, M. Liu, H.T. Cong, H.M. Cheng, M.S. Dresselhaus *Science*, 286 (1999) 1127.

[86] S. Yamashita, Y. Inoue, S. Maruyama, Y. Murakami, H. Yaguchi, M. Jablonski, S.Y. Set *Opt. Lett.*, 29 (2004) 1581.

[87] Z.-B. Liu, J.-G. Tian, Z. Guo, D.-M. Ren, F. Du, J.-Y. Zheng, Y.-S. Chen *Adv. Mater.*, 20 (2008) 511.

[88] A. Gambetta, C. Manzoni, E. Menna, M. Meneghetti, G. Cerullo, G. Lanzani, S. Tretiak, A. Piryatinski, A. Saxena, R.L. Martin, A.R. Bishop *Nature Physics*, 2 (2006) 515.

[89] G.Y. Guo, K.C. Chu, D-S Wang, C-G Duan *Phys. Rev. B: Condens. Matter*, 69 (2004) 205416-1.

[90] J. Wang, W.J. Blau *J. Phys. Chem. C*, 112 (2008) 2298.

[91] J.H. Yao, K.R. Elder, H. Guo, M. Grant *Phys. Rev. B: Condens. Matter*, 47 (1993) 14110.

[92] R. Finsy *Langmuir*, 20 (2004) 2975.

[93] W.W. Yu, L. Qu, W. Guo, X. Peng, *Chem. Mat.* 15 (2003) 2854.

[94] V. Drits, J. Środoń, D.D. Eberl *Clays Clay Miner.*, 45 (1997) 461.

[95] J.J. Bozzola, L.D. Russell. *Electron microscopy: principles and techniques for biologists.* Jones and Bartlett, Boston. (1992) 390.

[96] E. Meyer *Progress in Surface Science*, 41 (1992) 3.

[97] J. Drbohlavova, V. Adams, R. Kizek, J. Hubalek, *Int. J. Mol.*, *Sci.* 10 (2009) 656.

[98] T. Allen, *Particle Size Measurement 3rd edn*, London: Chapman and Hall (1981)

[99] S. Brunauer, P.H. Emmett, E. Teller, *J. Am. Chem. Soc.* 60 (1938) 309.

[100] C.P. Poole Jr., F.J. Owens, *Introduction to Nanotechnology*, New York: John Wiley and Sons (2003)

[101] P.W. Yu *J. Appl. Phys.*, 47 (1976) 677.

[102] M. D. Lampert, B. K. Meyer, M. Hornung, K. W. Benz, A. Petersson and L. Samuelson, *Journal of Crystal Growth*, 183 (1998) 377.

[103] P. Kubát, J. Mosinger, *J. Photochem. Photobiol. A: Chem.*, 96 (1996) 93.

[104] J.E. Ehrlich, X.L. Wu, I.-Y. S. Lee, Z.-Y. Hu, H. Rőckel, S.R. Marder, J.W. Perry *Opt. Lett.*, 22 (1997) 1843.

[105] Y. Xu, Z. Liu, X. Zhang, Y. Wang, J. Tian, Y. Huang, Y. Ma, X. Zhang, Y. Chen *Adv. Mater.*, 21 (2009) 1275.

[106] S. Shívt, W. JF, J. P. Lang, X. Q. Xin *J. Phys. Chem.*, 98 (1994) 3570.

[107] X. Sun, Y. Xiong, P. Chen, J. Lin, W. Ji, J. Hong Lim, S.S. Yang, D.J. Hagan, E.W. Van Stryland *Appl. Opt.*, 39 (2000) 1998.

[108] W. Ji, S. Shi, H. J. Du, P. Ge, S.H. Tang, X.Q. Xin *J. Phys. Chem.*, 99 (1995) 17297.

[109] D.I. Kovsh, S. Yang, D.J. Hagan, E.W. Van Stryland *Appl. Opt.*, 38 (1999) 5168.

[110] M.K.M. Low, H. Hou, H. Zheng, W. Wong, G. Jin, X. Xinb, W. Ji *Chem. Commun.* 4 (1998) 505.

[111] S. Shi, W. Ji, S.H. Tang *J. Am. Chem. Soc.*, 116 (1994) 3615.

[112] R.W. Boydy, R.J. Gehry, G.L. Fischery and J.E. Sipe *Pure Appl. Opt.*, 5 (1996) 505.

[113] X. Sun, R.Q. Yu, G.Q. Xu, T.S.A. Hor, W. Ji *Appl. Phys. Lett.*, 73 (1998) 3632.

[114] C.G. Claessens, W.J. Blau, M. Cook, M. Hanack, R.J.M. Nolte, T. Torres, D. Wöhrle *Monatshefte fü r Chemie*, 132 (2001) 3.

[115] S.J. Mathews, S. Chaitanya Kumar, L. Giribabu b, S. Venugopal Rao *Mater. Lett.*, 61 (2007) 4426.

[116] J.J Doyle, J. Wang, S.M. O'Flaherty, Y. Chen, A. Slodek, T. Hegarty, L.E. Carpenter II, D. Wőhrle, M. Hanack, W.J. Blau *J. Opt. A: Pure Appl. Opt.*, 10 (2008) 1.

[117] A. Santhi, V.V. Namboodiri, P. Radhakrishnan, V.P.N. Nampoori *J. Appl. Phys.*, 100 (2006) 053109-1.

[118] S.J. Mathews, S. Chaitanya Kumar, L. Giribabu, S. Venugopal Rao *Opt. Commun.*, 280 (2007) 206.

[119] S. Venugopal Rao, N. Venkatram, L. Giribabu, D. Narayana Rao *J. Appl. Phys.*, 105 (2009) 053109-1.

[120] J.M. Fox, T.J. Katz, S. Van Elshocht, T. Verbiest, M. Kauranen, A.Persoons, T. Thongpanchang, T. Krauss, L. Brus *J. Am. Chem. Soc.*, 121 (1999) 3453.

[121] P.D. Fuqua, B. Dunn, J.I. Zink *J. Sol-Gel Sci. Technol.*, 11 (1998) 241.

[122] E. Blanco, D. Narayana Rao, F.J. Aranda, D.V.G.L.N. Rao, J.A. Akkara, R. Litrán, M. Ramírez-del-Solar *J. Appl. Phys.*, 83 (1998) 3441.

[123] M. Hanack, T. Schneider, M. Barthel, J.S. Shirk, S.R. Flom, R.G.S. Pong *Coord. Chem. Rev.*, 219–221 (2001) 235.

[124] J.S. Shirk, R.G.S. Pong, F.J. Bartoli, A.W. Snow *Appl. Phys. Lett.*, 63 (1993) 1880.

[125] J.W. Perry, K. Mansour, I.Y.S. Lee, X.L. Wu, P.V. Bedworth, C.T. Chen, D. Ng, S.R. Marder, P. Miles, T. Wada, M. Tian, H. Sasabe *Science*, 273 (1996) 1533.

[126] D. Dini, M.J.F. Calvete, M. Hanack, M. Meneghetti, *J. Phys. Chem. A* 112 (2008) 8515.

[127] Y.Z. Gu, Z.J. Liang, F.X. Gan, *Opt. Mater.* 17 (2001) 471.

[128] J.W. Perry, K. Mansour, S.R. Marder, D. Alvarez Jr., K.J. Perry, I. Choong, *Opt. Lett.* 19 (1994) 625.

[129] C. Liu, X. Wang, G.Gong, Y. Liu, W. Qiu, D. Zhu, *Chem. Phys. Lett.* 347 (2001) 378.

[130] E. Agostinelli, D. Attanasio, I. Collamati, V. Fares. *Inorg. Chem.*, 23 (1984) 1162.

[131] G. de la Torre, P. Vazquez, F. Agullo-Lopez, T. Torres *J. Mat. Chem.*, 8 (1998) 1671.

[132] G. de la Torre, Vazquez P., F. Agullo-Lopez, T. Torres *Chem. Rev*., 104 (2004) 3723.

[133] G. Rojo, F. Agullo-Lopez, Cabezon B., T. Torres, S. Brasselet, I. Ledoux, J. Zyss *J. Phys. Chem. B*, 104 (2000) 4295.

[134] M.S. Rodriguez-Morgade, G.D. Pantos, E. Caballero, J.L. Sessler, T. Torres *Macroheterocycles*, 1 (2008) 40.

[135] F. Henari, J. Callaghan, H. Stiel, W. Blau, D.J. Cardin *Chem. Phys. Lett.*, 199 (1992) 144.

[136] J. Callaghan, W.J. Blau *J. Nonlinear Opt. Phys. Mater.*, 9 (2000) 505.

[137] W.J. Blau, H.J. Byrne, D.J. Cardin, T.J. Dennis, J.P. Hare, H.W. Kroto, R. Taylor, D.R.M. Walton *Phys. Rev. Lett.*, 67 (1991) 1423.

[138] S.R. Mishra, H.S. Rawat, S.C. Mehendale, K.C. Rustagi, A.K. Sood, R. Bandyopadhyay, A. Govindaraj, C.N.R. Rao *Chem. Phys. Lett.*, 317 (2000) 510.

[139] L. Vivien, P. Lancon, D. Riehl, F. Hache, E. Anglaret *Carbon*, 40 (2002) 1789.

[140] N. Izard, P. Billaud, D. Riehl, E. Anglaret *Opt. Lett.*, 30 (2005) 1509.

[141] Y. Chen, Y. Lin, Y. Liu, J. Doyle, N. He, X.D. Zhuang, J.R. Bai, W.J. Blau *J. Nanosci. Nanotechnol.*, 7 (2007) 1268.

[142] J. Wang, W.J. Blau *SPIE newsroom* (2007) doi:10.1117/2.1200711.0916, http://spie.org/x1789.xml? highlight=x2400

[143] J. Wang, W.J. Blau *Appl. Phys. B*, 91 (2008) 521.

[144] J. Wang, W.J. Blau *J. Phys. Chem. C*, 112 (2008) 2298.

[145] Y.P. Sun, J.E. Riggs *Int. Rev. Phys. Chem.*, 18 (1999) 43.

[146] Y.P. Sun, J.E. Riggs, K.B. Henbest, R.B. Martin *J. Nonlinear Opt. Phys. Mater.*, 9 (2000) 481.

[147] C. Zhang, Y.L. Song, X. Wang *Coord. Chem. Rev.*, 251 (2007) 111.

[148] X. Wang, C. Liu, Q. Gong, Y. Huang, C. Huang *Opt. Commun.*, 197 (2001) 83.

[149] W. Ji, H.J. Du, S.H. Tang, S. Shi *J. Opt. Soc. Am. B*, 12 (1995) 876.

[150] E.W. Van Stryland, M. Sheikh-Bahae in: *Characterization Techniques and Tabulations for Organic Nonlinear Materials*, Kuzyk MG, Dirk CW.Eds., page 655-692, Marcel Dekker, Inc., 1998.

[151] D. Dini, M. Hanack, in: K.M. Kadish, K.M. Smith, R. Guilard (Eds.), *The Porphyrin Handbook: Physical Properties of Phthalocyanine-based Materials, vol. 17*, Academic Press, USA, 2003, p. 22.

[152] D. Dini, M. Barthel, M. Hanack*, Eur. J. Org. Chem.* (2001) 3759.

[153] Y. Chen, M. Hanack, Y. Araki, O. Ito *Chem. Soc. Rev.*, 34 (2005) 517.

[154] J. Simon, C. Sirlin, *Pure Appl. Chem.*, 61 (1989) 1625.

[155] V. Chauke**,** M. Durmus, T. Nyokong, *J. Photochem. Photobiol. A: Chem.*, 192 (2007) 179

[156] A. Auger, W. J. Blau, P. M. Burnham, I. Chambrier, M. J. Cook, B. Isare, F. Nekelson, S. M. O'Flaherty, *J. Mater. Chem*., 13 (2003) 1042.

[157] M. Yüksek, A. Elmali, M. Durmus, H.G. Yaglioglu, H. Ünever, T. Nyokong *J. Opt.*, 12 (2010) 015208.

[158] Y–X Li, J. Zhu, Y. Chen, J. Zhang, J. Wang, B. Zhang,Y. He, W.J Blau *Nanotechnol.*, 22 (2011) 205704.

[159] Y. Liu, S.M. O'Flaherty, Y. Chen, Y. Araki, J. Bai, J. Doyle, W.J. Blau, O. Ito *Dyes Pigments*, 75 (2007) 88.

[160] S. Tekin, H.G. Yaglioglu, A. Elmali, U. Kürüm, H. Yanık, D.A. Tekdas, M. Durmus,V. Ahsen *Mater. Chem. Phys.*, 138 (2013) 270.

[161] D. Dini, M.J.F. Calvete, M. Hanack, W. Chen, W. Ji *ARKIVOC*, 3 (2006) 77.

[162] C.J. Ziegler in *Handbook of Porphyrin Science*, (K. M Kadish, K. M Smith, R. Guilard Eds) Vol 17, pages 113-238, World Scientific, Singapore, 2012.

[163] O.N. Trukhina, M. S. Rodríguez-Morgade, S. Wolfrum, E.Caballero, N. Snejko, E.A. Danilova, E. Gutiérrez-Puebla, M. K. Islyaikin, D. M. Guldi, T.Torres *J. Am. Chem. Soc.*, 132 (2010) 12991.

[164] S. Tekin, U. Kürüm, M. Durmuş, H.G. Yaglioglu, T. Nyokong, A. Elmali *Optics Commun.*, 283 (2010) 4749.

[165] M. Durmuş, T. Nyokong *Polyhedron*, 26 (2007) 2767.

[166] M. Durmuş, T. Nyokong *Spectrochim. Acta: A*, 69 (2008) 1170.

[167] M. Durmuş, T. Nyokong *Polyhedron*, 26 (2007) 3323.

[168] M. Durmuş, T. Nyokong *Tetrahedron*, 63 (2007) 1385.

[169] M.P. Somashekarappa, J. Keshavayya, S. Sampath *Pure Appl. Chem.* 74 (2002) 1609

[170] L. Ismaili, B. Refouvelet, A. Xicluna, US Patent number: 7217840 May 15 (2007)

[171] M. Idowu, J.Y. Chen, T. Nyokong *New J. Chem.*, 32 (2008) 290.

[172] A. Shavel, N. Gaponik, A. Eychmuller *J. Phys. Chem. B*, 110 (2006) 19280.

[173] Z.H. Zhang, W.S. Chin, J.J. Vittal *J. Phys. Chem. B*, 108 (2004) 18569.

[174] J.A. Kloepfer, S.E. Bradforth, J.L. Nadeau *J. Phys. Chem. B*, 109 (2005) 9996.

[175] C. W. Dirk, T. Marks *J. Inorg. Chem.*, 23 (1984) 4325–4332

[176] M. Bossa, E. Cervone, C. Garzillo, A. Peluso *J. Mol. Struct. (Theochem)*, 390 (1997) 101.

[177] M. Bossa, I. Grella, P. Nota, E. Cervone *J. Mol. Struct. (Theochem)*, 210 (1990) 267.

[178] S. Sam, L. Touahir, J.S. Andresa, P. Allongue, J.-N. Chazalviel, A.C. Gouget-Laemmel, C.H. de Villeneuve, A. Moraillon, F. Ozanam, N. Gabouze, S. Djebbar *Langmuir*, 26 (2010) 809.

[179] D. Gani, P.J. Hendra, W.F. Maddams, C. Passingham, I.A.M. Royaud, H.A. Willis, V. Zichy, M.E.A. Cudby *Analyst*., 115 (1990) 1313.

[180] B.N. Achar, K.S. Lokesh *J. Organomet. Chem*., 689 (2004) 2601.

[181] A.W. Snow, J.R. Griffith, N.P. Marullo *Macromolecules*, 17 (1984) 1614.

[182] N.E. Triggs, J.J. Valentini *J. Phys. Chem*., 96 (1992) 6922.

[183] M. Rodríguez-Baeza, A. Neira, C. Aguilera *J. Chil. Chem. Soc*., 48 (2003) 75.

[184] Z. Hongbing, C. Wenzhe, W. Minquan, Z. Chunlin, Z. Chan *Chem. Phy. Lett*., 389 (2004) 119.

[185] K. Ozoemena, N. Kuznetsova, T. Nyokong *J. Photochem. Photobiol. A: Chem*., 139 (2001) 217.

[186] T. Nyokong, (2010). in *Functional Phthalocyanine Molecular Materials, Structure and Bonding* (Jiang, J. Ed.) Springer, New York, Vol. 135

[187] M. Idowu, T. Nyokong *Spectrochim. Acta: A*, 75 (2010) 411.

[188] S. Moeno, T. Nyokong *J. Photochem. Photobiol. A: Chem.*, 215 (2010) 196.

[189] P.J. Camp, A.C. Jones, R.K. Neely, N.M. Speirs *J. Phys. Chem. A*, 106 (2002) 10725.

[190] E. Zenkevich, T. Blaudeck, M. Abdel-Mottaleb, F. Cichos, A. Shulga, C. von Borczyskowski *Inter. J. Photoenergy*, Article ID 90242 (2006) 1.

[191] S. Geyer, V.J. Porter, J.E. Halpert, T.S. Mentzel, M.A. Kastner, M.G. Bawendi *Phys. Rev. B,* 82 (2010)155201.

[192] D.M. Guldi, G.M.A. Rahman, F. Zerbetto, M. Prato *Acc. Chem. Res*., 38 (2005) 871.

[193] H.T. Xu, W.W. Xie, Y.C. Guo, Y. Ci, L.J. Chen, B.X. Peng *J. Chinese Chem. Soc.*, 54 (2007) 211.

[194] T.H. Tran-Thi, C. Desforge, C. Thiec *J. Phys. Chem.*, 93 (1989) 1226.

[195] M.G. Debacker, O. Deleplanque, B. Van Vlieberge, F.X. Sauvage *Laser Chem.*, 8 (1988) 1.

[196] A. Ogunsipe, J.-Y. Chen, T. Nyokong *New J. Chem.*, 28 (2004) 822.

[197] M. Idowu, T. Nyokong *J. Luminescence*, 129 (2009) 356.

[198] M. Falconieri *J. Opt. A: Pure Appl. Opt.*, **1** (1999) 662.

[199] S.M. Mian, S.B. McGee, N. Melikechi *Optics Commun.*, 207 (2002) 339.

[200] N.K.M.N. Srinivas, S.V. Rao, D.N. Rao *J. Opt. Soc. Am. B*, 20 (2003) 2470.

[201] J. Wang, B. Gu, H.-T. Wang, X.-W. Ni, *Optics Commun.*, 283 (2010) 3525.

[202] M. Sheik-Bahae, A.A. Said, T.H. Wei, D.J. Hagan, E.W. Van Stryland, *IEEE J. Quant. Electron.*, 26 (1990) 760.

[203] H.S. Nalwa, M. Hanack, G. Pawlowski, M.K. Engel, *Chem. Phy.*, 245 (1999) 17.

[204] Y. Chen, L. Gao, M. Feng, L. Gu, N. He, J. Wang, Y. Araki, W.J. Blau, O. Ito *Mini-Reviews in Organic Chemistry*, 6 (2009) 55.

[205] X.-F. Zhang, X. Li, L. Niu, L. Sun, L. Liu *J. Fluoresc.*, 19 (2009) 947.

[206] B. Derkowska, M. Wojdyla, W. Bala, K. Jaworowicz, M. Karpierz, R. Czaplicki, B. Sahraou *Mol. Cryst. Liq. Cryst.*, 485 (2008) 965.

[207] L.-S. Zheng, M. Feng, H.-B. Zhan *Acta Phys. Chim. Sin.*, 28 (2012) 208.

[208] R. Sreeja, J. John, P.M. Aneesh, M.K. Jayaraj *Optics Commun*. 283 (2010) 2908.

[209] E. Shahriari, E. Mahmood, W.M. Yunus *Am. Eng. Appl. Sci*. 3 (2010) 98.

[210] C. Nitschke, S.M. O'Flaherty, M. Kroll, W.J. Blau *J. Phys. Chem. B*, 108 (2004)1287.

[211] Y. Liu, Y. Chen, L. Cai, J. Wang, Y. Lin, J.J. Doyle, W.J. Blau *Mater. Chem. Phys.,* 107 (2008) 189.